Imperial College London

Department of Bioengineering

Thesis submitted in fulfilment of the requirements for the award of PhD degree of Imperial College London and the Diploma of Imperial College London

# A Platform to Restore Intra-Tissue Flow in Live Explant Assays

Author: Foivos Chatzidimitriou

Submitted in April 2021

Supervisors: Darryl R. Overby

Joseph M. van Batenburg-Sherwood

# i. Abstract

Tissue resection during first-line surgery is a standard strategy in the clinic for several life-threatening diseases, such as cancer. In case of malignancy, despite the benefits from surgery, cancer often becomes treatment-resistant and metastasises, limiting therapeutic options and patient survival. Due to tumour heterogeneity, treatment personalisation can improve patient outcomes, however tools based on native tissue samples, used for patient-specific drug screening remain very limited. This is primarily due to the diffusion-limited mass transport in static culture conditions, where tissue viability is rapidly reduced due to ischemia. Our aim is to develop a platform that restores intra-tissue flow through native tissue specimens to prolong their preservation *ex vivo*.

Flow of culture media around tissue specimens has been commonly used for sample preservation. However, the efficacy of most currently available platforms has been limited, as *ex vivo* specimen perfusion is not facilitated in these technologies. As fluid is allowed to travel around specimen periphery, intra-tissue flow is hydraulically disadvantaged and benefits from culture media renewal only affect cells within 200 μm from explant surface. In this thesis, a novel system is presented that comprises a channel-based device with a suitably-designed constriction to block peri-fusion (i.e. flow around the tissue) and facilitate specimen entrapment and perfusion.

Using a syringe pump, device efficacy to facilitate intra-tissue flow was investigated, showing that the induced perfusion occurred through both the vasculature and the interstitium. The effects of perfusion on specimen maintenance and function were also investigated. It was showed that healthy mouse liver and cancerous mouse and human omental specimens were better preserved under perfused conditions in the developed apparatus for 48h. Intra-tissue flow was also effective to inhibit cell metabolism after a 2h-specimen perfusion with a metabolic poison, suggesting this system may have great potential for predictive, live explant assays.

To my family and friends for their tireless support. To those distracted by others' projects as a result of their genuine interest for science.

# ii. Acknowledgements

First, I need to thank Professor Darryl Overby and Dr Joseph van Batenburg-Sherwood, who gave me the opportunity and resources to work on such an innovative and intriguing project. I am also grateful for their feedback throughout out the years.

Also, I need to thank all the researchers that contributed directly to my work, who can be found in detail in the Contributions Statement. Special thanks to Dr Lucy Collinson and Dr Anne Weston, for their collaboration on the micro-computed tomography. I am also grateful to Professor Christina Fotopoulou and Dr Paula Cunnea, for their genuine interest in my project since its early phases, providing access to human samples and contributing to the development of this device towards the clinic. Thank you to Dr Sam Au and Julian Ashby for providing their syringe pump when needed. A thank you also to Dr Periklis Pantazis, Konstantinos Kalyviotis and Elijah – See Swee Tang for allowing me to use their lab for imaging and Dr Claire Higgins for generously permitting department-wide use of her cryostat.

I would also like to thank Imperial's Commercialisation Office, and especially Dr Marika Reay and Dr Vaibhav Sharma for all their help with intellectual property protection and patent fillings. Also, a thank you to Dr Michael Newton and Tom Leonard, the patent attorneys drafting and filling our patent applications.

I also need to thank all the members of the Overby Lab for always being supportive and an amazing source of feedback. The Overby Lab members at present are (alphabetically): Jacques Bertrand, Dr Ester ReinaTorres, Justino Rodrigues, Lizzy Wheeler and Eva Zeringa. Past members of the Overby lab that I was fortunate to interact with are (alphabetically): Dr Anabela Cepa-Areias, Dr Michael Madekurozwa, Arianna Rech, Dr Alice Spenlehauer and Dr Pei-Jung Wu. Michael has been extremely helpful with all aspects of microfabrication and fluidics throughout the years, for which I am grateful for.

Thank you to the Facility for Imaging by Light Microscopy (FILM) personnel, and primarily to Stephen Rothery and Dr Andreas Bruckbauer, for their support and training in widefield and confocal imaging. Also, a big thank you to all the technicians at the department of Bioengineering for always trying to make our lives easier, and primarily to (alphabetically): Nana Asante Asamoah-Danso, Joel Eustaquio, Marta Garcia Bellmunt, Dr Miguel Hermida Ayala, Sharad Patel and Beth Wallis. Thank you also to Bioengineering's administration staff for their help, particularly to Christopher Sanders and Marc Livingstone for managing financial and order-related affairs, and their predecessors Alan Nyunt and Nazib Ahmed, respectively. Also, thank you to Britta Ross for giving a face to the department during my first months as a PhD student at Imperial. I am also grateful to the Estates staff and especially to the cleaning team for tirelessly maintaining a great environment for us to work in.

Last but not least, I want to thank Adele Lam, Konstantinos Kalyviotis, Christina Vagena Pantoula and Josefin Jansson Edqvist for their friendship and support.

# iii. Contribution Statement

The contributions of the several researchers, who contributed to the work presented in this thesis are acknowledged below:

Professor Darryl Overby and Dr Joseph van Batenburg-Sherwood conceptualised the stenosis-based design for a device that facilitates *ex vivo* specimen perfusion. Professor Michael Seckl and Dr Olivier Pardo also contributed to the concept during the early phases of platform development.

**All chapters**

Professor Darryl Overby, Dr Joseph van Batenburg-Sherwood and Foivos Chatzidimitriou were involved in the design and planning of experiments and discussions on data analysis.

**Chapter 2**

- Dr Joseph van Batenburg-Sherwood assisted with hydraulic resistance measurements using the 3D-printed, multichannel device with the iPerfusion system (data not shown).
- Foivos Chatzidimitriou did all other experiments and data analysis.

**Chapter 3**

- Dr Lucy Collinson and Dr Anne Weston designed the imaging protocol for microCT and Dr Anne Weston run the imaging cycle at the Francis Crick Institute (London, UK).
- Professor Thomas Brand and Dr Ursula Herbort-Brand kindly provided zebrafish cadavers and training on tissue isolation.
- Konstantinos Kalyviotis assisted with the confocal imaging of perfused zebrafish tissue with fluorescent tracers.
- Professor Christina Lo Celso kindly provided Flk1-GFP mice, which were used for some of the preliminary experiments for perfusion demonstration (data not shown).
- Neophytos Vroullides run simulations of fluid flow and oxygen delivery through perfused specimens using COMSOL Multiphysics based on a first-order mathematical model of oxygen diffusion developed by Professor Darryl Overby and Foivos Chatzidimitriou.
- Foivos Chatzidimitriou did all other experiments and data analysis.

**Chapter 4**

- Professor Iain McNeish consulted on the mouse omental tumour experiments and analysis of the results.
- Professor Christina Fotopoulou provided the human omental tumour specimens from debulking surgeries.
- Dr Paula Cunnea consulted on the human omental tumour experiments.
- Dr Carmen Aguirre Hernandez prepared the ID8 mouse models and culture media used for experiments.
- Dr Darren Ennis consulted on the processing and staining of mouse omental tumour specimens. He also consulted on discussions about the results.
- Tissue specimen dehydration, paraffin-embedment, sectioning and staining of mouse omental tumour samples was done at the Histopathology Laboratory of Barts Cancer Institute, Queen Mary University of London.
- Foivos Chatzidimitriou did all other experiments and data analysis.

# iv. Copyright and Financial Disclosure

I hereby certify that the work presented in this thesis is my own, contributions by others have been acknowledged and all else is accurately referenced. I certify that this thesis complies with copyright laws of the UK and does not comprise any instance of plagiarism.

Funding for the work presented in this thesis was provided by an Imperial College Joint Translation Fund (supported by MRC Confidence in Concept, NIHR Imperial Biomedical Research Centre, The Royal Marsden Hospital NHS Foundation Trust, Wellcome Institutional Strategic Support Fund and EPSRC Impact Acceleration Account) and an NIH grant (EY022359) acquired by Professor Darryl R. Overby.

# v. Conference Presentations

**Chatzidimitriou F.**, van Batenburg-Sherwood J.M., NG S.S., Rashid T., Overby D.R. (2020), A liver-in-chip platform for preserving *ex vivo* tissue viability, at the MicroTAS 2020 Virtual Conference, online. Virtual poster presentation

# vi. Associated patents and publications

Patents

A patent application has been filled for the device and method for *ex vivo* specimen perfusion described in this thesis (Title: "Device for perfusion and preservation of tissue specimens *ex vivo*", Greek Patent Application No: 20200100136 - UK Patent Application No: 2004177.8 – PCT filling No: PCT/EP2021/056739).

Publications

**Chatzidimitriou F.**, van Batenburg-Sherwood J.M., Cunnea P., Fotopoulou C., McNeish I.A., Overby D.R. A novel platform to restore intra-tissue flow and preserve *ex vivo* specimens. *In preparation*.

# vii. List of abbreviations

| | |
|---|---|
| **ABC** | ATP-binding cassette |
| **ADP** | Adenosine diphosphate |
| **AFM** | Atomic force microscopy |
| **ANOVA** | Analysis of variance |
| **Atk** | Serine/threonine-specific protein kinase |
| **ATP** | Adenosine triphosphate |
| **BAK1** | BCL2 antagonist/killer 1 |
| **BAX** | Bcl-2-associated X protein |
| **BCA** | Bicinchoninic acid |
| **BCL2** | B-cell lymphoma 2 |
| **bFGF** | Basic fibroblast growth factor |
| **BRAF** | Serine/threonine-protein kinase B-Raf |
| **BSEP** | Bile salt export pump |
| **CAF** | Cancer associated fibroblast |
| **CAM-DR** | Cell adhesion-mediated drug resistance |
| **cC3** | Cleaved caspase 3 |
| **CTLA4** | Cytotoxic T-lymphocyte-associated protein 4 |
| **DMEM** | Dulbecco's Modified Eagle Medium |
| **DPX** | Dibutylphthalate-Polystyrene-Xylene |
| **ECM** | Extracellular matrix |
| **EDTA** | Ethylenediaminetetraacetic acid |
| **EGFR** | Epidermal growth factor receptor |
| **eNOS** | Endothelial nitric oxide synthase |

| | |
|---|---|
| **ER** | Endoplasmic reticulum |
| **$F_C$** | Compressive force acting on the specimen from the inclined channel surface, |
| **GFP** | Green fluorescent protein |
| **GLUT-1** | Glucose transporter 1 |
| **H&E** | Haematoxylin & Eosin |
| **HBSS** | Hank's Balanced Salt Solution |
| **HEPES** | 4-(2-hydroxyethyl)-1-piperazineethanesulfonic acid |
| **HER1,2** | Epidermal growth factor receptor 1,2 |
| **HIF-1a** | Hypoxia-inducible factor 1-alpha |
| **HMGB1** | High-mobility group box-1 |
| **ICGC** | International Cancer Genome Consortium |
| **IFP** | Interstitial fluid pressure |
| **IL-1** | Interleukin-1 |
| **KRAS** | Kirsten rat sarcoma viral oncogene homologue |
| **LDH** | Lactate dehydrogenase |
| **MPTP** | Mitochondrial permeability transition pore |
| **MTMP** | Mitochondrial permeability transition pore |
| **MTS** | 3-(4,5-Dimethylthiazol-2-yl)-5-(3-carboxymethoxyphenyl)-2-(4-sulfophenyl)-2*H*-tetrazolium |
| **MTT** | 3-(4,5-dimethylthiazol-2-yl)-2,5-diphenyltetrazolium bromide |
| **NAD** | Nicotinamide adenine dinucleotide |
| **NGS** | Normal goat serum |
| **NO** | Nitric oxide |
| **NOS** | Nitric oxide synthase |
| **OCT** | Optimal cutting temperature compound |

| | |
|---|---|
| **PARP** | Poly (ADP-ribose) polymerase |
| **PAS** | Periodic acid Schiff's staining |
| **PD1** | Programmed cell death protein 1 receptor |
| **PD-L1** | Programmed death-ligand 1 |
| **PDMS** | Polydimethylsiloxane |
| **PFA** | Formaldehyde |
| **$Re_L$** | Reynolds number |
| **SD** | Standard deviation |
| **SH** | Standard histopathology |
| **SMC** | Smooth muscle cell |
| **T** | Friction |
| **TCGA** | The Cancer Genome Atlas |
| **TME** | Tumour microenvironment |
| **TNFa** | Tumor necrosis factor alpha |
| **Tris** | Tris(hydroxymethyl)aminomethane |
| **UW** | University of Wisconsin medium |
| **VEGF** | Vascular endothelial growth factor |
| **WGA** | Wheat germ agglutinin |
| **WST-1** | 2-(4-Iodophenyl)-3-(4-nitrophenyl)-5-(2,4-disulfophenyl)-2H-tetrazolium, monosodium salt |
| **WT1** | Wilm's tumour protein 1 |
| **XTT** | 2,3-Bis-(2-Methoxy-4-Nitro-5-Sulfophenyl)-2*H*-Tetrazolium-5-Carboxanilide |
| **θ** | Constriction slope |
| **μ** | Friction coefficient between the specimen and channel surface |

# viii. List of figures

# Table of Contents

# Chapter 1

# Introduction, Specific Aims and Background

## 1.1 Introduction

In medical practice, clinicians collect tissue specimens from patients to perform tests when they need to screen a tissue for abnormalities and assess their pathologic potential. To preserve cell identifying features, pathologists process tissue samples with fixatives, a process that stops proteolytic degradation, but also kills the cells. Although fixed specimens can be used for clinical examination of a patient's condition, fixed specimens no longer actively respond to external stimuli, limiting their applicability for personalised medicine applications. However, complex diseases, such as cancer, are induced by several driver and passenger mutations, in an environment characterised by thicker and stiffer extracellular matrix, and modified endothelial and stromal cell populations (Hanahan and Weinberg 2011). Analysing the complex interplay between these factors for every patient is not yet possible, with histological analysis only informing treatment according to the stage and molecular profile of the tumour. In this context, outlooks remain poor for most patients, making clear that there is no one drug that fits all those with the same type of cancer (Bedard, Hansen et al. 2013).

To better understand the initiation and progression of diseases researchers use a range of laboratory platforms that mimic systems within the human body. Such models have been successfully used to unravel the mechanisms shaping cell events in health and disease, and to predict the potential benefit of a given medical intervention. Currently, numerous examples of such platforms are commercially available that comprise primary or cell line-derived cells, spheroids, organoids or microtissues together with several stimuli necessary for cell well-being such as extracellular matrix proteins, growth factors and shear stress (Pauli, Hopkins et al. 2017). However, "bottom-up" development of these *in vitro* systems and lack of tissue-relevant structures limit cell responsiveness to environmental cues and the ability to study patient-relevant features. Despite the increasing application of these models in research and drug development, such platforms are considered as poor predictors of how the organism responds to a given agent (Amoedo, Obre et al. 2017, Hoarau-Véchot, Rafii et al. 2018, Don and Huch 2021).

Although complex and expensive *in vitro* models of human tissues are the gold standard for drug assays, they are often insufficiently relevant compared to intact tissue samples, which comprise practically all structural features of the *in vivo* environment. Indeed, live patient tissues are the optimal approach for studying phenotypic characteristics. However, specimen maintenance after isolation remains challenging due to the limited lifetime of *ex vivo* tissue without vascular perfusion to supply nutrients and oxygen. Disconnection from the circulation exposes the tissue to ischemia, disrupting intracellular calcium balance, adenosine triphosphate (ATP) production and reactive species levels, which eventually leads to cell death. Currently, tissue explants are commonly cultured while submerged in culture media, where mass transport

is exclusively restricted to diffusion through the surface of the specimen. Passive diffusion through and consumption of nutrients by serial cell layers limits the delivery of nutrients into the tissue beyond 100 μm (Helmlinger, Yuan et al. 1997), hence poorly meeting cell energy demands. Inadequate nutrient delivery across the tissue results in reduced explant viability, insignificant response to external stimuli and technical limitations in biological assay performance.

The fundamental challenge for most isolated tissue-based platforms is that the induced flow travels around the sample rather than through it. This is due to the significant hydraulic resistance difference between the available routes for perfusion with the explant and the free volume in the fluidic device around the sample. Indeed, most mammal tissues are characterised by significant hydraulic resistance (Levick 1987), rendering most currently available technologies for explant perfusion ineffective.

**The central hypothesis of the current work is that establishment of intra-tissue flow will preserve the viability function of *ex vivo* biopsies and provide an efficient route for delivery of compounds for the evaluation of tissue response.** Knowledge of the effects of ischemia *in vivo* supports the notion that perfusion of *ex vivo* specimens as soon as possible after the isolation will benefit the maintenance of their viability and function. Furthermore, the induced flow through the tissue may also provide an advective route for *ex vivo* delivery of a compound within the explant.

In this thesis, I examined whether a suitably designed channel with a constriction could be used to fluidically load, immobilise and perfuse *ex vivo* thick tissue specimens, using a commercially available syringe pump. Moreover, I explored the effects mediated by the induced flow on cell viability and function of liver and ovarian tumour specimens. To assess whether perfusion-mediated compound delivery influenced tissue response to treatment, I perfused explants with a metabolic poison to evaluate whether a known drug-induced toxic effect can be replicated using this platform.

## 1.2 Background

This section provides a background on how tissues specimens are used in clinical practice, the events that occur within tissue following isolation, and currently available models for laboratory testing using patient cells. Then, the heterogenous nature of human tissues and tumours is discussed to appreciate the necessity for fluidic technologies for *ex vivo* tissue specimens. Finally, the state-of-the-art and the limitations of such platforms are presented to introduce the reader to the need for the work done in the context of this thesis.

### 1.2.1 Patient specimens in clinical practice

Biological samples are routinely collected in clinical practice for various purposes, from basic science and clinical trials to diagnosis and surgery. Diagnostic specimens may be biological fluids (such as blood and blood fractions, urine and saliva) or tissue samples from any region within the human body. Biological fluid samples are primarily collected for preventive health testing and condition monitoring, whereas tissue specimens are only collected after clinical examination or medical imaging has suggested abnormal organ structure, tissue density or cell morphology within an organ. Unlike fluid samples, most tissue biopsies are processed according to the method used for specimen analysis, whilst most solid biological samples are fixed and then embedded in paraffin for further examination.

---

Chemical and physical methods for fixation[1] preserve specimens by preventing autolysis, a process induced by intracellular proteolytic enzymes that results in cell digestion. Chemical fixation (mainly with

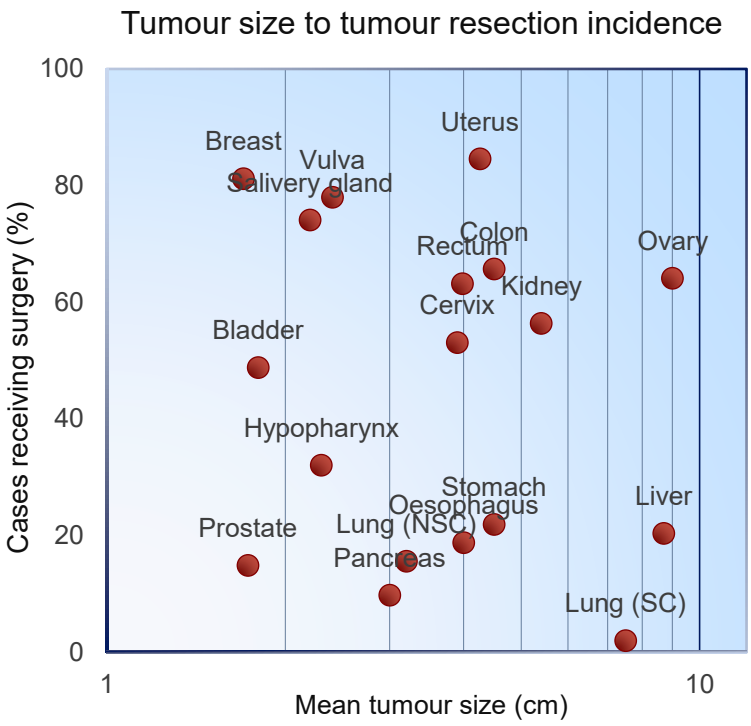


**Figure 1.1** Graph illustrating median tumour size in centimeters to the percentage of those patients receiving surgery to the total number of patients treated for a given type of malignancy. Cancer types: Bladder (Wakai, Utsumi et al. 2016), breast (Bosch, Kessels et al. 2003), cervical (Lambin, Kramar et al. 1998), colon (Kornprat, Pollheimer et al. 2011), hypopharynx (Kim, Lee et al. 2016), kidney (Thompson, Kurta et al. 2009), liver (Zhao, Wu et al. 2016), lung – non-small cell lung cancer (Zhang, Gold et al. 2015), lung – small-cell lung cancer (Gerber, Dahlberg et al. 2013), oesophagus (Zeybek, Erdoğan et al. 2013), oral cavity (Lodder, Teertstra et al. 2011), ovary (Moore, Chung et al. 2004), pancreas (Petermann, Demartines et al. 2013), prostate (Eichelberger, Koch et al. 2005), rectum (Wang, Xu et al. 2020), salivary glands (Seethala, Thompson et al. 2012), stomach (Im, Kim et al. 2012), uterine (Berretta, Patrelli et al. 2014) and vulva (Cırık, Kalyoncu et al. 2014). The percentage of cancer patients receiving tumour resection as part of their therapy is based on data provided by the NHS (UK) for the period 2013-2015.

---

[1]Fixation refers to the process biological samples undergo to be preserved against autolysis and putrefaction. Fixation is often induced chemically and fixed specimens are characterized by increased stability and stiffness.

neutrally buffered formalin/formaldehyde) deactivates such enzymes irreversibly via stabilisation of the tertiary and quaternary protein structure by cross-link formation between the fixative and protein subgroups (Howat and Wilson 2014). This enables the preservation of shape and dimensions, nucleus to cytoplasm size ratio and position within a specimen of each cell, which are key features for histopathological analysis. For this reason, it is crucial that tissue specimens are placed in fixative as soon as possible after isolation until further processing, analysis and treatment decisions are made. As an alternative to chemical fixation, tissue specimens may be cryopreserved after embedment in a water-soluble blend of glycols and resins and freezing with dry ice (~ -78.5˚C) or liquid nitrogen (~ -196˚C). This physical method for tissue fixation is used only when histopathological analysis must take place soon after retrieval, such as in the case of histopathological analysis during surgery. It is worth noting that even in the case of physical fixation, cut sections of a specimen need to be chemically fixed for staining and archiving. Specimen fixation is necessary to permanently stop tissue degeneration and preserve histology. However, stabilisation renders any fixed specimen unable to produce an active biological response to an external stimulus. Indeed, although fixed specimen sections are an invaluable source of information for diagnosis, they are used mainly for patient classification rather than to predict the effect of a medical intervention. Therefore, use of tissue sections in clinical practice is currently limited to cancer type and molecular marker identification. However, it is now evident that the mutational burden, the microbiome and environmental factors influencing protein production result in significant differences in treatment response, even among patients with the same condition (Marusyk, Almendro et al. 2012, Bedard, Hansen et al. 2013, Dagogo-Jack and Shaw 2018). For example, high tumour mutational burden has been associated with a higher response to chemotherapy and checkpoint inhibitors in non-small cell lung cancer (Willis, Fiander et al. 2019), and antibiotic treatment prior to immunotherapy may reduce patient response and survival (Pinato, Howlett et al. 2019). Although standard histological examination cannot account for these parameters that influence cell response to a compound, drug screening with live explant-based systems can inform, personalise and eventually optimise patient treatment. Such platforms that preserve a biological sample viable and facilitate its treatment with a drug to measure changes in selected marker levels are herein referred to as “drug assays”.

The range of applicability of a specimen-based technology depends significantly on the availability of appropriate samples. Especially for tissue samples, the timing, method and purpose of specimen collection by a pathologist greatly influence whether enough material can be provided in sufficient time for use in a functional assay. For example, although biopsy examinations are standard diagnostic procedures, the quantity of material collected is often insufficient for personalised assays. On that basis, such technologies should focus primarily on resected tissue after primary or secondary debulking surgery,

which is usually followed by chemotherapy. In fact, surgical tumour resection is the most used treatment for neoplasms and the most frequent first-line intervention for urological, gynaecological, oral, colorectal, breast and kidney tumours. Resected tumour size ranges from a few millimetres to several centimetres, allowing in some cases (mainly when the resected tissue is more than two centimetres) for enough of the available material to be used with tissue-based platforms after histopathological samples have been secured (Fig. 1.1). A larger number of samples from a tumour allows better recapitulation of tissue spatial heterogeneity and increases the confidence of the observations, both of which are necessary for a clinically-relevant drug assay (Dagogo-Jack and Shaw 2018). In this context, explant-based platforms, including the device presented in this thesis, hold significant potential for treatment personalisation, primarily to inform adjuvant chemotherapy prescription after primary debulking surgery. More specifically, a significant number of patients presents innate resistance to adjuvant chemotherapy administrated after surgery, who cannot be currently identified early as tools for non-responder identification are lacking. Additionally, explants provided after surgical recession of tumours that have recurred or metastasise can be used in tissue-based systems to inform chemotherapy prescription (Hall, Savvatis et al. 2019).

Tissue resected during surgery is the main source of biological material to use in a personalised, live, drug response assay. However, the material collected during surgery typically needs to be processed into isolated cells, tissue fragments or equal sized samples that can be then incorporated in the system used for a given assay. Tissue specimens can be digested into isolated cells using proteolytic enzymes (such as collagenases) or mechanical means. For tissue-based live assays, which are used very rarely and predominantly for scientific research, the original explant needs to be cut into smaller samples using a microtome or fine blades. Such tissue processing methods are extremely laborious and often result in limited *ex vivo* and *in vitro* viability, which constrain the wide applicability of patient-specific diagnostic assays. The viability of explants is rapidly reduced *ex vivo* mainly due to cutting damage, cold and warm ischemia and diffusion-limited mass transport (will be discussed in detail further below). For these reasons, past attempts to use patient specimens to predict drug response have been very limited. Therefore, to update personalised assays, new means for explant preservation *ex vivo* are needed.

### 1.2.2 Ischemia and reperfusion injury

To maintain tissue homeostasis blood must flow within the vasculature with physiologic shear stress, viscosity and flow rate. In the extreme event of temporary or permanent arterial blood flow occlusion (termed “ischemia”) hypoxia, metabolic imbalance and lack of shear initiate a cascade of processes resulting in tissue damage. Similarly, when a tissue specimen is isolated from a patient, ischemic cues begin to compromise biological functions and decrease explant viability (Fig. 1.2). However, as cell survival primarily depends on the severity and duration of ischemia, restoration of flow at the earliest time

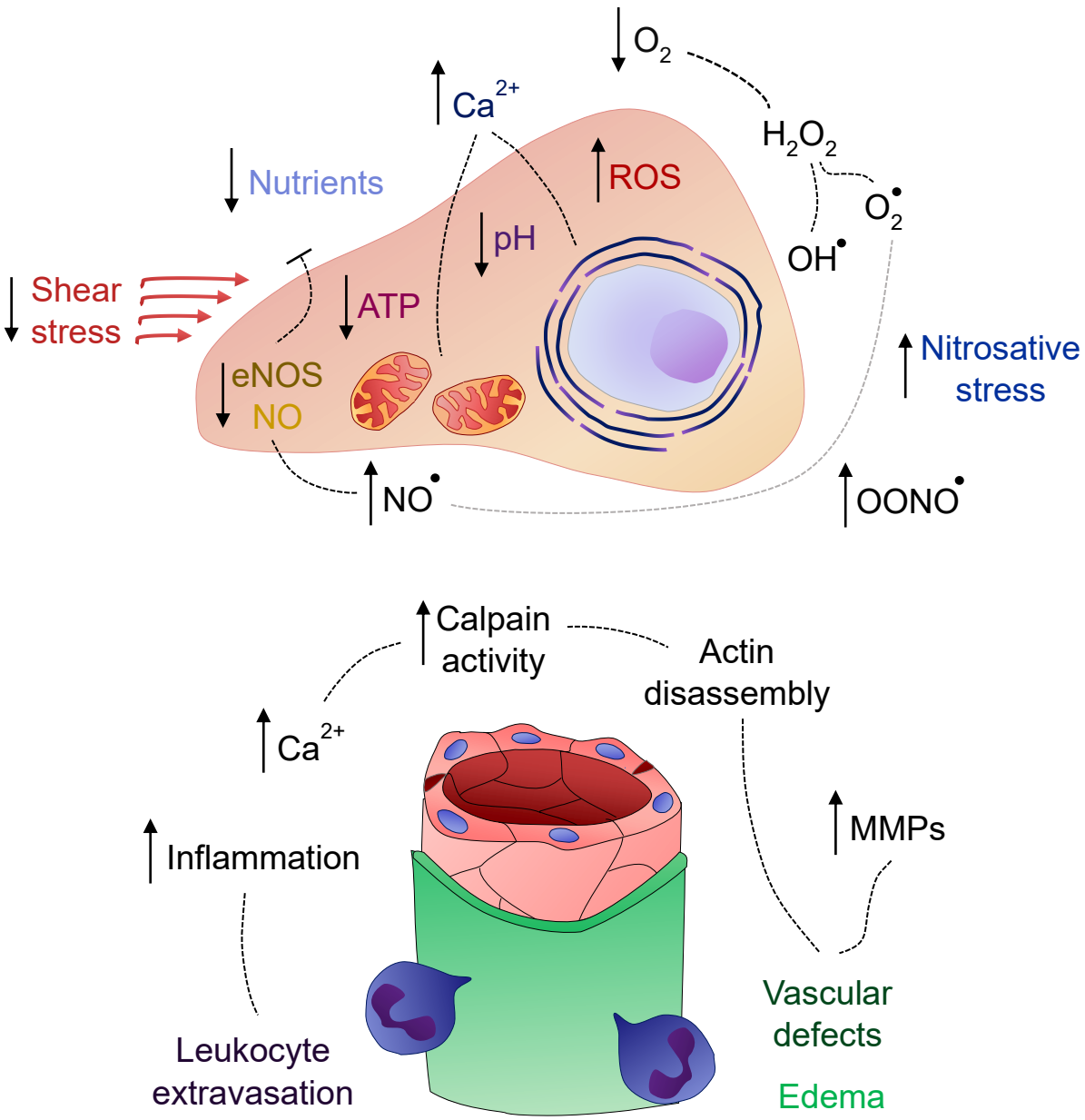


**Figure 1.2** Ischemic effects on endothelial cells (top) and the vasculature (bottom). (Top) Lack of shear stress and rapid reduction in oxygen and nutrient availability result in increased intracellular $Ca^{2+}$ levels, lower pH, decreased ATP and nitrosative and oxidative stress to endothelial cells. Similar events are induced to adjacent parenchymal cells. (Bottom) Proinflammatory stimuli, elevated $Ca^{2+}$ levels and increased metalloproteinases (MMPs) disrupt the endothelium and result to leukocyte extravasation and edema.

possible determines the extent of tissue injury and post-reperfusion dysfunction (Kalogeris, Baines et al. 2012, Wu, Yiang et al. 2018). In the context of this thesis, ischemia and reperfusion injury effects on tissues are discussed to increase understanding of the necessity for a technology that timely facilitates intra-tissue flow in *ex vivo* specimens and the inherent limitations any such system will have.

Although limited periods of ischemia do not result in long-term functional deficits or tissue injury, once ischemia occurs for longer than a critical duration, cell death-leading pathways are activated. This threshold for tolerable ischemia varies significantly by cell type and tissue and is often different among species even for the same organ. Despite increasing understanding of ischemia dynamics, the exact

mechanism whereby reversible ischemia progresses to irreversible cell death remains unclear. Ischemic effects are further exacerbated by “reperfusion injury”, a phenomenon occurring when flow is restored. Although reperfusion is necessary for tissue reoxygenation and nutrient delivery, it tends to further aggravate ischemic effects and tissue damage.

During ischemia, as nutrient and oxygen availability is rapidly reduced, cells switch to anaerobic glycolysis to meet their energy needs. Hypoxia inhibits electron flow via the respiratory chain, which stops ADP phosphorylation and promotes ATP hydrolysis (Cave, Ingwall et al. 2000, Liu, Shoji-Kawata et al. 2013). Anaerobic ATP production increases lactate, proton and NAD+ levels within cells, resulting in the development of an acidic cytosolic environment (De Backer 2003). Enhanced net $Ca^{2+}$ influx and limited uptake by the endoplasmic reticulum (ER) result in calcium accumulation within the cell (Kristián, Katsura et al. 1994, Kristián and Siesjö 1998, Szydlowska and Tymianski 2010). Unphysiologically high cytosolic calcium levels lead to mitochondrial permeability transition pore (MPTP) opening, which further impairs ATP production and results in intracellular accumulation of toxic fatty acids, reactive oxygen species (ROS) production and eventually necrosis (Di Lisa, Canton et al. 2007, Baines 2009, Solaini, Baracca et al. 2010).

In ischemia and reperfusion injury, reactive species produced by various sources within the cell inactivate or damage macromolecules and disrupt chemical balances (such as thiol redox circuits), eventually impairing cell signalling (Granger and Kvietys 2015). Furthermore, oxidative and nitrosative stress decrease nitric oxide (NO) bioavailability and promote the development of a pro-inflammatory environment in absence of pathogens (“sterile inflammation”). Hypoxia and ROS decrease $BH_4$, an important nitric oxide synthase (NOS) cofactor, which induces NOS uncoupling, a phenomenon resulting in increased superoxide anion production (by uncoupled NOS) and lower levels of NO (Kalogeris, Baines et al. 2012, Luo, Lei et al. 2014). As NO is an antiadhesive signalling molecule, lower NO levels also translate to increased adhesion of transient cell populations within tissues, such as leukocytes. This effect is further exacerbated by ROS, which modifies the expression of adhesion molecules on the surface of leukocytes and endothelial cells, with the latter further reducing NO production. In this setting, activated neutrophils infiltrate ischemic tissues and secrete pore-forming molecules, which together with ROS and released hydrolytic enzymes induce extensive damage to parenchymal tissues (Kvietys and Granger 2012, Granger and Kvietys 2015).

Sterile inflammation, an inflammatory response occurring during reperfusion and in absence of pathogens, plays a key role in reperfusion injury. Although this type of inflammation remains poorly understood, it is suggested that antigen presenting cells are activated by alarm antigenic signals (rather than antigens *per se*), eventually triggering the immune response cascade (Matzinger 2002, Land 2005). Gradually,

leukocytes alter their morphology, polarisation and surface receptors so that they eventually transform in a “flattened” phenotype that facilitates extravasation. Through this process, leukocytes adhere to endothelial cells across the microcirculation resulting in arteriolar, capillary, and postcapillary venular dysfunction, an early and characteristic event in reperfusion injury (Eltzschig and Collard 2004, Eltzschig and Eckle 2011). Similarly, neutrophils are recruited in reperfused tissues, primarily in post-capillary venules, whilst mast cells get activated and degranulated, promoting vascular fluid leakage and oedema. In response to inflammatory, hypoxic and low-shear stimuli all major endothelial cell functions are compromised, including vascular permeability regulation, and control of immune cell migration and adhesion (Welbourn, Goldman et al. 1991, Vinten-Johansen 2004).

When perfusion is restored, about 40% of capillaries may fail to reperfuse in what is known as “no-reflow phenomenon” (Niccoli, Burzotta et al. 2009, Schwartz and Kloner 2012). Postischemic capillary no-reflow is not caused by microvessel thrombosis and is mainly associated with neutrophil activation, leukocyte extravasation and physical entrapment of immune cells within capillary lumena (Engler, Schmid-Schönbein et al. 1983, Ge, Zhou et al. 2015). Especially in the case of neutrophils, which are large (8.3 µm mean diameter (Downey, Doherty et al. 1990)), stiff, viscoelastic cells, significant cytoskeletal deformation is required so that they fit through capillaries. Hypoxia and acidosis increase cell stiffness, which results in the entrapment of such large cells within the microvasculature. Intra-capillary immune cell arrest is further promoted by endothelial cell swelling and corresponding capillary lumen narrowing. As oedema increases, the interstitial pressure surrounding blood vessel rises, which together with parenchymal cell swelling eventually result in microvessel collapse (Eltzschig and Eckle 2011, Kalogeris, Baines et al. 2012).

Organs such as the brain, heart, liver and the kidneys present significant oxygen and energy demands, therefore showing limited resistance to oxidative stress and highly susceptibility to ischemic injury (Kalogeris, Baines et al. 2012). In this context, the brain is by far the most sensitive organ to blood supply reductions, with detectable ischemic damage occurring within 20 minutes. This is mainly due to its high oxygen consumption (about 25% of total) and the exclusive use of glucose as an energy substrate. The increased sensitivity of the brain to ischemia is also attributed to limited glycogen storage, lower levels of antioxidants and high polyunsaturated fatty acid content, with the latter being greatly prone to oxidative damage (Oliver, Starke-Reed et al. 1990, Sanderson, Reynolds et al. 2013).

Despite its ability to utilise alternative energy sources and high antioxidant levels, the liver is amongst the most susceptible organs to ischemic injury (St Peter, Imber et al. 2002). Prolonged glycolytic metabolism, hypoxia, calcium net influx and immune cell activation are considered as key mediators of hepatic damage. Moreover, high-mobility group box-1 (HMGB1) nuclear protein leaking from damaged and dying

hepatocytes, mitochondrial permeability transition pore (MTMP) dysfunction and neutrophil and CD4+ immune cell recruitment mediate reperfusion injury in the liver. Interestingly, temperature significantly influences which liver cell population will primarily be injured, with microvessel endothelial cells being damaged during cold ischemia whilst hepatocytes are the ones harmed the most under ischemic, ambient temperature conditions (McKeown, Edwards et al. 1988). Similar rapid ischemic damage dynamics have been reported in heart and kidney tissue (McKeown, Edwards et al. 1988, Yellon and Hausenloy 2007). On the contrary, skeletal muscle demonstrates higher tolerance of short periods of ischemia, mainly due to its ability to remain fully functional under hypoxia using glycolysis. Similarly, tissues with little or no vasculature can withstand long periods of ischemia without substantial loss of viability or function. A characteristic example is the cornea, which is avascular and can be stored in common culture media for more than 20 days with minimal loss of viability (Kalogeris, Baines et al. 2012).

### 1.2.3 *In vivo, ex vivo* and *in vitro* models in therapy personalisation

The limitations in native tissue specimen preservation imposed by ischemia have promoted the use of several *in vitro*, *ex vivo* and xenograft models to study cancer and treatment efficacy (Fig. 1.3). Currently, cell-based platforms are considered powerful tools to evaluate the effect a drug may have. Monolayer cultures of primary cells and/or immortalised cell lines have dominated preclinical evaluation studies for decades, mainly due to their technical simplicity, ease of access and low cost. However, monolayer cultures have significant limitations in mimicking the functions of living tissues (Harunaga and Yamada 2011, Kapałczyńska, Kolenda et al. 2018). *In vitro*, primary cells rapidly dedifferentiate due to poor interaction with adjacent cells and their surroundings (cell-cell and cell-ECM adhesions) and lack of three-dimensional structure formation (Bissell 1981, Schnabel, Marlovits et al. 2002). Although cells from cell

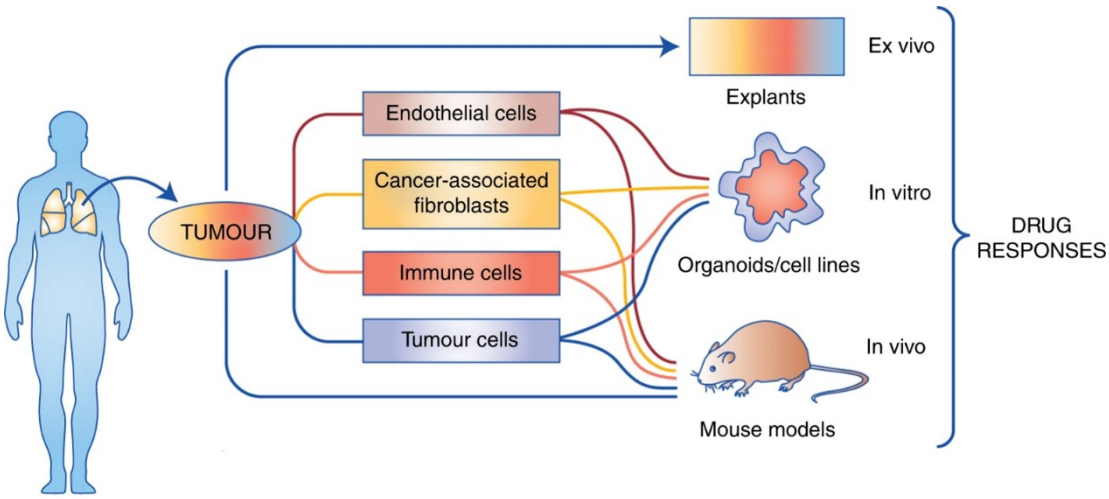


**Figure 1.3** Specimens from a surgically removed tumour explant can be used either directly in technologies based on native tissue specimens and/or *in vivo* (xenografts), or indirectly in cell-based models after digestion of the original sample into a cell suspension (adapted from (Powley, Patel et al. 2020), following the Creative Commons Attribution 4.0 International License (http://creativecommons.org/licenses/by/4.0/).

lines can be cultured in such conditions for several months, the immortalisation process (that cells undergo to proliferate practically infinitely) drastically diminishes the *in vivo* relevance of their behaviour (Geraghty, Capes-Davis et al. 2014). To increase the relevance of culturing conditions, ECM components have been used as an alternative surface for cells to be cultured upon or within (Du, Han et al. 2008, Duval, Grover et al. 2017). Such substances (mainly proteins and glycoproteins) enable cells to establish some of the cell-ECM adhesions they normally develop *in vivo*, which allows them to maintain several functions and features of their cytoskeleton (Geiger, Bershadsky et al. 2001, Cukierman, Pankov et al. 2002).

Three-dimensional cultures based on gels and scaffolds can overcome some of monolayer culture limitations (such as non-*in vivo* relevant matrix stiffness, cytosceletical adaptation in 2D, poor cell-to-cell adhesions) and facilitate *in vivo*-like structure development. ECM protein-based gels with embedded cells have pores of less than five microns so that mass transport is allowed whilst cells remain immobilised (Jen, Wake et al. 1996, Caliari and Burdick 2016). The merit of this type of culturing system is that cells can establish cell-ECM connections in an easily developed and controlled setting. However, embedment limits cell-cell communication and cell proliferation, while difficulty in isolating cells from within the gels constrains their laboratory use (Wu, Zhang et al. 2005). Such limitations are partially overcome in scaffold-based models, which are open-porous structures with suitable pore size and mechanical properties to promote cell residence and proliferation within them (O'Brien, Harley et al. 2005). Scaffolds can be designed to mimic the elasticity and stiffness of the extracellular matrix and have been also successfully applied for skin and neuron regeneration *in vivo* (Compton, Butler et al. 1998, Soller, Tzeranis et al. 2012) and *in vitro* (Karageorgiou and Kaplan 2005, Fischbach, Chen et al. 2007). Most of these constructs are manufactured via lyophilisation, solvent exclusion and rapid prototyping, where innovative 3D printing techniques have enabled manipulation of scaffolds architecture and properties down to the nanoscale (Zhao, Gu et al. 2018, Weisgrab, Ovsianikov et al. 2019).

To further enhance the *in vivo* relevance of cell-based platforms, perfusion has been incorporated to increase nutrient delivery, gas supply and waste removal, whilst recreating several biophysical cues cells experience within tissues. Recent advances in microfabrication and rapid prototyping have enabled the wide use of macro- and microfluidic devices in cell and explant culture (Verpoorte and De Rooij 2003, Ren, Zhou et al. 2013). Perfusion in such platforms partially mimics the effects blood flow mediates on cells *in vivo,* such as shear stress and the turnover of nutrients (Bhatia and Ingber 2014). Moreover, fluidic devices can be easily compartmentalised, enabling the recapitulation of the spatial arrangement of cells within an organ. Organ-on-a-chip approaches have shown promising results for drug response studies, however, their set up remains complex and often case-specific, limiting the use of a given model for a different experiment.

On the contrary, spheroids (spherical constructs formed by cell aggregates) are technically easy to develop and most fabrication methods are effective for several cell types. Indeed, spheroids can be developed using cell suspensions of one or more cell types in suitable wells, bioreactors or through the "hanging drop" method. As an *in vitro* model, they are currently in widespread use in cancer research as they recapitulate several of the diffusion gradients that often occur within tumours (Zanoni, Piccinini et al. 2016). Within spheroids cell-cell interaction is promoted, helping cells to maintain several cytoskeletal features, exhibit higher metabolic rates and remain differentiated for longer periods (Achilli, Meyer et al. 2012). Control of spheroid thickness enables the study of a hypoxic environment and necrotic core formation typically occurring within neoplasms, factors known to influence the potential clinical benefit and delivery of a drug (Mehta, Hsiao et al. 2012). Despite these advantages, spheroids often lack cell-ECM adhesions and acquire an agglomerate conformation with poor relevance to *in vivo* architecture (Benam, Dauth et al. 2015).

Organoids developed from patient cell suspensions in ECM components (such as Matrigel™) are considered as an emerging alternative with significant potential for clinical applications. Patient-derived organoids (PDOs) are developed from isolated patient cells after biopsy digestion and may recapitulate the original tumour characteristics enough to predict response to several treatments (Vlachogiannis, Hedayat et al. 2018, Ooft, Weeber et al. 2019). In a recent example, patient-derived organoids were reported to accurately predict treatment outcome in patients with third or fourth grade, metastatic, heavily pre-treated gastrointestinal cancers. Despite promising results of this application, similar models for other types of healthy or malignant tissue may not be as effective (Huch, Knoblich et al. 2017, Bhaduri, Andrews et al. 2020). The reason for this limitation is that metastatic, pretreated cancer cells in later tumour grades are poorly- or non-differentiated, no longer resembling their non-neoplastic counterparts. Such characteristics limit the applicability of organoids to well-differentiated cell populations present within earlier stage, treatment-naïve tumours, which are sensitive to environmental changes. However, even in absence of this limitation, such models are rarely translatable to the clinics for personalised diagnostics, as their development is laborious, time-consuming and cannot be produced at scale with the currently available technologies (Weeber, Ooft et al. 2017, Powley, Patel et al. 2020).

In the laboratory setting, as 3D models present higher morphological complexity, it is technically challenging to systematically assess their use. Compared to typical monolayer cultures, 3D models remain poorly developed in terms of imaging, assays and automation if compared with typical monolayer cultures. Moreover, the diversity of currently available 3D model characteristics limits the comparability of the output data across developed culture platforms. Notably, complex models are usually developed to study specific phenomena (e.g. drug-induced toxic effects, bacterial infection, atherosclerosis) on a given cell structure

or interface. This renders them more relevant for experimentation within the context they have been developed, while narrowing the width of applications a 3D model could be utilised for. In parallel, although ECM materials and fluid flow have overcome some of the common limitations of 2D and static cultures, these advanced models are still under development and validation. In addition, the benefit for cells and tissues of different origin varies significantly.

Models based on explants processed into thin tissue slices, microtissues or punched-out specimens have been utilised in the development of more biologically relevant and clinically translatable assays. Native tissue specimens comprise most cell types and matrix features forming the tumour microenvironment, which are known to influence treatment efficacy, holding therefore significant potential in platforms recapitulating aspects of *in vivo* tissue function (Powley, Patel et al. 2020) (Fig. 1.4). Also, compatible tissue specimens with such platforms can be easily isolated from a tissue resection or *ex vivo* organ and then incorporated in a culture system, without tissue digestion and/or model expansion that are usually required for cell-based models and xenografts (Byrne, Alférez et al. 2017, Don and Huch 2021). However, tumours are heterogeneous, often comprising necrotic and/or inflamed regions, which may increase the variability between different samples coming from the same tumour (Marusyk, Almendro et al. 2012, Junttila and de Sauvage 2013). The inability to macroscopically identify these regions may compromise specimen integrity while within culture and induces the requirement for a larger number of samples per donor to control for inter-tumour heterogeneity. As most currently available explant-based platforms depend on diffusion-limited mass transport and specimens cut with not widely accessible equipment, the use of such technologies in the clinics remains extremely limited.

As an alternative to different methods of *ex vivo* tissue culture, explants can be transplanted into immunocompromised animals, where tumours can develop vascular connections to the circulation, grow

| | Monolayer | Gels | Scaffolds | Spheroids | Organoids | Microfluidics | Xenografts | Explants |
|---|---|---|---|---|---|---|---|---|
| (+) | Technical simplicity<br>Standarised<br>High-throuput & Imaging friendly | 3D cell configuration<br>Cell-matrix adhesions<br>Diffusion gradients | Manipulation of matrix properties (e.g. pore size)<br>3D cell configuration<br>Cell-matrix adhesions | Co-culture<br>3D cell-constructs<br>Diffusion gradients exploration | Recapitulate aspects of patient response to treatment<br>3D cell configuration<br>Fabrication | Mass transport control<br>Shear stress<br>Compart-mentalisation | TME preservation<br>Recapitulate aspects of patient response to treatment<br>Systemic drug delivery | Comprise most cell-types and aspects of TME<br>No requirement for grow/ expantion<br>Translatability to clinic |
| (-) | Lack of 3D cell conformation<br>No mimicry of matrix materials and stiffness<br>Poor for co-culture | Cell-cell communication<br>Cell isolation | Variability<br>Challenges in scaffold fabrication<br>Cell isolation | Cell-matrix adhesions<br>Matrix stiffness<br>Imaging complications | Expantion timeline<br>Loss of micro-environment<br>Poorly applicable for some tissues | Complex fluidic set ups<br>Cell-cell communication<br>Challenging Perfusate recollection | Model set up timeline<br>Cost<br>Evolutionary differences in toxicity | Variability<br>Tissue opacity<br>Scaling limitations |

**Figure 1.4** Summary of advantages and disadvantages for different types of models using cell suspensions or native tissue specimens for *in vitro* and/or *ex vivo* tissue culture applications, including drug screening.

and metastasise following cancer progression. Similarly, tumour cell suspensions isolated from a patient's tumour can be injected into animals to form xenografts in a technically easier manner (compared to the surgical transplantation required for explants). In either type of xenograft, an incubation time of at least a month is required for the cells or explant to grow and become a part of the animal organism. After this period, animals can be treated with different treatments and provide meaningful insights about how the original tumour would respond to a given compound. Despite the evidence suggesting robust recapitulation of patient response, the number of xenografts needed to inform a given patient's treatment plan raise ethical concerns and involve significant costs that render animal use for clinical purposes unlikely. Also, evolutionary differences between species often complicate the identification of toxicity events, as for example rodents can tolerate higher dosages of chemotherapy than humans (Hoffman 2015, Byrne, Alférez et al. 2017)

### 1.2.4 Tumour heterogeneity

In the past, various diseases were attributed to single-gene mutations and patient differentiation was overlooked. Currently, there is mounting evidence that human diseases are genetically complex (Hanahan and Weinberg 2011, Bedard, Hansen et al. 2013, Berkowitz 2020) and that often there is no one drug fitting all those suffering from the same condition (Spear, Heath-Chiozzi et al. 2001). Despite enormous research efforts in the field of cancer treatment, chemotherapy remains the backbone for neoplasm therapy, irrespective of the limited benefits for most patients (Morgan, Ward et al. 2004, Prigerson, Bao et al. 2015, Miller, Siegel et al. 2016). Notably, a significant number of patients has inherent resistance to first-line chemotherapy (Moulder 2010, Holohan, Van Schaeybroeck et al. 2013, Gu, Zhang et al. 2016, McDonald, Salinas et al. 2019), but early identification and prescription of different treatment for non-responders is not yet possible.

Tumour initiation and progression require several driver mutations to occur so that pro-oncogenic pathways are activated and tumour suppressing mechanisms are silenced. Such mutations are developed due to Darwinian, evolutionary pressure on cells, which also results in the occurrence of several (so called "passenger") mutations with no selective fitness advantage (Marusyk, Almendro et al. 2012, Pon and Marra 2015). The spatiotemporal interplay between driver and passenger mutations results in clinical phenotype heterogeneity even for tumours of the same histological subtype (Navin, Kendall et al. 2011). Indeed, large scale sequencing projects, such as The Cancer Genome Atlas (TCGA) and the International Cancer Genome Consortium (ICGC), have confirmed significant inter- and intra-patient heterogeneity even for tumours with the same driver mutations (Bedard, Hansen et al. 2013, Dagogo-Jack and Shaw 2018). For that reason, although several genes have been recognised as prognostic biomarkers and can be targeted for correction by drugs (such as BRAF in melanoma, EGFR in non-small cell lung cancer,

KRAS in colorectal cancer and HER1 and HER2 in breast cancer), administration of targeted therapy to suitable patients has had limited success (Marquart, Chen et al. 2018). For example, EGFR inhibitors are approved for metastatic colorectal (non KRAS mutated) cancer therapy, but less than 20% of treated patients benefit from treatment (Cunningham, Humblet et al. 2004, Siena, Sartore-Bianchi et al. 2009). Apart from genomic variations in cancer cells, driver and passenger mutation differentiation is based on epidemiological data and tissue sections, where a molecular subtype may be mis- or over-represented (Marusyk, Almendro et al. 2012, Pauli, Hopkins et al. 2017). The standard clinical practice of linking patient condition to a specific genetic type regardless of the dynamically changing nature of tumours may explain suboptimal targeted therapy results.

The non-cellular component of the tissues drastically influences cell behaviour in health and disease. In cancer, the tumour microenvironment (TME) is a key mediator of disease initiation, progression and metastasis because it physically and biologically determines drug delivery and response within tumours (Cox and Erler 2011, Dewhirst and Secomb 2017, Wu and Dai 2017). ECM components and cell-ECM adhesions increase cancer cell tolerance to anticancer therapies, differentiating treatment efficacy among patients with the same malignancy type (Hakanson, Cukierman et al. 2014, Nallanthighal, Heiserman et al. 2019). For example, ECM remodelling due to collagen IV (Col IV) over-production results in drug resistance to cisplatin in ovarian cancer, while expression levels of this gene correlate with tumour grade (Sherman-Baust, Weeraratna et al. 2003). Similarly, several ECM components (e.g. collagen IV, fibronectin, laminin) are known to protect lung cancer cells from apoptotic death due to increased protein tyrosine kinase (PTK) activity (Sethi, Rintoul et al. 1999, RINTOUL and SETHI 2002). ECM remodelling increases cell-ECM adhesions, which induce cancer cell tolerance to chemotherapy in what is phenotypically described as cell adhesion-mediated drug resistance (CAM-DR) (Damiano, Cress et al. 1999, Correia and Bissell 2012). Integrins, which have a key role in CAM-DR, interact with the Arg-Gly-Asp (RGD) binding site found in several ECM proteins and protect cancer cells from the deleterious effects of chemotherapy and radiotherapy by activation of DNA repair mechanisms and pro-survival signalling (Cooper and Giancotti 2019). Cells may also undergo cytoskeletal rearrangements in response to ECM remodelling that induces metabolic changes and enable cancer cells to hijack existing tissue structures to survive nutrient deprivation. Indeed, stiffened matrix has been recently shown to control directly pancreatic cancer metabolism via a mechanosensitive transcriptional target of YAP (Papalazarou, Zhang et al. 2020), an observation suggesting that ECM mechanical properties may actively determine cancer cell fate (Park, Burckhardt et al. 2020).

The quantity of drug that successfully reaches a malignant tissue is influenced by the factors shaping the tissue microenvironment (Dewhirst and Secomb 2017). These include hypoxia, cell plasticity, proteolytic

enzyme expression and cytokine secretion (Lu, Takai et al. 2011, Junttila and de Sauvage 2013, da Silva-Diz, Lorenzo-Sanz et al. 2018), with the complex and dynamic interplay between them controlling tumour remodelling. pH within cancerous tissues is often acidic as glucose uptake by cancer cells is increased even under normoxic conditions (Warburg Effect) (Liberti and Locasale 2016). During hypoxia, intra-tumour acidity is further enhanced as cells switch to anaerobic metabolism. In an acidic environment, pharmaceutical compounds and several ECM molecules become charged and electrostatic interactions between them limit drug delivery to cells (Stylianopoulos, Poh et al. 2010, Manallack, Prankerd et al. 2013). Moreover, low pH obstructs drug penetration deeper than the hydrophobic plasma membrane of cells, leading to compound entrapment within acidic endosomes (Gotink, Broxterman et al. 2011). Poor drug response and immune suppression allow tumour growth and tissue milieu remodelling to proceed.

Transformation of cell environment is not mediated by tumour cells alone. Rather, it is characterised by fibroblast recruitment, matrix modification and vascular remodelling. Cancer associated fibroblast (CAF) plasticity and intra-tumour gradients of environmental factors result in significant stromal and vascular heterogeneity within the TME (Junttila and de Sauvage 2013, Farnsworth, Lackmann et al. 2014, Liu, Zhou et al. 2019). Contrary to what was previously believed, there are several well-differentiated, tissue-specific CAF subpopulations with key roles in almost all stromal processes, such as cytokine, ECM and metalloproteinase production. CAF-controlled matrix degradation releases several growth factors, such as bFGF and VEGF, that are normally trapped within the ECM by various proteoglycans, affecting cell behaviour. These processes progressively replace physiologic microenvironment with a pro-tumourigenic one that is defined by enhanced matrix deposition, higher collagen type IV, fibronectin and laminin content and increased stiffness (Xing, Saidou et al. 2010, Sahai, Astsaturov et al. 2020).

Cancerous tissue vasculature has a characteristic, irregularly branched and disorganised architecture resulting from persistent pro-angiogenic signalling within the TME. Disrupted tight junctions, reduced pericyte coverage and higher permeability (Jain 2005, Farnsworth, Lackmann et al. 2014) are also distinctive features of intra-tumour vessels. Although several chemical factors promote new vessel formation, the developing vascular routes may never completely mature or differentiate to standard size and function vasculature (arterioles, venules and capillaries) (Eberhard, Kahlert et al. 2000). These functional and structural defects lead to increased vascular leakage into and elevated interstitial fluid pressure (IFP) in the surrounding tissue. Moreover, lymphatic system communication with tissue vasculature is impaired at the tumour site and therefore the increasing IFP cannot be equilibrated. Tumour growth also leads to vascular and lymphatic vessel compression, further exacerbating the IFP build up. High IFP levels and unphysiologically thick ECM within the tumour (Netti, Berk et al. 2000, Heldin, Rubin et al. 2004) decrease drug penetration and result in perivascular localisation of therapeutic substances,

despite the increased permeability of tumour vasculature (Stylianopoulos and Jain 2015). Poor nutrient, oxygen and drug delivery together with hypoxia directly contribute in the pro-angiogenic and tumourigenic loop (De Palma, Biziato et al. 2017).

Cancer progression depends on antitumour immune surveillance impairment, which is often mediated by endothelial remodelling. Capillaries and some types of small vessels lack or have lower smooth muscle cell protection than large vessels (such as veins and arteries), and therefore are more exposed to cancerogenic remodelling. As capillaries and small-sized vessels are less protected from such modifications, tumour growth renders them prone to pericyte detachment (Raza, Franklin et al. 2010) and the prime site for angiogenic sprouting. Notably, high microvessel density has been suggested as a prognostic marker for poor outcome in several cancers (Weidner 1995, Hasan, Byers et al. 2002). Moreover, despite high levels of inflammatory cytokines, such as TNFa and IL-1, tumour endothelium is characterised by anergy to such signals and persistent pro-angiogenic signalling-induced downregulation of leukocyte adhesion molecules (such as E-selectin, CD34, intercellular adhesion molecule-1 and vascular cell adhesion molecule-1) (Farnsworth, Lackmann et al. 2014). This effect directly decreases immune cell recruitment and adhesion (Griffioen, Damen et al. 1996), promotes immune evasion of cancer cells and reduces tumour infiltration by T-cells (Dirkx, oude Egbrink et al. 2006, Schaaf, Garg et al. 2018). Immune cell populations and the degree of leukocyte infiltration and localisation within the tumour positively correlate with patient response to chemotherapy (Liu, Hu et al. 2020) and immunotherapy (Thorsson, Gibbs et al. 2018). The latter greatly depends on receptors on the immune cell surface, which greatly influence antitumour function and response to treatment. CTLA4, PD1/PD-L1 and several other T-cell surface markers have been acknowledged as molecular switches for immunosuppression and their blockade has proven to be a successful anticancer clinical strategy (Seidel, Otsuka et al. 2018, Rotte 2019).

Despite angiogenesis having long been considered to be a required process for tumour initiation and growth, it is now evident that cancer may proceed even without pro-angiogenic signalling (Sakariassen, Prestegarden et al. 2006, Lugano, Ramachandran et al. 2019). Alternative routes for tumour perfusion can be established via vascular co-option, a process where cancer cells migrate along and eventually control existing vessels at the tumour site (Kuczynski, Vermeulen et al. 2019, Latacz, Caspani et al. 2019). When tumour growth is enabled along sinusoidal blood vessels, cancer cells may acquire multiple resistance mechanisms to treatments (chemotherapy, immunotherapy and angiogenesis inhibitors) (Frentzas, Simoneau et al. 2016). However, tubular structure formation for tissue perfusion can occur even in absence of endothelial cells. Indeed, tumour cell differentiation into a phenotype that resembles endothelial cells and the development of vessel-like structures of characteristic thickness and lamination

have been observed in several tumours (Lin, Maniotis et al. 2005, Lugano, Ramachandran et al. 2019). Notably, this process that is known as “vasculogenic mimicry” is directly influenced by ECM, as collagens and matrix proteoglycans are necessary for non-endothelial vessel stabilisation within the tumour milieu. More specifically, ECM components may surround the cancer cells forming the vessel or even directly form a globular structure with tumour cells on its periphery (Ge and Luo 2018). As tools to differentiate vessel co-option and vasculogenic mimicry from normal tumour vasculature are insufficient, drug and diagnostic targeting of these factors remains unsuccessful.

### 1.2.5 State-of-the-art models to preserve *ex vivo* tissue specimens

To better understand the limitations of current *ex vivo* flow models, a differentiation is introduced between “perfusion” referring to intra-tissue flow *through* the extracellular space and/or tissue vasculature and “peri-fusion” being used to describe continuous media supply and renewal *around* a tissue specimen, where mass transport remains diffusion-limited.

After isolation, a cascade of degenerating processes rapidly reduces tissue specimen viability and function. To address this issue, several models have been developed and demonstrated to provide prolonged maintenance of tissue discs or slices has been demonstrated (Schumacher, Khong et al. 2007, Rambani, Vukasinovic et al. 2009, Huang, Williams et al. 2012, Ataç, Wagner et al. 2013, Chang, Mikheev et al. 2014, Astolfi, Peant et al. 2016, Holton, Sinatra et al. 2017, Beckwith, Borenstein et al. 2018). In most of these platforms, restoration of intra-tissue flow is claimed as the main cause of maintained tissue viability. However, evidence of advective flow within the specimens used in currently available technologies is lacking. This limits the reliability and reproducibility of such flow models and their translatability to the clinical setting remains poor (Rohr, Binder et al. 2016, McLean, Schwerdtfeger et al. 2018, Morgan, Hanna et al. 2020). Alternatively, intact organs (Sherwood, Reina-Torres et al. 2016, Bral, Gala-Lopez et al. 2017) and small vessels (Bergh, Ekman et al. 2005, Kornuta and Dixon 2014) can be cultured and preserved for a short period of time via cannulation, however it can be hardly used for smaller parenchymal tissue specimens. This is due to the difficulty to cannulate small vessels and capillaries, which are the only vascular routes present within millimetre-thick tissue samples.

Compared to static culture, peri-fused models employ continuous media renewal as the main strategy employed to maintain the tissue viable. Most peri-fused systems comprise a chamber with one or more compartments where the tissue sample is placed, connected to an inlet, an outlet and potentially more routes for exchanging the media interfaced with the sample. For example, one or more fluid flow routes have been used for drug screening applications, where each route carries a drug that is directly interfaced with the device (Chang, Mikheev et al. 2014). In most applications one or two streams of culture media

are incorporated in one device, with the latter case being used for enhanced culture media mixing within the tissue chamber. For several types of tissue, such as the lung, the skin, the brain, the gut, the liver and the retina, an air-liquid interface may also be used to culture a tissue slice (Randall, Turton et al. 2011, Huang, Williams et al. 2012). In either case, specimen culture takes place in standard incubator conditions (37$^{o}$C, 5% $CO_2$).

With respect to tissue type and as a result of continuous progress in fabrication methods, chamber size and architecture, media flowrate and composition, and specimen slicing method have been suggested as the main design parameters for such platforms (Huang, Williams et al. 2012, McLean, Schwerdtfeger et al. 2018). More specificsally, chamber geometry, culture media flowrate and tissue to chamber volume ratio define the turnover time of the culture media around the explant, which is the time period required for the entire volume within the chamber to be renewed. As oxygen and nutrient consumption by the explant rapidly reduces the concentration of such elements in the culture media, minimisation of turnover time can improve tissue slice culture *ex vivo*. Lower turnover time can be achieved by increasing the flowrate and/or decreasing the chamber size, however chamber design is often determined as a compromise between mass transport and empirical considerations that enable easy specimen incorporation in the set up (usually possible for larger chamber dimensions).

Culture media content will not be covered in detail as this is beyond the scope of this thesis and it greatly depends on the kind of tissue used and assay to be performed. Briefly, culture media supplemented with antibiotics, Hank's Balanced Salt Solution (HBSS) or University of Wisconsin (UW) medium for isolation and ice-cold conditions during isolation are evidently necessary for successful peri-fused culture. In peri-fused models, culture media flow rate is considered as the main parameter controlling tissue preservation (Helgason and Miller 2005, Godoy, Hewitt et al. 2013).

Tissue sample size and shape are critical factors for any technology based on primary tissue material, for *ex vivo assays* and biological experimentation. The cutting of explants into identical samples for incorporation into such platforms is considered to be a key. Failure to uniformly process tissues during the preparation stage may produce variable assay results (Kanter, Monshouwer et al. 2002, Bowers, Burns et al. 2014, Abdelaal, Kim et al. 2015). The incorporated sample may be an intact-organ slice (mainly in the case of brain or heart) or smaller size specimens generated by punching out samples from an explant or whole-organ slice. If whole-organ slices are required, the organ is often first embedded in gelling agent, most commonly agarose, to be kept immobile and enable fine slice cutting. Sharp cutting equipment is required as blunt parts compromise several cell layers deep within the tissue.

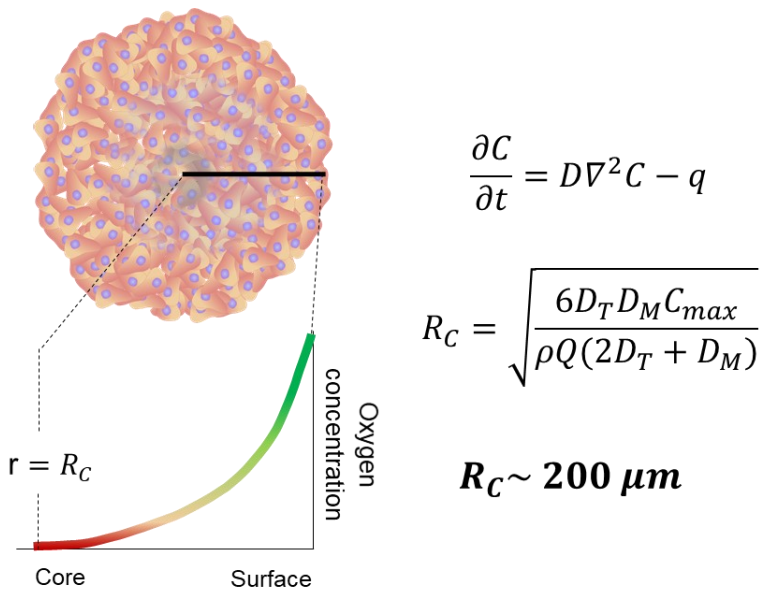


**Figure 1.5** Oxygen concentration gradient within tissue due to diffusion and consumption by cells. $R_c$ is the critical radius beyond which an anoxic core is developed within a tissue sample. Other variables: C is the solute concentration within the tissue, t is time, D is the diffusion constant of the solute and q the solute consumption rate per volume· $D_T$ and $D_M$ are the diffusion constants for oxygen in the tissue and in the media respectively, $C_{max}$ is the maximum concentration of oxygen and is equal to that of the media, ρ is cell density within the tissue and Q is the constant oxygen consumption rate per cell.

Tissue specimen thickness in peri-fused models ranges between 200 to 700 µm, with approximately 400 µm being considered the maximum specimen diameter without anoxia occurring in sample core (Astolfi, Peant et al. 2016) (Fig. 1.5). This is consistent with experimental measurements of oxygen saturation *in vivo*. However, consumption of oxygen by serial cell layers significantly reduces its delivery within tissue, with less than 40% of the original oxygen concentration being available to cells 100 µm from specimen surface (Helmlinger, Yuan et al. 1997). This significant oxygen gradient between specimen surface and sample core is rapidly established and is steeper than what would be anticipated using theoretical models for tissue oxygenation *ex vivo* (Milotti, Stella et al. 2017).

Specimen incorporation in most tissue-based platforms is done either manually or fluidically. In the former (and most frequent setting) the cut sample is placed on a surface that has suitable coating or features (e.g. pores, posts and microneedles) (Huang, Williams et al. 2012) to support efficient specimen immobilisation whilst maximising tissue contact with culture media. However, recently, delivery via fluid flow of cut specimens to the cavities to reside within has been suggested (Astolfi, Peant et al. 2016, Rousset, Monet et al. 2017) as a more high-throughput alternative for sample loading. In either case, most platforms are fabricated with bioinert, transparent or translucent, gas permeable materials, which enable quick equilibration to incubator conditions, direct specimen observation and compatibility with various imaging methods (e.g. fluorescence microscopy, Raman microscopy). Also, device fabrication of such constructs can be fast and economic with polymer processing and microfabrication techniques (Becker and Locascio 2002, Ren, Zhou et al. 2013, McLean, Schwerdtfeger et al. 2018).

### 1.2.6 Limitations of peri-fused tissue culture

Maintenance of tissue viability after isolation is dependent on re-establishment of intra-tissue flow as soon as possible, which cannot be accomplished via peri-fusion. In *ex vivo* peri-fused models, culture media flow occurs around the employed samples whilst they are positioned on a porous surface or within a cavity. In either case media surrounds the specimen and therefore when a pressure gradient is applied the induced flow occurs around the tissue sample rather than through it. Indeed, for a given pressure gradient across a rigid porous solid, the flow occurring through it is linearly dependent on its hydraulic resistance, which is the difficulty experienced by a fluid whilst flowing through a body (Levick 1987). Tissue resistance is, at least, a hundred times higher than that of the fluid channel (Fig. 1.6). This effect is aggravated if the sample is entrapped at channel bottom (Fig. 1.7(A)) or positioned away from the flow profile centre, such as within a cavity that protrudes from the main channel (Fig. 1.7(B),(F)). In another form of peri-fusion model, the tissue plane is perpendicular to the flow profile whilst the whole specimen is interfaced with it (Fig. 1.7(C)). Also, peri-fusion occurs in systems facilitating explant attachment on a plane of microneedles (Fig. 1.7(D) or sample entrapment by posts (Fig. 1.7(E)) under flow. Generally, in peri-fused systems, flow only travels *around* the tissue, where resistance is negligible compared to that within the explant (Fig. 1.7(G)), limiting tissue-media interaction to diffusion via the explant's surface. This method could, in principle, force limited flow only through a thin tissue slice lumen, however media delivery to lumen periphery and the rest of the specimen would remain diffusion restricted, with insignificant benefit for the whole sample.

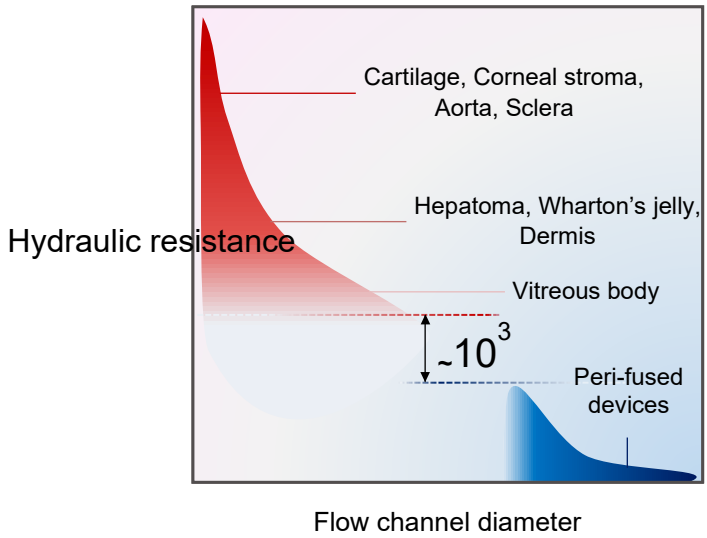


**Figure 1.6** The hydraulic resistance primarily depends on the channel diameter of the route where flow travels through, resulting in a three-orders of magnitude difference between the bibliographically available ranges for the hydraulic resistance of several tissues and that of most channels for peri-fused tissue culutre.

Oxygen requirements vary with tissue type and assay environment (e.g. hypoxic or hyperoxic), however gas delivery to tissue in any peri-fused model is diffusion limited. For this reason, maintaining optimal oxygen and nutrient concentration on the sample's surface greatly influences tissue viability. Indeed, increasing flow rate within the cavity where the specimen is entrapped has been found to improve oxygen and nutrient availability on the tissue interface and enhancing compound concentration within the sample. Although flow travels only around the specimen in peri-fused tissue culture, an optimal flow rate for viability maintenance may be identified (Rambani, Vukasinovic et al. 2009). Likely, this value is the result of the competing effect between the oxygen delivery and mechanical stress on surficial cell layers (Place, Domann et al. 2017). Indeed, a lower flowrate can result in prolonged turnover time, allowing significant oxygen concentration gradients to develop between the flowing liquid and the cells within the explant's surficial layers. On the contrary a higher flowrate of culture media can lead to lower turnover time, which decreases the oxygen concentration gradient established between the tissue and the culture media.

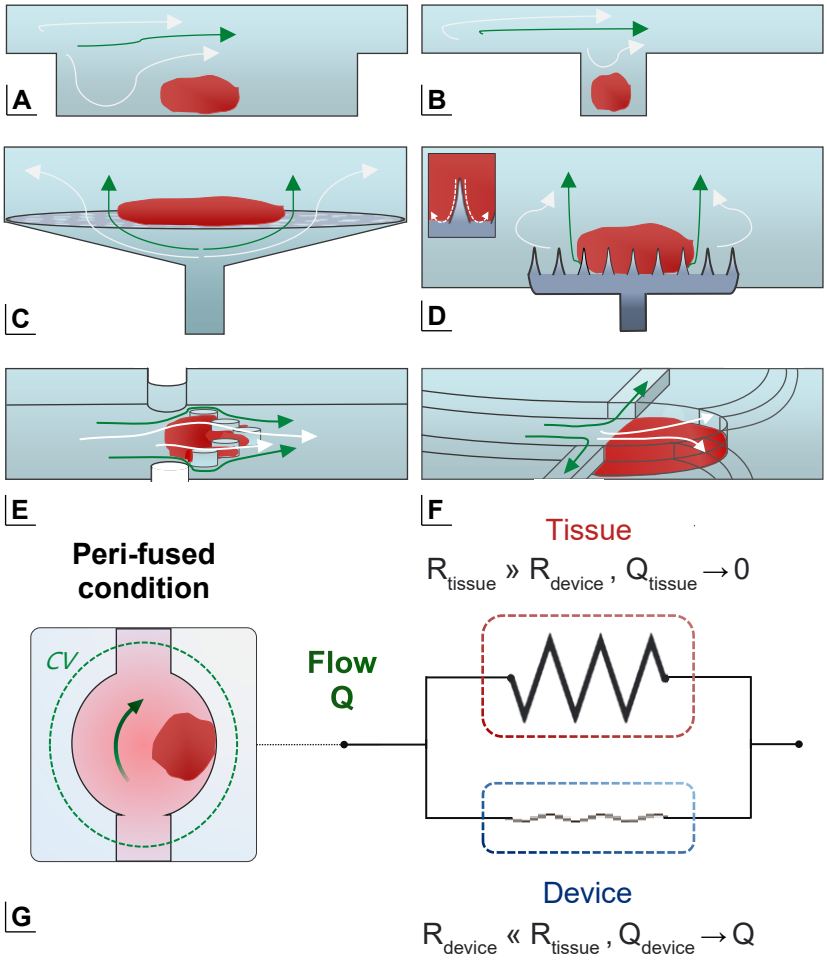


**Figure 1.7** Schematic visualisation of currently available designs for explant culture in presence of fluid flow. A specimen may be cultured at the bottom of a chamber (A), within a protruding cavity (B), on a mesh (C), on microneedles (D) or trapped by posts (e) or within a "pocket" structure (F) - Circuit analog (G) demonstrating the significant hydraulic resistance gradient between the channel and the tissue. Q is the flowrate at the inlet and the outlet of the system, $Q_{tissue}$ is the flowrate of the fluid travelling through the tissue and $Q_{device}$ is the flowrate of the fluid travelling through the channel and around the explant; $R_{tissue}$ is the hydraulic resistance of the explant and $R_{device}$ is the hydraulic resistance of the channel, for fluid flow through the channel and around the explant.

However, increasing the flowrate beyond a threshold defined by the tissue type and the chamber design may result in insignificant benefits for mass transport whilst aggravating the injury a flow jet may induce to the explant.

Irrespective of optimisation of flow conditions, the issue of no re-establishment of intra-tissue flow remains unaddressed in peri-fused models. As ischemia harms energy consuming organs the most, hypoxia and nutrient deprivation rapidly impair cell function in brain, liver, heart, kidney and other sensitive tissue samples *ex vivo* within hours under peri-fused conditions. High oxygen consumption by cells allows enough oxygenation only for the few cell layers near the surface (Shweiki, Neeman et al. 1995, Grimes, Kelly et al. 2014, Place, Domann et al. 2017). Below these layers, oxygen availability is drastically reduced, promoting HIF-1a stabilisation and translocation to the nucleus. There, HIF-1a dimerises with its beta unit, forming a complex that upregulates several angiogenic, proliferating and metabolic genes (Kaelin Jr and Ratcliffe 2008), including lactate dehydrogenase (LDH) (Peek, Levine et al. 2017). LDH converts reversibly pyruvate to lactate, enabling cell energy needs to be covered via glycolysis. GLUT-1, a cell surface receptor controlling glucose uptake is also upregulated to increase glucose internalisation during hypoxia (Chen, Pore et al. 2001, Majmundar, Wong et al. 2010). Glycolysis can support cell energy demand during limited periods of hypoxia, however diffusion-restricted mass transport limits glucose availability within a peri-fused explant. *In vivo*, glucose is delivered via the circulation across the human body, transported into cells by mediated transport with GLUT1 transporters (Bell, Kayano et al. 1990). The interplay of advective and GLUT-1 mediated delivery is sufficient to satisfy cell glucose demand under aerobic and anaerobic conditions, effectively rendering passive diffusion of glucose negligible.

*Ex vivo*, in the absence of advective transport within the tissue, as in the case of static and peri-fused models, glucose is forced to be transported via passive diffusion through explant surface. As cells switch to glycolysis during hypoxia, glucose consumption increases so that cells cover their needs through the less energy-efficient anaerobic cycle. However, as compared to oxygen, glucose diffusion into tissue occurs at less than a tenth of the rate (Androjna, Gatica et al. 2008, Bashkatov, Genina et al. 2009), poorly matching the glycolysis rate, which is about 25 times faster than oxidative phosphorylation (Mookerjee, Gerencser et al. 2017). For these reasons, only a small fraction of explant cells have access to glucose. As a result of starvation, pro-apoptotic, pro-autophagic and pro-necroptotic pathways are activated, rapidly reducing explant viability (Altman and Rathmell 2012, Graham, Tahmasian et al. 2012, Nikoletopoulou, Markaki et al. 2013, Iurlaro, Püschel et al. 2017).

Similarly to static culture of explants, diffusion-restricted oxygen delivery is insufficient to enable reoxygenation and perpetuates hypoxia in peri-fused models. Anaerobic conditions promote acidosis and calcium influx, which impair mitochondrial function and lead to necrosis (Szydlowska and Tymianski 2010,

Kalogeris, Baines et al. 2012). The accumulation of metabolic byproducts and substances leaking from dying cells (such as HMGB1 from injured hepatocytes) establishes an inflammatory milieu that further impairs effective mass transport through the tissue (Boudreault and Grygorczyk 2004, Cauwels, Rogge et al. 2014). In this context, the viability preservation benefit (however limited that might be) observed in peri-fused *versus* static cultures may be the result of tissue oxygenation post-ischemia. More specifically, in the peri-fused case, oxygen concentration and waste removal close to tissue surface are constantly maximal, whilst media quality in static cultures reduces rapidly until it is renewed. However, as the ischemic cues persist, necrotic mechanisms are activated, resulting in rapid loss of viability from specimen core towards the outer layers in peri-fused culture models.

### 1.2.7 Challenges in tissue-based system characterisation

Specimen preservation after the tissue has been isolated from the human body is the main challenge for tissue-based platforms when an active biological response is to be assayed. Viability maintenance is the starting point to characterise the efficacy of an *ex vivo* tissue culture model, however reliably identifying and quantifying viable cells within thick biological samples is challenging (Breeuwer and Abee 2000, Ramirez, Antczak et al. 2010, Piccinini, Tesei et al. 2017, Idrees, Chiono et al. 2018). Limitations in viability measurements scale with specimen thickness and are mainly caused by diffusion-limited reagent transport and imaging difficulties deep into tissue (Griffith, Miller et al. 2005, Richardson and Lichtman 2015). Additionally, current protocols for specimen cutting limit the applicability of tissue-based assays in a high-throughput context, which further limits their use in academic, industrial and clinical settings.

Cell viability maintenance is necessary for any live tissue platform, however how it is quantified varies with specimen size and technological setting. Fluorescent and luminescent dyes indicating live and dead cells are the gold standard for viability assessment in monolayer and 3D cell cultures. Depending on the dye type, the signal may be measured spectrometrically in the supernatant or directly within cells using microscopy. In live-cell imaging applications, a substrate diffuses into cells and is converted to a fluorescent product when activated by light. Similarly, for assays where the signal is measured in culture media, a substance either diffuses into cells to be converted to a fluorescent product and then diffuses back into the bulk fluid, or a protein leaking from dying cells reacts with a substrate in the media. In either case, diffusion of the assay reagent into, or dying cell protein out of, the explant is needed for a meaningful measurement in tissue samples. In monolayer cultures diffusion through cell membrane is the rate limiting step for detecting a signal. However, thick biological samples comprise several cell layers closely packed upon each other, increasing the difficulty for assay reagent to reach all cells within a specimen. Indeed, diffusion through tissue samples is slow and reagents often do not reach the explant core following standard protocol incubation (<2 hours). As such, there is essentially no meaningful signal from within the

sample (Sekine, Haraguchi et al. 2011, Zanoni, Piccinini et al. 2016, Leary, Rhee et al. 2018). Even when a dye molecule is small enough to diffuse within thick specimens in the incubating period, means for fast, high-resolution imaging through the entire specimen remain limited.

Standard Histopathology (SH) is an alternative approach to real-time and endpoint viability and/or cytotoxicity measurements that enables visualisation of molecular and structural features within cells and tissues. In most SH applications, frozen or paraffin-embedded tissue sections are stained either using antibodies (i.e. a primary antibody is used for target detection and a secondary antibody to visualise the primary) or stains probing distinct cell components, such as lipid droplets (stained with Oil Red O) or positively charged structures (stained with Eosin, which is negatively charged). SH presents significant advantages, enabling the extraction of spatial information from a specimen and allowing multiplexed detection of several markers on the same sample if using immunofluorescence. However, despite recent advancements in microscopy and tissue processing, section thickness of no more than 50 μm and more often of about 10 μm is recommended for cell labelling and tissue visualisation, which can limit the relevance of the information provided from a single section of a millimetre- or centimetre-thick sample. Additionally, sectioning requires trained personnel and tissue staining is laborious, both of which may limit the applicability of SH for large numbers of samples (Slaoui and Fiette 2011, Musumeci 2014).

3D microscopy is possible by spatial reconstruction of images from serial tissue sections, however this has proven to be challenging due to cutting artifacts, section detachment and time-consuming imaging procedures. An alternative is the “blockface approach”, where imaging is done on the surface of a mounted specimen as sections are sequentially shaved off (Denk and Horstmann 2004, Ragan, Kadiri et al. 2012). With this technique, alignment and serial sectioning are guaranteed. However, expensive equipment and complex sample preparation, acquisition settings and image analysis are required (Wanner, Kirschmann et al. 2015). Section recollection is also often problematic, limiting further use of sections from specific regions of interest, which is a standard process in histology. Non-sectioning approaches allow whole specimen volumetric imaging while also keeping the sample structurally intact for other assays or archiving purposes. However, when a region is excited by light, the recollected signal is generated by all the serial layers reached by it, regardless of where the focus plane is, in what is known as “out-of-focus blur”.

This obstacle in volumetric imaging has been partially overcome by the development of confocal microscopy (Minsky 1988), where a pinhole is used to block light from areas below or above the focus plane from reaching the detector. Despite achieving “optical sectioning” using this imaging modality, difficulties in deep-tissue imaging persist. Inherent optical properties of tissues limit light penetration and reduce signal-to-noise ratio when imaging thick specimens in 3D. For example, pigmentation, auto-

fluorescent tissue molecules and inhomogeneity-induced light scattering decrease imaging depth and quality (Monici 2005, Jun, Kim et al. 2017). More specifically, melatonin, hemoglobin and myoglobin are the main tissue chromophores in tissues, significantly absorbing light in the optical range (Tainaka, Kubota et al. 2014). However, the prime reason for tissue opacity is the lateral light scattering induced by heterogeneously distributed biological molecules and structures within tissues. Water, minerals, lipids, proteins, organelles and a few cell types (e.g. erythrocytes) exhibit significant differences in refractive index and dimensions, resulting in light transmittance perpendicularly to the beam direction, limiting light penetration into the tissue (Mourant, Freyer et al. 1998, Kienle and Hibst 2006, Susaki and Ueda 2016).

## 1.3 Engineering a perfused tissue model

Tissue explants collected from patients represent an invaluable source of material to study disease phenotypes and inform clinical decisions. However, cell morphology and tissue function are greatly altered when biological samples are removed from their original environment and acclimatised to the laboratory setting. This drastic transition compromises biological sample viability and differentiation, despite the numerous advances in *ex vivo* models. Among the several limitations of currently developed models have, diffusion-restricted mass transport is the main one responsible for the degeneration of explants soon after the isolation (Place, Domann et al. 2017, Rodenhizer, Dean et al. 2018). Despite culture media flow has been incorporated to several platforms, high hydraulic resistance of tissues renders them perfused, whilst the specimens are only peri-fused. To overcome this issue, a culturing system that supports resected tissue perfusion is needed. In this context, the term “perfusion” refers to flow of nutrient media *through* the extracellular and/or interstitial space, and possibly pre-existing vascular routes inside the sample. By introducing advective solute transport, perfusion can more effectively provide for cell nutrient and oxygen demands, clear metabolic waste and enable delivery of testing pharmaceutics inside the specimen than presently available *ex vivo* flow models. Therefore, a perfused biopsy-based model could facilitate robust, easily performed and personalised drug testing, with the aim of improving patient therapy and treatment outcome.

### 1.3.1 Motivation of thesis

*In vivo*, hypoxia, nutrient deprivation and lack of advection induce metabolic and functional changes in cells and result in chemical and mechanical imbalance within tissues, leading to cell death and irreversible tissue injury. Such processes mediate the ischemic effects after a tissue is isolated from the human body or when blood flow through a tissue or organ has been stopped. Despite ischemia remaining inconclusively understood and poorly treated in the clinic, reperfusion as soon as possible remains the crucial step for minimal damage to the tissue of interest (Kalogeris, Baines et al. 2012). However, intra-

tissue flow has not been incorporated evidently in currently available technologies for explant maintenance. Most *ex vivo* platforms facilitate culture media flow around the specimen, with nutrient and oxygen delivery within the tissue remaining diffusion-limited. This may be the main reason for their poor performance in specimen preservation and limited use in standard clinical oncology. The central hypothesis of this thesis focuses on the idea that re-initiation of perfusion in *ex vivo* specimens can preserve tissue viability and function for longer than currently possible in static and peri-fused systems. Based on evidence from the *in vivo* setting, re-establishment of flow within the explant should increase the availability of glucose and oxygen via advection, providing for the energy demands of cells close to the perfused routes. This would allow cells to resume aerobic metabolism, decrease reactive species formation and improve metabolic product washout within the explant. Advective mass transport within the specimen can also enable the direct delivery of xenobiotics, such as pharmaceutical compounds, to assess the effects they may have on cells. A validated perfused tissue model for drug response prediction would be a powerful tool for treatment personalisation, as it would enable for the first time the direct use of routinely collected patient tissue in a live drug assay.

### 1.3.2 Specific aims

**Specific aim 1:** To design and fabricate a device for *ex vivo* native tissue sample perfusion.

Available technologies allow fluid flow *around* the specimen, which renders any mass transport occurring *through* the tissue negligible. Therefore, a device with a suitable constriction that surrounds the specimen was designed, as an alternative setting to induce fluid flow through *ex vivo* tissue samples. 3D printed molds were utilised for polymer fabrication of polydimethylsiloxane (PDMS) layers with desired conformation that were then bonded to each other using plasma treatment. Liver tissues from wild-type (C57BL/6J) mice were cut into 3 mm-thick specimens and were used to characterise platform efficacy to entrap parenchymal tissue specimens and to demonstrate that induced flow does not travel through the device-tissue interface. *This specific aim is addressed in Chapter 2.*

**Specific aim 2:** To demonstrate that the developed device and method for *ex vivo* explant perfusion can induce intra-tissue flow and identify the routes of perfusion through the specimen.

Peri-fusion result to negligible advection through *ex vivo* tissue specimens. Therefore, liver tissues from wild-type (C57BL/6) mice and transgenic mice with GFP-tagged Tie2 expression (Tie2-GFPtg) were used to explore the efficacy of the developed device and method to provide intra-tissue flow and examine through what routes perfusion occurs. Tissue sample morphology was examined after culture under perfused, static and peri-fused conditions. Also, specimens were perfused with a fluorescent lectin (WGA),

fluorescent tracers and gold nanoparticles to quantify and visualise intra-tissue flow in 2D and 3D. *This specific aim is addressed in Chapter 3.*

**Specific aim 3:** To study the effects the induced flow has on *ex vivo* specimen viability and function.

Isolated tissue samples are typically ischemic until intra-tissue flow is re-established. To demonstrate perfusion's benefit for tissue preservation, wild-type (C57BL/6) mouse liver specimen viability was assessed by measuring intracellular proteases, lactate dehydrogenase and ATP in specimen lysate after a 48-hour perfusion. Dying cells were also identified on specimen cryosections with cleaved-caspase 3 immunolabelling. Also, maintenance of tumour specimens was assessed using specimens from an ID8 mouse model of ovarian cancer and immunostaining for cleaved-caspase 3, Wilm's Tumour protein 1 (WT1) and Ki67. Ability of liver specimens to respond to a 2h-treatment with a metabolic poison was assessed with ATP quantifications and Periodic-Acid-Schiff's and Oil Red O staining. *This specific aim is addressed in Chapter 4.*

Each chapter was written so that it is self-contained and independent from the rest of the chapters that are comprised in this dissertation. Also, the experimental evidence provided for each experiment were generated from an independent set of tissue specimens and subjects, as described in the corresponding method sections.

# Chapter 2

# Design and Methods

## 2.1 Introduction

### 2.1.1 Intra-tissue flow

Tissues require vascular perfusion to maintain homeostasis. Cessation of blood and interstitial fluid renewal within tissues can be tolerated only for very limited periods, as processes deteriorating cell chemical equilibria, tissue structures and organ viability rapidly progress. Indeed, restoration of intra-tissue flow is critical for graft function and survival of transplants, despite suboptimal means to re-establish flow (Ardehali, Esmailian et al. 2015, Cypel, Neyrinck et al. 2019, Pinezich and Vunjak-Novakovic 2019) and the complex injurious effect re-perfusion can independently induce (see 1.2.2) (Eltzschig and Collard 2004, Eltzschig and Eckle 2011). Although perfusion restoration for *ex vivo* whole organs is an increasingly applicable technology for transplantations in the clinic (Ardehali, Esmailian et al. 2015, Bral, Gala-Lopez et al. 2017), technologies for perfusion of native tissue specimens collected during surgery or biopsy examination remain underdeveloped.

*In vivo*, heart pulses generate the pressure necessary to deliver blood flow to the rest of the body (Opie 2004). Blood flow is also regulated via the compliance of large arteries, which expand during diastole and contract during systole to provide more stable flow between pulses (Yamaguchi and Garceau 1980, O'Leary 1991, Dinenno, Jones et al. 1999). Local distribution of blood in arteries and arterioles is regulated by resistances to flow, induced by the contraction and/or relaxation of smooth muscle cells (SMCs). Vasomotion, the synchronic oscillation of SMC tension in response to intracellular $Ca^{2+}$ levels, directly controls vascular resistance and capillary perfusion independently of the heart.(Aalkjaer and Nilsson 2005, Davis, Hill et al. 2008). Despite these mechanisms controlling blood flow, tissue reperfusion (after an ischemic event or a transplant), can fail to re-establish fluid flow through capillaries, with irreversible damage caused on the affected organs. Although the exact reasons for this phenomenon remain poorly understood (and are not linked to vessel blockage by clots for instance), the interplay of surface tension, cell extravasation and high capillary hydraulic resistance is highlighted as a key regulator for it (Engler, Schmid-Schönbein et al. 1983, Eltzschig and Collard 2004, Ge, Zhou et al. 2015).

Immediately after tissue resection from an organ nutrient and oxygen availability is compromised, whilst intercellular proteases leaking from damaged cells aggravate stress experienced by their adjacent counterparts. These effects are suppressed during standard cold storage of explants, as lowered metabolic rates prolong cell survival under ischemic conditions. However, cold storage itself can increase sodium and chloride influx, resulting in disrupted intracellular calcium levels, cell swelling and apoptosis (Rauen and de Groot 2004), particularly in sinusoidal endothelial cells (McKeown, Edwards et al. 1988, Bilzer and Gerbes 2000). Hypothermia and absence of perfusion within a tissue rapidly establish an

ischemic milieu that progressively impairs cell functions and eventually tissue viability, rendering re-establishment of intra-tissue flow necessary. Nevertheless, restoration of perfusion in explanted tissue specimens has been poorly addressed at present, due to the limited technologies for inducing intra-tissue flow and limited understanding of ischemia and reperfusion injury dynamics.

### 2.1.2 Moving beyond peri-fusion

The high hydraulic resistance of narrow-lumen capillary networks and ECM gaps shapes the design criteria for the development of a technology, where minimally processed native tissue specimens can be perfused *ex vivo*. In standard approaches, a channel "must be sufficiently large to prevent (…) clogging by tumor samples" (Beckwith, Borenstein et al. 2018), allowing flow to travel around the specimen. The several-orders-of-magnitude gradient between the hydraulic resistance of the explant and that of the channel results in absence of flow within the tissue specimen. Notably, this is the case in any setting where flow can travel through any route with a hydraulic resistance that is significantly lower than that of the explant. Limited publications directly address the restoration of advection in explants and allegedly achieve some level of intra-tissue flow. However, in these publications, no direct evidence of intra-tissue flow is provided, and the mechanisms used would not be expected to generate fluid flow through a native tissue specimen (Parrish, Gandolfi et al. 1995, Kanter, Monshouwer et al. 2002, Schumacher, Khong et al. 2007, Rambani, Vukasinovic et al. 2009, Huang, Williams et al. 2012, Chang, Mikheev et al. 2014, Gerpe, van Vloten et al. 2018).

Several platforms have been developed that interface an explant with culture media under flow, but the flow acts only as a means to continuously renew the fluid close to the tissue. Such technologies improve tissue residence, as nutrient and oxygen gradients, and metabolic waste accumulation are ameliorated by constant volume turnover. However, the tissue culture platforms where fluid flow travels around the specimen - referred to as *peri-fused* cultures in the context of this thesis - can only benefit the few cell layers within a maximum of 200 µm from sample surface, as diffusion rapidly limits mass transport deep into the tissue (Grimes, Kelly et al. 2014, Milotti, Stella et al. 2017, Place, Domann et al. 2017). For these reasons, most currently available models depend on thin slices of tissue, which poorly recapitulate tissue heterogeneity, and require sophisticated cutting equipment and complicated set-ups (Powley, Patel et al. 2020). For these reasons, development of peri-fused systems has been limited and there has been little incorporation into standard clinical practice and pre-clinical assessment.

To move beyond from peri-fusion, where only cells close to specimen surface might benefit from media turnover, fluid flow must be re-established *within* the tissue. *In vivo*, where the vasculature remains intact and functional, restoration of advective transport depends mainly on normal cardiac function and absence

of clots. *Ex vivo*, tissue explantation compromises several vascular routes in specimen periphery, whilst entrapped blood within the explant rapidly coagulates. These peculiarities of the *ex vivo* setting complicate the process and means required to perfuse a native tissue specimen post-resection. Canulation, which is often employed in the perfusion of whole organs, cannot be meaningfully applied in this context due to the significantly small dimensions of the perfusable routes within the explant. For this reason, a novel design for a device where tissue specimens can be loaded, immobilised and perfused is required to re-establish *flow through* in live explant assays.

The device presented herein utilised specimen compression within a constriction with a slope to facilitate specimen entrapment and block peri-fusion, so that the externally induced flow (using a syringe pump) was forced to travel *through* the tissue. However, various tissue properties and explant parameters (such as which areas of the specimen expose vascular routes) that can influence perfusion efficacy of *ex vivo* tissue samples cannot be controlled experimentally. More specifically, dimensions of vascular routes greatly vary within organs, resulting in variability in specimen permeability, which cannot be known in advance. Moreover, even if prior mapping of the vascular route size range within an explant was possible, specimen positioning inside a channel so that perfusion was promoted would be impossible without cannulation. On another aspect, several organs and diseased tissues (such as tumours) are characterised by significant spatial variations in mechanical properties (such as stiffness) (Handorf, Zhou et al. 2015, Guimarães, Gasperini et al. 2020), which is impossible to reproducibly account for experimentally.

On this basis, device development was focused on factors that could be experimentally explored and manipulated, such as the dimensions of the stenotic channel, the constriction design and the specimen size. The main objective in the trial-and-error approach that was followed was to first achieve specimen entrapment, block peri-fusion and then study perfusion's efficacy and its effects on tissues (explored in Chapter 4). Shear stress is known to determine key aspects of cell function and influence mechanotransduction, especially in endothelial cell types. The mechanobiological effects of fluid flow on epithelial cells remain understudied, however several functional aspects of the epithelium have been shown to be regulated by shear (Tanaka, Yamato et al. 2006, Steward Jr, Tambe et al. 2015). Since methods to directly measure the flow and/or the pressure experienced by the cells within a perfused explant are lacking, advection's impact on cell mechanotransduction was not explored.

## 2.2 System design

### 2.2.1 Channel for specimen perfusion

To overcome the limitations of the peri-fused culture conditions, we hypothesised that directing a native tissue specimen in a channel with a suitably designed constriction could induce intra-tissue flow through

native parenchymal tissue specimens. As such specimens are characterised by low stiffness (~3-10 kPa) (Handorf, Zhou et al. 2015, Guimarães, Gasperini et al. 2020), the identification of an effective channel design for tissue specimen immobilisation and perfusion depends on the interplay between tissue properties and device features. Mechanical properties of tissues have been increasingly investigated using atomic force microscopy (AFM) and systems designed to study compressive deformation of biological samples. The evidence originated with these methods have informed a plethora of theoretical and empirical models connecting tissue compression, friction and perfusion. However, most of these measurements and models are based on unconfined specimens or one-directional tissue confinement, which greatly limit the translatability of such findings and approaches to a channel-based platform. Moreover, the applicability of standard approaches for the development of a prototype is further complicated by inter-specimen heterogeneity and stochastic positioning within channel constriction.

In an attempt to directly inform the design process by case-specific evidence, a trial-and-error empirical process was followed, providing a promising system. The key parameters determining channel design and effectiveness are briefly described below.

Constriction geometry is a key parameter for a channel, where specimens are entrapped within, while fluid flow around them is obstructed. Cross-sectional area reduction is the primary mean to immobilise a tissue specimen, as the tighter the constriction the higher the compressive force acting on the specimen, thus increasing the friction (and the corresponding effective[1] friction coefficient μ) at the interface between the tissue and the device. However, specimen compression results in increased tissue density and eventually to reduced tissue permeability due to collapse of perfusable routes. In this thesis, changes in permeability of uncollapsed routes were not considered and collapse of perfusable routes was only examined at the level of cytotoxicity (cleaved-caspase 3 signal), necrosis (areas of nonnucleated cells) and absence of intra-tissue flow signal during perfusion visualisation. Therefore, successful constriction design requires the selection of a suitable original to minimum cross-sectional area ratio (A/B) (Fig. 2.1(A)) that results in specimen immobilisation for at least 48 hours whilst enabling perfusion. The induced perfusion

Constriction length is another parameter that directly influences specimen entrapment and perfusion within the channel. For a given cross-sectional area gradient, constriction length determines the angle at which channel stenosis is formed (θ), therefore influencing the efficacy of tissue entrapment (Fig. 2.1(B)). Lower θ values lead to reduced specimen support from channel surface and lower friction at the tissue-

[1] Effective friction coefficient refers to the friction coefficient after correcting for the level of specimen deformation as a result of specimen compression.

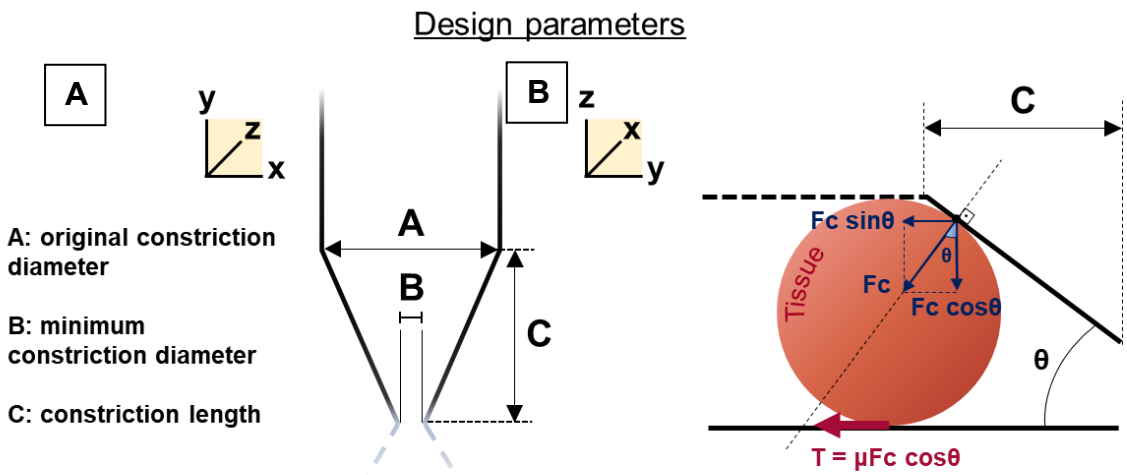


**Figure 2.1** Design considerations for channel design (A) Design parameters influencing tissue positioning, immobilisation and perfusion within the constriction region (B) Force balance on a specimen reaching the stenosis, where $F_C$ is the compressive force acting on the specimen from the inclined channel surface, T is friction, μ is the effective friction coefficient between the specimen and channel surface and θ is the angle of the constriction slope.

channel interface, resulting in poorer immobilisation. On the contrary, for increasing θ values, both specimen support from channel wall and friction between the tissue sample and channel surface are enhanced, resulting in increasingly effective immobilisation.

In summary, in order to induce flow through a native tissue specimen, a channel design based on a constriction, which an explant can seal within, was developed. The constriction design was defined by the compromise between two competing effects:

1. the need for narrowing channel diameter so that the specimen is entrapped whilst sealing channel's lumen and
2. the necessity for stenosis diameter to be wide enough so that tissue compression does not force the perfusable intra-tissue routes to collapse.

### 2.2.2 Material considerations

The development of a device that can facilitate tissue loading, immobilisation and perfusion within a confined space depends (apart from geometric considerations) on the properties of the material employed for prototype microfabrication. The interplay between the tissue specimen and its surroundings and the necessity for the development of an assay-friendly system are key elements in material selection for this device. On this basis, in the constriction-based design described in the previous section, tissue entrapment within and sealing of the stenosis result in the formation of a tissue-channel interface, where there is absence of a direct culture media supply. This interface may expose the tissue to compressive injury and material-induced toxicity due to prolonged contact of the specimen with the device wall. This tissue-channel interaction introduces the requirement for using a material that is bioinert (does not initiate

a response or induce an effect when introduced to a biological tissue) and gas-permeable. Moreover, tissue culture *ex vivo* depends on the presence of a human body mimicking pH, temperature and solute environment in the media used to provide nutrients and oxygen to the specimen. For these reasons, standard cell and/or tissue culture takes place within $CO_2$ incubators, at 37ºC and 5% $CO_2$ atmosphere. As such, the material used should have sufficient tolerance to a high humidity environment whilst solute absorption remains negligible. Also, the material should be compatible with standard physical and chemical sterilisation methods, such as autoclavation and cleaning with ethanol, respectively.

Several other considerations are important to launch a practical and low-cost technology. The optical, physicochemical and surface properties of the material used can play a major role in the applicability of the system within standard operating procedures in a clinical setting and multiplex assays commonly run in a lab. A prototype-friendly material should be low-cost, provide micrometre-scale resolution structures with relatively simple processing and be compatible with surface treatment methods to create fluidically-sealed, multi-layer structures. Also, optical access during early incorporation of the specimen into the device and throughout perfusion is required for effective tissue handling, positioning and system set up. Apart from tissue monitoring, a material that provides superior imaging accessibility during microscopy applications is highly preferred.

### 2.2.3 Flow-driving system

To drive flow through a porous body, a pressure gradient is required to be established across it. Apart from cannulation-based approaches, to successfully establish such a pressure difference across a native tissue specimen, fluid must only travel through the sample (see 1.2.5 and 1.2.6). To assure this, any flow around the sample, particularly through the interface between the specimen and the holding equipment must be blocked by a sufficiently tight seal. Once this has been achieved, a system connected to the inlet and/or the outlet of a device will induce fluid flow through a pressure-driven or flow-controlled mechanism.

Pressure-driven systems typically externally apply a manometric height difference to either the inlet or the outlet of a perfused channel, with the outlet or inlet respectively being open to atmosphere. Such systems benefit from lower response times than flow-based systems (BÁRÁNY 1964, Madekurozwa 2019) and allow direct control of the pressure gradient experienced by the biological specimen employed, which shall be maintained to *in vivo*-relevant levels. However, pressure build up within tissue compartments can be significant, reaching 60 mmHg or more within some tumours (Boucher, Baxter et al. 1990, Heldin, Rubin et al. 2004). This translates to ~82 $cmH_2O$, which often requires complicated set ups since such manometric heights are impractical to implement in a clinical setting. This limitation can be partially overcome by a stream of compressed air or vacuum connected to the fluidic channel as an alternative.

However, such pressure sources are not applicable for systems where several channels need to be perfused simultaneously, each at the same flowrate.

Flow-controlled systems (such as positive displacement pumps) can directly control the flowrate through a specimen. For this reason, simpler perfusion systems can be used to drive flow through resistive bodies, where high pressure levels will be exhibited. Despite being more expensive if compared with systems for pressure control, most pump types enable direct and independent control of the flow in each channel, allowing easier design and use of multi-channel platforms, which are often necessary for biological experiments. Nevertheless, flow-controlled systems are characterised by higher response times, with the difference between the two types of systems increasing with the hydraulic resistance of the porous medium. Indicatively, pressure-controlled systems have an order of magnitude lower response times for mouse eye perfusions (BÁRÁNY 1964, Madekurozwa 2019). This difference renders flow-controlled systems less useful in cases where pressure – flow relationships need to be measured. Additionally, interface with independent pressure sensing equipment is required to monitor the pressure gradient experienced by the perfused biological sample.

Theoretically, as described by Darcy's law (Darcy 1856), under laminar flow conditions and for a rigid (non-deformable) porous medium, flow and pressure are linearly connected (for steady state single phase flow of an incompressible fluid). This approach sufficiently describes porous media flow under non-inertial conditions, where friction between the fluid and the porous body is considered as negligible. For reasons that are not fully understood, significant non-linearities have been observed experimentally in pressure-flow measurements through porous solid media even for [2]$Re_D$<1. Indeed, even for low fluid velocities in complex solids (such as tissues), gas solubility changes (influencing viscosity), surface tension and porous solid microstructure and heterogeneity complicate the characterisation of flow profiles through solids. Therefore, whether flow or pressure is controlled in a perfusion system might result in different culture media delivery conditions within an *ex vivo* perfused organ or tissue. As nutrient needs and relevant biomechanical cues are cell- and tissue-specific, different systems for *ex vivo* perfusion have been developed, using either a constant pressure gradient across the tissue/organ or a constant flowrate of culture media through it. For reasons that remain speculative, flow-based technologies have been

[2] Reynolds number (1883) $Re_L$ is a widely, non-dimensional quantity used to differentiate laminar to viscous flow as it represents the ratio between the inertial forces to the viscous forces in a flowing fluid. It can be calculated using the following formula:

$$Re_D = \frac{\rho u D}{\mu}$$

where ρ is the density of the flowing fluid, u is the fluid velocity, D is channel diameter and μ is the dynamic viscosity of the fluid. Typically, for fully developed flow through a pipe, a flow is considered laminar when $Re_L \leq 2300$.

reported to be more effective in preserving tissue viability and function in some cases (Bastien, Piriou et al. 2000, Azau, Markowicz et al. 2014, Halsøy, Kondratiev et al. 2016). However, ischemic injury of organs during bypass surgery remains possible despite the use of external perfusion support systems (Mir, Pavan et al. 2016, Zhou, Meng et al. 2016) and optimal solutions for *ex vivo* perfusion of native tissues generally remain elusive.

The main aim for this chapter was to design and fabricate a constriction-based platform that would enable sample self-sealing in the constriction, so that a pressure gradient applied across the specimen would inhibit peri-fusion and promote perfusion.

## 2.3 Materials & Methods

### 2.3.1 Sample origin

Platform design was focused on 3 mm-thick (~10-20 mg) parenchymal tissue (e.g. mouse liver, human omentum) specimens. Such specimens can be easily collected using a common biopsy punch, while parenchymal tissues share several properties, enabling wide applicability of the platform.

Specimens used for platform testing were from C57BL/6J male mice (Charles River Ltd, UK), aged 8-18 weeks at the time of the experiment. All mice were first allowed at least one week to acclimatise to the housing environment and were housed in clear individually ventilated cages at 21˚C, with a 12h light dark cycle. Food and water were supplied *ad libitum*. Mice were culled via neck dislocation, with decapitation as a secondary culling method to confirm death. For the standard experimental protocol, animal tissue was resected only once the set up was ready for sample incorporation and as soon as possible after animal culling (typically ~15min). Specimen isolation from mouse liver was carried out by under aseptic conditions for biological experiments or within a ventilated cabinet for perfusion characterisation experiments. In either case, using autoclaved surgical equipment, the whole mouse liver was resected and washed 3 times with ice-cold, sterile modified Krebs – Henseleit (KH) buffer[3] (Sigma-Aldrich Company Ltd, UK). Using a biopsy punch (Integra LifeSciences Corporation, USA), 3-mm thick mouse liver specimens were punched out of the liver lobes, washed once with KH buffer and placed in a Falcon tube with buffer on ice. All experiments were carried out under the authority of a UK Home Office project license.

[3] The Krebs-Henseleit buffer is a modified Ringer solution used for liver tissue preservation by postulating the urea cycle Cohen, P. P. and M. Hayano (1946). "Urea synthesis by liver homogenates." J. biol. Chem **166**: 251.

### 2.3.2 Channel-based device

To assure that the platform would be sufficiently practical, a design where a specimen is loaded via an open inlet reservoir to a channel bearing a constriction was employed, with flow downstream of the sample being driven through channel outlet by a syringe pump in withdrawal mode. Constriction geometry was designed so that the stenosis produced would be sufficiently narrow to entrap the specimen and allow it to self-seal the constriction. In parallel, the chosen dimensions should result in a stenosis wide enough to protect the perfusable routes within the specimen from collapse due to compression. The significantly low stiffness of liver (and most parenchymal tissue) specimens allows them to deform even under minimal compression. Therefore, to enable specimen immobilisation and maintenance at the entrapment site during perfusion a constriction of about a fourth of sample original diameter was chosen.

Beyond constriction dimensions, constriction length and slope are also paramount for specimen immobilisation and perfusion. A constriction long enough for the whole specimen to fit within would enable sample's unhindered slipping further into the constriction due to the compression from the flowing fluid. This would eventually lead to sample extrusion downstream of the stenosis. On the contrary, a sudden constriction would be more effective for specimen entrapment, however a larger part of the specimen could be exposed to lower media turnover due to the flow profile established in the channel.

#### 2.3.2.1 Preliminary prototype

First, the impact of constriction length (C) (Fig. 2.1(A)) and shape was explored using a 3D printed (Objet30 Pro – Stratasys, USA) device comprising six different channel architectures, based on different combinations of three cases of constriction length (1, 2 and 3 mm) and two constriction shapes (round or flat-bottom) (Appendix A, SF1). The round shape would facilitate more isotropic compression of the specimen during loading and perfusion whilst a flat-bottom constriction would be useful for imaging applications. Notably, all testing channels had the same cross-sectional area at the original channel region and at the minimum constriction point. As tissue immobilisation was poor for constriction length of 3 mm and was independent of constriction shape, the channel with a flat bottom constriction shape and a 2-mm constriction length from the parallel-channel 3D printed device was used for hydraulic resistance measurements with entrapped murine liver specimens (C57BL6 mice, 11-16 weeks – Charles River Ltd, UK) utilising the *iPerfusion* system (Sherwood, Reina-Torres et al. 2016).

#### 2.3.2.2 Final PDMS-based platform

Experimentation with the preliminary prototype (see 2.3.2.1) provided insights for the design of the final version of the device. A constriction comprising a maximum cross-section (A) (if round) of about half the specimen diameter (i.e. 1.8 mm) and a minimum cross section (B) of a fourth of sample diameter (i.e. 0.75

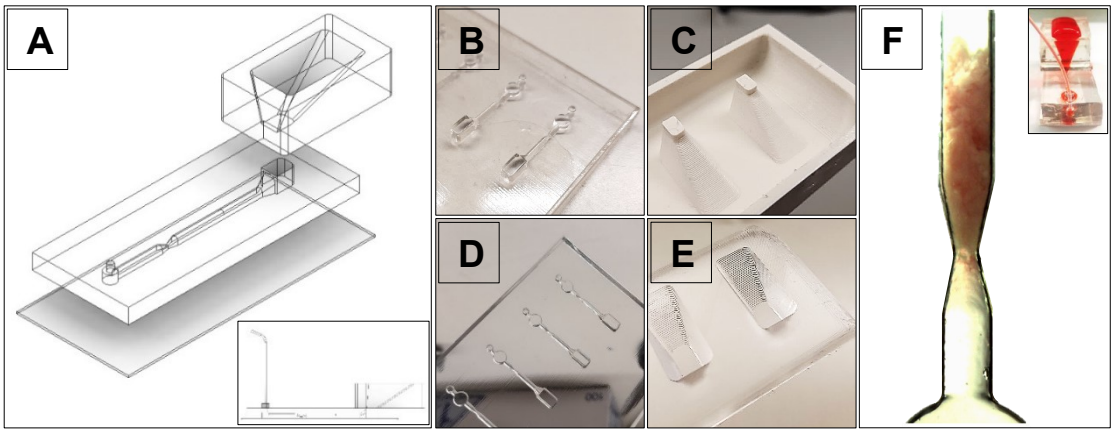


**Figure 2.2** Device for perfusion of native tissue specimens: (A) multi-layer fabrication process comprising a top/open-air reservoir layer, a middle/channel layer, and a flat bottom layer, mould and polymerised PDMS layer for the channel (B, D respectively) and the reservoirs (C,E), (F) a 3 millimeter mouse liver specimen immobilised at the device constriction region, with inset showing the front view of a fully-assembled device filled with saline with food colouring.

mm) was hypothesised to be sufficient for the entrapment of native liver specimens, at least for a given range of constriction length (C) values (Fig. 2.1(A)). Prototype and moulds for PDMS casting were designed using Autodesk Inventor (Autodesk, USA). Counteracting between the necessity for a tight seal and sufficient perfusion, a constriction length of 2 mm was selected, resulting to a slope of 27.7 degrees for the chosen minimum constriction diameter.

Each platform was formed using three Polydimethylsiloxane (PDMS) layers (Fig. 2.2(A)). A Petri dish was used to fabricate the flat bottom layer, and two different 3D printed moulds (Fig. 2.2(B)(C)), which were used to cast in the layer comprising the channel structures required (Fig. 2.2(D)) and a top layer that was an open-air reservoir (Fig. 2.2(E)). For all layers, Sylgard 184 (Dow Corning Corporation, USA) was used, at an elastomer to curing agent mixing ratio of 10:1. The mixture was degassed in a vacuum chamber until optically transparent and then used to fill the moulds and left to cure in a 65˚C oven overnight. To form the three-layer construct, each surface to be bonded to another one was first treated with plasma[4] using a corona treater (Electro-Technic Products, USA), at maximum power for 30 seconds. Then, the two treated surfaces were aligned and manually compressed against each other. Each platform was then left to cure on a hot plate (~80˚C) for at least 2 hours. Withdrawal of fluid through tissue specimens of significant hydraulic resistance would generate negative pressures downstream of the specimen in the channel, given the open-air reservoir. Therefore, as a protection against leaks, the tubing (PTFE

[4] Surface treatment with plasma refers to the process where a beam of highly reactive species (mainly charged molecules, ions and electrons) activates groups on a surface. For example, treatment of PDMS surfaces with plasma exposes silanol groups (Si-OH) and provides the energy necessary for them to form bonds with other excited Si-OH groups when interfaced with treated PDMS or glass surfaces, see Nicholas, et al. (2019). Study of plasma treatment for PDMS surface modification on the fabrication of microfluidic devices. AIP Conference Proceedings, AIP Publishing LLC.

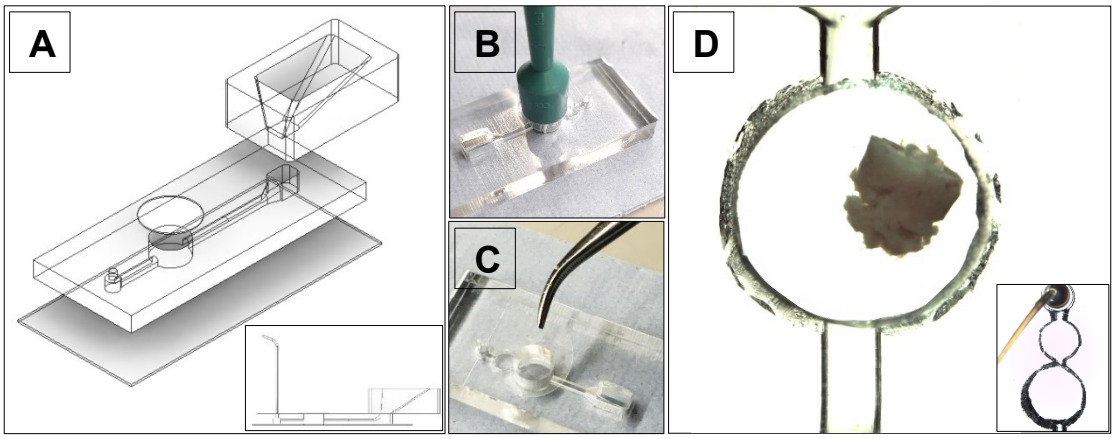


**Figure 2.3** Control device used for peri-fusion of native tissue specimens: (A) multi-layer fabrication process, (B) peri-fusion chamber, which is formed with a (C) biopsy punch and a (D) round coverslip. A 3-millimeter mouse liver specimen in the peri-fusion chamber, with the inset showing an empty fully assembled device for peri-fusion.

microbore tubing 0.56 mm ID, 1.07 mm OD – Fisher Scientific UK Ltd, UK) incorporated at channel outlet was sealed with PDMS and polymerised as above.

### 2.3.3 'Peri-fused control' device

In order to fully validate the platform and its use in *ex vivo* specimen perfusion a fair control of peri-fusion was required. Using the same mould, materials and fabrication process as for the prototype for perfusion, a modified device was fabricated, which had wide round region (diameter: ~8 mm, height: ~6 mm) for tissue residence instead of a constriction (Fig. 2.3). This region was formed by cutting off an 8 mm-cylinder at the constriction region of the middle PDMS layer ("channel layer") using a biopsy punch (Integra LifeSciences Corporation, USA) and sealing the top of the channel with a ten-millimeter round coverslip (Fisher Scientific UK Ltd, UK) after plasma bonding.

### 2.3.4 Perfusion system

To examine device efficacy in liver specimen perfusion and preservation, a flow-driven system was employed using two identical syringe pumps (PHD Ultra - Harvard Apparatus, USA). Characterisation of flowrate output of one of these pumps in the context of another project had shown (as it was expected for a flow – controlled system) accurate but pulsatile flow rate control (indicatively 119.9 ± 34.0 nl/min (mean ± 2SD) when output is set at 120 nl/min) (Madekurozwa, Reina-Torres et al. 2017). To enable parallel and independent perfusion of individual devices, a 3-part adapter was developed, allowing simultaneous control of six 1 ml syringes (Terumo Europe, Belgium) (Appendix A, SF2). All parts of the adapter were fabricated using an Ultimaker 2+ 3D printer (Ultimaker BV, Netherlands) with acrylonitrile butadiene styrene (ABS) as the printing material (Ultimaker BV, Netherlands). Based on the hydraulic resistance measurements performed with mouse liver specimens (see 2.3.2) and to avoid an extreme pressure gradient occurring across a specimen, a maximum flowrate of 200 nl/min was used for the perfusions.

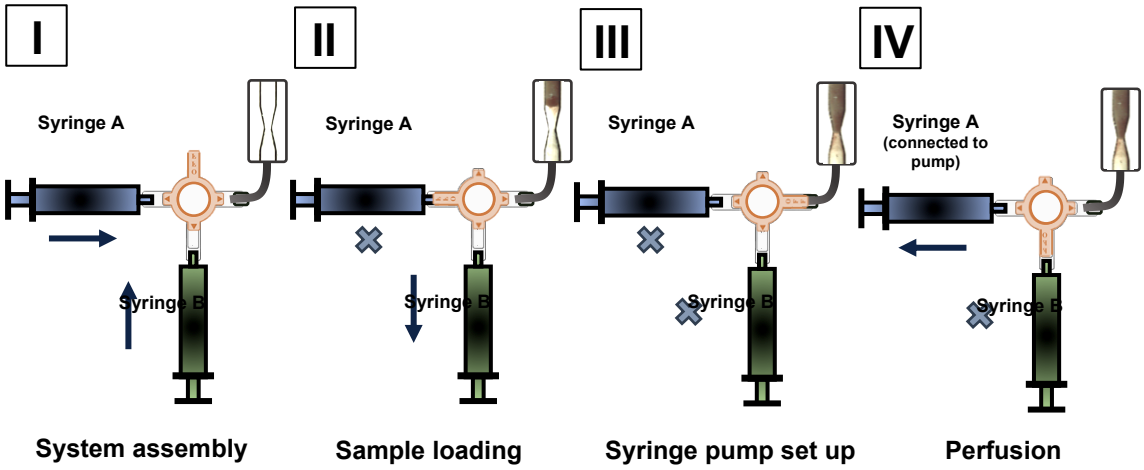


**Figure 2.4** Three-way valve and syringes used for system assembly and specimen manipulation within the device from sample loading to perfusion. Arrows show the direction of the flow and the x signs indicate no flow.

Further considerations and adjustments regarding the employed flowrate are included in Chapter 3 and Chapter 4.

### 2.3.5 Experimental set-up and procedure

The device was tested and validated with mouse liver samples. Each device (perfused and/or peri-fused) was connected to a sterile three-way valve and each valve was connected to two 1 ml syringes; syringe A (parallel to device tubing; volume depends on syringe pump and/or syringe pump adapter allowance) and syringe B (perpendicular to device tubing; volume depends on total dead volume) (Fig. 2.4). The two syringes enable the user to manually induce flow perturbations so that the specimen can be introduced to the constriction and perfusion can be controlled via the syringe pump. First, each device-valve-syringes

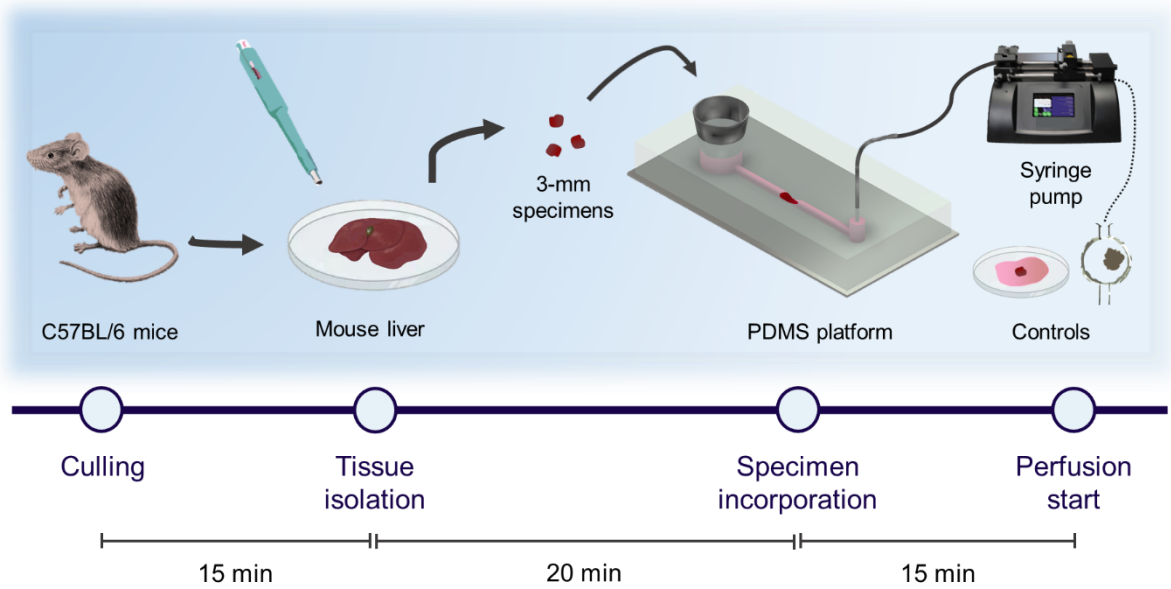


**Figure 2.5** Flow chart and timeline between animal culling, tissue and specimen isolation, sample incorporation and culture within the platform and the control settings

complex was filled with sterile PBS, which was subsequently exchanged with culture media or any other perfusate as required.

Using sterile tweezers, one sample was placed (submerged) in each device's inlet reservoir and allowed to sink. Once the specimen reached the bottom of the reservoir, media withdrawal was manually induced using syringe B (Fig. 2.4(II)) until the specimen reached and sealed the constriction. Then valve conformation was changed so that the flow towards the device was blocked to assure the specimen would remain within the constriction (Fig. 2.4(III)). Once this process was followed for all devices, they were placed and sealed within sterile containers, and kept in a tissue culture incubator, with the end of the tubing with the valve and the syringes outside. Syringe B for each device was then connected to the syringe pump adapter and after all devices were connected to the syringe pump, valve conformation was changed so that flow to syringe A is blocked (Fig. 2.4(IV)). Then, withdrawal of perfusate was controlled by the syringe pump (Fig. 2.5).

Unless otherwise stated, perfusion took place with equipment (devices, tubing, adapters, pipette tip containers for device residence and surgical equipment) sterilised via autoclavation (121˚C, 15 min) using sterile-filtered (0.22 µm-pore filter) media or saline. Full protocols for the perfusion experiments can be found in Appendix B.

### 2.3.6 Imaging

Microscopy was employed to image the tissue during specimen incorporation in the perfused device and visualise fluid flow during early stages of perfusion and peri-fusion. An inverted light stereoscope was utilised to observe erythrocyte washout as the sample was directed to the constriction. Similarly, a light microscope was used to examine if cells were present in the perfusate (10x magnification) and whether any of these cells were erythrocytes (40x magnification). A fluorescence stereoscope (connected to a mercury lamp) was used to demonstrate fluid flow in perfused and peri-fused conditions, where fluorescent tracers (0.2 µm carboxyl-mediated, red ($555_{EX}/565_{EM}$) latex beads – Invitrogen, UK) were suspended in the perfusate.

## 2.4 Results

Using the 3D printed device (Appendix A, SF1), it became evident that a constriction length of 3 mm produced a constriction insufficiently tight to entrap a liver specimen, whilst constriction shape did not have an effect on entrapment. Therefore, a 2-millimeter-long constriction and a flat-bottom (imaging friendly) constriction shape were selected as design parameters of the final prototype. Using a pressure-step method (5 steps, 5 mmHg each), indicative measurements with this channel design and the

*iPerfusion* system (Sherwood, Reina-Torres et al. 2016) showed that immobilised specimen resistance in the constriction can be 450-900 mmHg/(µl/min), informing the range of flowrates that would be employable with a flow-driven perfusion system.

The final platform version fabricated via layering of plasma treated PDMS constructs was successful and the device coped well with autoclavation and the humid incubator environment. Wetting by culture media, specimen compression against the constriction and the negative pressure downstream of the specimen (due to continuous media withdrawal) did not affect device structure or sealing throughout 48h cultures. Importantly, for these perfusion durations, the constriction design supported tissue immobilisation even at flowrates beyond the relevant range (up to 1 µl/min). In limited instances progressive slipping of the tissue specimen was observed, largely due to the lower friction between the tissue and the flat PDMS bottom surface of the device. However, that never resulted in the specimen extruding significantly into the downstream region of the channel and/or sample passing the constriction region did not occur, and therefore slipping was considered insignificant for the perfusion durations tested.

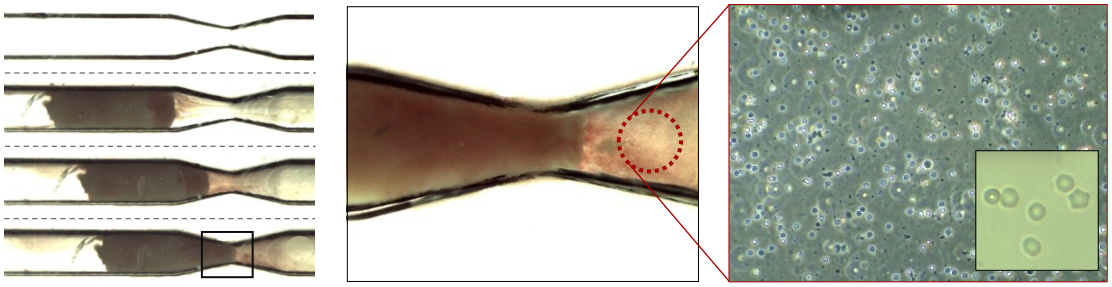

**Figure 2.6** Tissue specimen loading and immobilisation within the constriction under flow result in blood washout as confirmed by light microscopy (right: blood washout image scale: 10x, inset image scale: 40x)

Tissue specimens were easily loaded into the platform reservoir and were directed to the channel constriction after manual perturbation of the flow within the channel. During loading, specimens reached the constriction and adapted to constriction geometry (Fig. 2.6). As specimens reached the constriction, blood was washed out of the samples (Fig. 2.6). Blood presence in the perfusate downstream of the constriction was confirmed by collecting the perfusate immediately after tissue direction to the stenosis and examination under a common light microscope. This blood washout effect was further promoted once the sample reached the stenosis as a result of specimen compression against the constriction and the flow induced by the manual control of syringe A.

To examine whether specimen-constriction sealing was sufficiently tight to obstruct peri-fusion, fluorescent tracers (0.2 µm carboxyl-mediated, red ($555_{EX}/565_{EM}$) latex beads – Invitrogen, UK) were added to the perfusate upstream of the sample after it had been directed to the stenosis. After 30 minutes of perfusion, tracers covered the whole upstream region but were not found at the channel-tissue interface. On the contrary, in the peri-fused (control) device, tracers were able to travel all around the

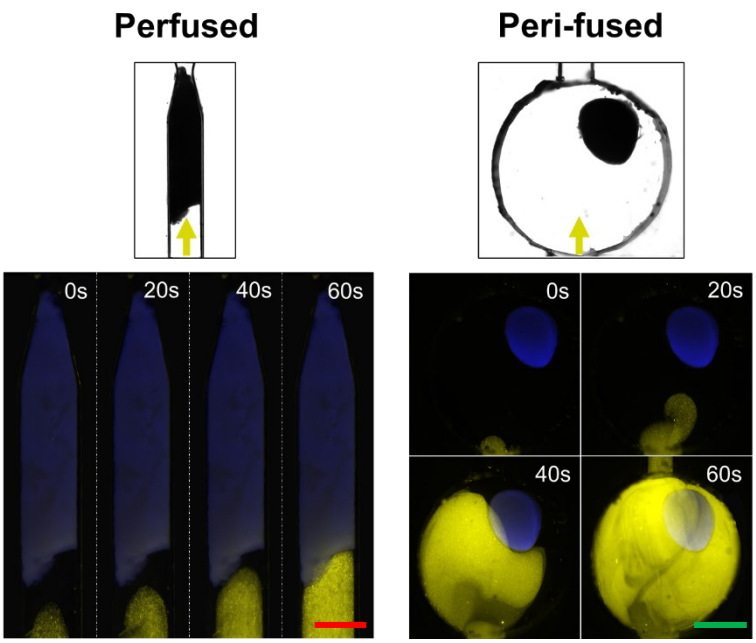


**Figure 2.7** Visualisation of fluid flow using fluorescent tracers (yellow) in a perfused and a peri-fused specimen (red scale bar: 1.5 mm, green scale bar: 3 mm).

specimen, probing the available paths for fluid flow to travel around the specimen rather than through it (Fig. 2.7).

## 2.5 Discussion

Prototypes' validation was carried out using murine liver specimens, as mouse tissues from a given strain have low biological variability and are readily available. Notably, mouse liver tissues are characterised by similar mechanical properties (Guimarães, Gasperini et al. 2020, MacManus, Menichetti et al. 2020) and sensitivity to ischemia (Abe, Hines et al. 2009, De Villiers and Riley 2020) to human tissues, and therefore serving as a suitable model for platform validation.

Preliminary testing using mouse samples in the 3D printed prototype informed final platform version design, which included a 2-millimeter-long constriction and a flat-bottom stenosis shape. Also, the 3D printed multichannel device informed material selection for the final prototype. Despite micrometre-scale resolution of the printer used, channel internal surfaces were quite rough as a result of material deposition on top of the support material for lumen formation. This artifact was absent on 3D printed surfaces that had not been printed on support material. For that reason, the same 3D printing process and printing material (VeroClear – Stratasys, USA) were used for the fabrication of moulds (Fig. 2.2(B)), were PDMS (Sylgard 184 formulation - Dow Corning Corporation, USA) layers with channel architecture were cast in. PDMS is a gas-permeable, imaging-friendly, bioinert and transparent material, widely accessible at a relatively low cost.

Fabrication of device layers with PDMS provided smooth, low friction surfaces that enabled the specimens to reach channel constriction with limited deformation. In spite of the flat bottom layer forming the constriction of the device, specimen slipping due to compressive load by fluid flow was limited and did not appear to endanger tissue immobilisation and constriction sealing. It is worth noting that neither the employed specimens nor the channels tested were pre-treated or functionalised to promote specimen adherence within the channel. Absence of artificially induced specimen adherence allowed independent exploration of the device design efficacy for tissue loading, immobilisation and sealing and the effects that perfusion (regardless of adhering substances) might have on specimens. It should be noted that, although an adherence-promoting substance was not necessary in the examined culture window (48h, characterised in Chapter 4 - see 4.2.2, 4.2.3, 4.3), it might be required for longer perfusions, higher flowrates (>1 μl/min) or samples of a different origin. Also, the flow-controlled system employed (see 2.3.4) was successful to control up to 6 devices per pump, each device independently of another.

For a fair experimental design, a control device was needed that would provide to the cultured specimens the cues that they would be exposed to in currently available technologies employing peri-fusion to extend tissue viability *ex vivo*. As is the case for the field of 3D cell culture systems, tissue-based culture models are greatly heterogenous, covering a range from channels with media capacity of less than a milliliter (Astolfi, Peant et al. 2016) to several-microliter-large bioreactors (Rambani, Vukasinovic et al. 2009). Similarly, the range of employed flowrates varies from <0.5 μl/hour (Rambani, Vukasinovic et al. 2009, Astolfi, Peant et al. 2016) to 300 μl/hour (Beckwith, Borenstein et al. 2018). Given this significant variability of available alternatives, a peri-fused control device was designed and fabricated so that a 3 mm-thick tissue sample can be cultured in a setting where media is renewed around the specimen.

Blood washout during specimen direction towards the constriction suggests that at least a minimal amount of perfusate travels through the sample even before it fills the stenosis. This observation suggests that the sample seals sufficiently even the upstream non-constriction region of the channel (further evidence of peri-fusion blockage can be found in Chapter 3 – see 3.2.6, 3.3). Moreover, the enhanced washout observed when the specimen reaches the constriction support the notion that the sample seals the stenosis, blocking peri-fusion from occurring. Importantly, this effect also demonstrates that intra-tissue flow is established early through the specimen, without an acclimatisation period being necessary to restore advection through the sample. Finally, washout removes residual blood and clots from specimen vasculature, thus providing unobstructed routes for intra-tissue flow.

The selected design provided a channel that was effective to facilitate specimen loading under flow, tissue entrapment at the constriction region and maintenance of the sample in the stenosis throughout the perfusion period (up to 48h - characterised in Chapter 4 - see 4.2.2, 4.2.3, 4.3). Notably, the device

efficiently obstructed peri-fusion around entrapped specimens, which was necessary for the induced flow to travel through the tissue rather than around it. Also, channel design allowed specimen sealing of the entire area occupied by the explant, even before the stenosis, which minimised the possibility for poor perfusion of specimen regions close to the upstream front of the sample.

Although this prototype served as a promising set up to induce flow through native tissue specimens, several aspects of this technology can be further optimised, particularly with respect to the different mechanical properties of various tissues. Poroelastic modelling of specimens perfused in this device would enable better understanding of the role of constriction's slope for tissue entrapment and compression, enabling informed modifications on specimen size and constriction design. Also, computational modelling of fluid flow through an entrapped specimen could provide valuable insights on oxygen and other solute delivery within the tissue, accounting for the higher tissue density within the constriction. Combined theoretical and computational approaches could improve understanding on the competing effect between higher flowrates in more constricting stenoses and higher permeability (due to lower compression) in wider constrictions, to account for higher oxygen and energy needs in lower permeability regions. Additionally, empirical testing of different constriction shapes and sizes with flow visualisation and histology could contribute towards the identification of more effective channel conformations to induce intra-tissue flow through specimens and improve the preservation of their viability *ex vivo*.

Beyond the technical optimisation that could benefit the device presented herein, the constriction-based approach to induce intra-tissue flow through *ex vivo* specimens has inherent limitations that may limit its applicability in specific contexts. First, the concept of employing a stenotic channel to block specimen peri-fusion and induce perfusion depends on explant compression, which may be harmful for tissues that are sensitive to strain. On another aspect, at the current device, where specimens are fluidically loaded to the channel's constriction, the user is unable to control specimen positioning and orientation during loading. Additionally, similarly to most channel-based and microfluidics set ups, the current design is not directly compatible with methods for perfusate collection downstream of the specimen, which could be used in assays determining explant viability and function. Notably, this effect is aggravated in the perfused device due to the negative pressure developed downstream of the specimen for perfusion to occur. Also, the current system depends on perfusion equipment that resides outside the incubator environment, where the perfused tissue specimens are cultured, a set up that can involve several practical complications for the user and the applicability of this system in a clinical setting. It is also worth noting that insights from the *ex vivo* organ perfusion field regarding optimal flowrate and pressure value ranges to maintain high levels of viability are poorly translatable to the system presented herein. This limitation is generated by

the increased tissue density of the compressed specimens in the device and the fundamental differences in solutes' consumption along the perfusable routes between the two cases.

## 2.6 Conclusions

In this study, we present the first platform, to the best of our knowledge, that can facilitate tissue immobilisation under flow whilst obstructing peri-fusion from occurring through the interface between the employed tissue sample and the channel wall. The developed platform serves as a prototype to test the hypothesis that inducing intra-tissue flow through native tissue specimens can preserve thick tissue specimens for longer than peri-fusion technologies for explant culture and drug assays.

# Chapter 3

# Demonstration of Intra-Tissue Flow

## 3.1 Introduction

### 3.1.1 The importance of advection for tissues

Mammalian cells require continuous access to oxygen, nutrients, signaling molecules and metabolic waste clearance routes to maintain their homeostatic functions. Transport of such substances occurs primarily via the circulatory system, through advection along the vascular routes and diffusion across capillary walls and cell membranes. Vasculature size and density vary by organ due to differences in metabolic rates and oxygen consumption. However, throughout the human body, capillaries hold the largest surface area for mass exchange among all blood vessels (Schmidt-Nielsen and Pennycuik 1961, Schmidt and Thews 2013). Most capillaries are less than 10 microns wide (Schmidt-Nielsen and Pennycuik 1961, Schmidt and Thews 2013), which renders them among the most resistive routes for fluid flow within tissues after arterioles (Gould, Tsai et al. 2017).

Apart from the vasculature's role in establishing chemical gradients, substantial solute mass balances in the human body are also controlled through interstitial fluid transport within the extracellular space. Gaps of varying dimension (from a few nanometres to micrometres) between cell cytoskeleton and tissue matrix, or within the matrix itself, work as an intact fluid compartment that contributes to mass exchange between cells and their microenvironment (Swartz and Fleury 2007). As the vast majority of vascular routes and matrix gaps are less than 10 microns wide, human tissues are defined by significant hydraulic resistance, which greatly depends on (perfused route) diameter[1].

Advection is the prime mechanism for fluid transport across the human body and perfusion regulation is necessary for normal organ activities. Physiologic function of tissues not only depends on the presence of fluid flow, but it also requires constant control of the perfusion parameters as well. Indicatively, in several types of bypass surgeries, tissue function may be compromised due to insufficient mimicry of heart-controlled perfusion and partial disruption of physiologic vascular tone (Mir, Pavan et al. 2016, Zhou, Meng et al. 2016). Despite the essential role of perfusion for tissues, most currently available systems to interface *ex vivo* specimens with a stream of culture media (see 1.2.6), although being described as "perfused", have not truly established advection within the tissue itself. In the absence of advection, oxygen and nutrient delivery can be facilitated only via diffusion, which can be effective for mass transport only within 200 μm into the tissue from the source (Helmlinger, Yuan et al. 1997, Milotti, Stella et al. 2017). Therefore, for specimen dimensions greater than ~400 μm (Astolfi, Peant et al. 2016), necrotic core development is predicted to occur within samples used in an *ex vivo* set up. To preserve large (>1 mm) native tissue samples alive within culture, establishment of intra-tissue flow through perfusable routes (e.g. vasculature,

[1] At steady state, for pressure-driven and fully-developed laminar flow of an incompressible fluid through a straight, constant-diameter and round channel, hydraulic resistance can be calculated using the following formula: $R = \frac{\Delta P}{Q} = \frac{8\mu L}{\pi r^4}$ where R is the hydraulic resistance, ΔP the pressure drop across the channel, Q the flowrate of the flowing fluid through the channel, μ is the dynamic viscosity of the fluid, L is channel length and r is channel radius Fox, R. W., et al. (2020). Fox and McDonald's introduction to fluid mechanics, John Wiley & Sons.

matrix gaps) is necessary. The number and flow capacity of each of these routes will define whether an explant employed in a perfused platform can be sufficiently supplied with media and therefore its survival. For these reasons, demonstration of intra-tissue flow in any *ex vivo* specimen perfusion platform should be considered essential for its validation.

The difficulty to induce fluid flow through tissues increases the complexity of re-establishing perfusion after temporary or permanent occlusion of the circulation *in vivo* and that of restoring intra-tissue flow *ex vivo*. Especially for explanted samples, suitably designed platforms are required so that flow is driven through the specimen rather than around it. In most models available in the literature, flow around the samples is unrestricted, which translates to the absence of advection within the employed explant. This can only be overcome if the boundary between the channel(s) delivering the flow and the sample is sealed and potential leaks through this interface are negligible (see 2.2 for specimen sealing of the device). As the device presented herein depends on specimen compression within a confined channel to block peri-fusion, intra-tissue flow evidence is required to assure that compression does not result in perfusable route collapse within then sample.

### 3.1.2 Platform validation: Flow through explants

Culture media and supplements have been a fundamental feature of biological laboratory research and their role for *ex vivo* cell and/or microorganism maintenance, grow and proliferation is unquestionable (Yao and Asayama 2017). Active metabolism requires frequent renewal of culture media components and media turnover is considered a key design parameter for cell- and tissue-based models that requires optimisation. Evidence from 3D cell models have shown that physical boundaries partially obstructing or delaying fresh media delivery to cells can result in poorer cell functions and death (Karageorgiou and Kaplan 2005, Du, Han et al. 2008, Gomes, Guillaume et al. 2016). For example, cells cultured within scaffolds may be exposed to lower levels of nutrients, hypoxia and metabolic byproducts as mass exchange is partially obstructed by the scaffold and cells in the outer regions consume most of the media components. Similarly, cellular aggregates (spheroids) can become several hundreds of micrometers thick, however beyond about 400 μm a necrotic core develops as a result of anoxia and nutrients deprivation. Despite the effects of diffusion-limited culture being well understood, a platform that interfaces directly regions from within a native tissue specimen with culture media are lacking.

The available systems that interface native tissue specimens with a stream of culture media are diffusion-limited, as flow can travel around the sample. This means that cells on specimen periphery and the outer layers of the sample can benefit from media turnover, whilst specimen core remains isolated. Nutrient and gas delivery within a tissue sample can be improved by inducing flow through the available routes for perfusion, such as the interstitial space and the vasculature. Cells within or at the periphery of these compartments can survive in culture if interfaced with media via perfusion and support specimen preservation for longer. Therefore, to validate a technology that

aspires to overcome diffusion limitations of common tissue-culture models, evidence of intra-tissue flow needs to be demonstrated.

### 3.1.3 Challenges in perfusion visualisation, imaging and markers

Intra-tissue flow is necessary to preserve explant viability, however, identifying the regions within a specimen where perfusion occurs through is challenging. Most approaches for perfusion visualisation depend either on tracers and/or contrast agents within the perfusate or on functional readouts regarding flow's effect on tissues (Daly and Leahy 2013, Zhao, Chen et al. 2018). Regarding functional readouts, preservation of specimen viability is the main parameter to decide if a testing prototype is effective to perfuse native samples. However, even for ischemia-susceptible organs, activation of cell death mechanisms and progression of primary and/or secondary necrosis that induce measurable differences in explant viability markers may require several hours. In such timeframes nutrient delivery may be dominated by diffusion and therefore examination of advection's direct role in specimen preservation may be challenging. For example, peri-fused culture improves specimen preservation by maintaining maximum oxygen and nutrient levels on explant's surface, however this benefit is independent of perfusion. Similarly, several cytoplasmic proteins, cell junctions or receptors that could be used as indicators of advection are affected by nutrient deprivation, hypoxia and shear. Therefore, identifying a group of markers that clearly demonstrates effective induction of intra-tissue flow in an explant is challenging (Hasanin, Mukhtar et al. 2017).

Light-based imaging approaches have been employed in order to map intra-tissue flow and functional markers within biological samples. Recent advances in microscopy (such as confocal and multiphoton microscopes) have enabled imaging of biological systems *in situ*, with high spatial resolution (Qiang and Wang 2020). The efficacy of such approaches has been limited with thick parenchymal specimens, nevertheless (Richardson and Lichtman 2015). Limited light penetration within tissues and light scattering induced by refractive index mismatch between the different components of tissues (proteins, lipids, water) render such specimens significantly opaque. Also, pigmented and inherently fluorescent tissue structures further limit light penetration and signal recollection from within the tissue (Monici 2005). Higher wavelength light and multi-photon technologies can be used to achieve deeper light penetration, however tissue imaging with cell-level resolution beyond 200 µm has not been successful in pigment-rich tissues, such as the liver. Tissue clearing protocols, which employ organic solvents to replace and/or decolorize some of tissue components (fat or erythrocytes for instance) have been successful to increase volumetric imaging efficacy even beyond one-millimeter thickness (Tainaka, Kubota et al. 2014, Susaki and Ueda 2016). Despite their advantages, currently available imaging modalities require long imaging cycles for several millimeter large specimens, which renders them impractical for the validation of novel systems, where testing sessions with a multitude of samples are required. Therefore, using specimen sections (usually 6 to 30 µm thick) is an alternative that overcomes most of these limitations, however it is worth noting that preserving perfusion-

carried tracers on their original location within samples for imaging may be challenging due to washing steps and standard methods used in histology applications.

*In vivo*, tissue perfusion can be visualised using x-rays (e.g. CT scan) or magnetic fields (e.g. MRI) in resolution high enough for clinical information extraction yet low for imaging submicron features, such as tracers within an explant (Du Plessis, Broeckhoven et al. 2017). Novel benchmark systems for microCT imaging on biological samples have been developed and are able to provide meaningful insights for cell function, reaching even submicron resolution (de Castro Fonseca, Araujo et al. 2018). However, imaging quality still greatly varies due to the effects of fixatives, embedding material (if any), water content and specimen orientation. This variation together with the higher cost and longer imaging cycle per specimen reduce the applicability of such imaging methods during early phases of system validation.

In that context, the main aim for this chapter was to evaluate the efficacy of the developed device to facilitate intra-tissue flow and/or vascular perfusion within parenchymal tissue specimens. Histology and visualisation of fluorescent tracer and gold nanoparticle distributions were utilised to assess the device's ability to facilitate intra-tissue flow. Induction of advection in *ex vivo* native tissue samples without cannulation would be a significant development compared to currently available diffusion-limited technologies. Also, re-establishment of perfusion in *ex vivo* specimens would mark a step forward for their prolonged preservation after explanation and their use for experimentation under conditions that better mimic mass transport *in vivo*.

## 3.2 Methods

### 3.2.1 Tissue specimens

To examine the ability of this device to induce intra-tissue flow, mouse liver specimens were used as a model tissue with comparable permeability and mechanical properties to those of human tissues (MacManus, Maillet et al. 2019, MacManus, Menichetti et al. 2020). Tissue samples were taken from C57BL/6J (Charles River Ltd, UK) or Tie2-GFP Balb/c mice that were bred *in house*. Specimens from C57BL/6J mice were used as a source of wildtype material and samples from the livers of Tie2-GFP Balb/c mice were used in applications where a fluorescently tagged endothelium (via the incorporation of a Green Fluorescent Protein molecule on the TEK gene, which is cytoplasmically expressed in endothelial cells) could provide insights regarding where the induced flow was travelling through. Also, mouse liver vasculature is considered isotopically developed and therefore permeability differences between specimens from different regions of the liver were not considered (Sänger, Schenk et al. 2015). Mice were male and aged 8-18 weeks at the time of culling. All mice were housed in clear individually ventilated cages at 21ºC, with a 12h light dark cycle, where food and water were supplied *ad libitum*. Mice were culled via neck dislocation and decapitation as a secondary culling method to confirm death. As soon as possible after culling, the mouse liver was resected within a ventilated cabinet and was washed 3 times with ice-cold, KH buffer (Sigma-

Aldrich Company Ltd, UK). Using a biopsy punch (Integra LifeSciences Corporation, USA), 3-mm thick mouse liver specimens from one a single C57BL6/J mouse were punched out of the liver lobes, washed once with KH buffer and placed in a falcon tube with 30ml buffer on ice. All experiments were done under the authority of a UK Home Office project license (PPL 70/9064).

As a less opaque alternative to mouse liver specimens, tissue samples from zebrafish (*Dario rerio*) skeletal muscle were used for a live imaging experiment. 3-mm specimens were collected from (30 to 40 week-old) adult fish that were kept in accordance with standard conditions. Animal breeding and culling was performed under the authority of a UK Home Office project license (PPL 70/7171). Animals were culled by immersion in 0.1% 3-aminobenzoate methanesulfonate in PBS (Sigma-Aldrich, USA) until 5 minutes after the loss of respiratory movement. After this, fish were placed in ice-cold water and then pinned in a PDMS-coated plate. Under a stereoscope, using sterile tweezers and a scalpel the epixialis part of the musculature was collected and placed in PBS, until specimen incorporation to the device.

### 3.2.2 Tissue sectioning

After each experiment specimens were fixed (unless otherwise stated) with 4% methanol-free formaldehyde (PFA – Thermofisher Scientific, UK) at ambient temperature. Fixation duration varied with application to account for issues such as autofluorescence, sensitive fluorophores (such as GFP), reagent diffusion and/or particle washout when necessary. After fixation, specimens were cryoprotected with 30% sucrose until sink and then embedded in Optimal Cutting Temperature compound (OCT) (VWR Chemicals, USA). The OCT containing the tissue sample was then incubated on dry ice until fully frozen and kept at -80$^{o}$C until sectioning. Sectioning took place with an NX70 Cryostat (chamber temperature: -20$^{o}$C, blade temperature: -20$^{o}$C) (Thermofisher Scientific, UK) after each OCT block had acclimatised in the cryostat chamber for at least 30 minutes. In all cases, sections were collected on SuperFrost Plus slides (VWR, UK).

### 3.2.3 Cell morphology

To inspect cell morphology and orientation with respect to specimen immobilisation and perfusion within the developed device, 3-mm liver specimens collected with a biopsy punch were washed three times with ice-cold KH[2] buffer (Thermofisher Scientific, UK) and then cultured in three different settings: (i) perfused culture in the developed device, (ii) peri-fused culture within the peri-fused control device and (iii) static culture wherein the specimen was submerged in media in a common 24-well plate with 1.5 ml of media. Additionally, a compression control was included, which was a specimen loaded in the constriction of a perfused device, with fluid flow only

[2] The Krebs-Henseleit buffer is a modified Ringer solution used for liver tissue preservation by postulating the urea cycle Cohen, P. P. and M. Hayano (1946). "Urea synthesis by liver homogenates." J. biol. Chem **166**: 251.

used to load the sample in the constriction (flow was obstructed after specimen immobilisation). All specimens used for this experiment came from a single animal's liver and two samples were cultured in each condition. The culture media used for all cases was high glucose Dulbecco's Modified Eagle Medium (DMEM – Life Technologies ltd, UK), supplemented with 20 mM HEPES buffer (Thermofisher Scientific, UK), which enables maintenance of pH=7.4 at ambient conditions. For the two flow-controlled cases (perfused and peri-fused), a flowrate of 100 nl/min was applied using a syringe pump (PHD ultra, Harvard Apparatus, USA). After 2.5h of perfusion, specimens were recollected from each system, washed three times each with PBS (without $Ca^{2+}$ or $Mg^{2+}$) and fixed for 2.5h with 4% PFA at ambient temperature. After fixation, specimens were cryoprotected with 30% sucrose until sink and then embedded in Optimal Cutting Temperature compound (OCT) (VWR Chemicals, USA) on dry ice and kept at -80$^{o}$C until sectioning. 10-μm-thick specimen slices were cut and kept at -80$^{o}$C until further processing. Before microscopy, specimen slides were let to acclimatise at ambient environment in an opaque container for 45 minutes. Then, sections were fixed with 4% PFA for 10 minutes at ambient temperature and were then washed three times with PBS (with $Ca^{2+}$ and $Mg^{2+}$).

Sections were stained with a red ($650_{EX}/668_{EM}$) fluorescent Phalloidin formulation (Thermofisher Scientific Ltd, UK) that stains actin filaments to visualise cell shape, at a 1:40 dilution in a 0.1% Triton X-100, 5% normal goat serum (NGS) mixture for 20 minutes at ambient temperature. Finally, sections were washed with PBS (with $Ca^{2+}$ and $Mg^{2+}$) and then mounted with a few drops of aqueous mounting medium (Fluoromount™ – Thermofisher Scientific Ltd, UK) with 1.2 μg/ml Hoechst 33342 (Thermofisher Scientific Ltd, UK) and a coverslip. After allowing enough time for the mounting medium to spread across the slide (~30 minutes), slides were sealed with clear nail polish and were stored at 4$^{o}$C until imaging. A Leica SP8 Confocal microscope (Leica, Germany) was used for imaging indicative regions within specimen core (beyond 200 μm from explant's surface), from two sections per specimen, collected with 100 μm distance between them.

### 3.2.4 Dye delivery

Efficacy of substance delivery within the employed specimens was probed by supplementing the culture media for all culture conditions (static, peri-fused and perfused) with a fluorescent wheat germ agglutinin (WGA). The fluorescently tagged WGA has a size of about 49.5kDa, which matches the size of several proteins, whilst its ability to be fixable and bind on cell membranes rendered it useful to probe the areas where the molecule was transported through via advection and diffusion. Nine 3-mm liver specimens were collected as above (see 3.2.2) and were then divided to static, peri-fused and perfused (in the developed device) culturing conditions, where samples were first cultured with high glucose DMEM[3] without phenol red (to minimise autofluorescence), supplemented with 20 mM

[3] In the experiments presented in this chapter, unless otherwise stated, high glucose culture media was used in perfusion experiments to minimise the effects of nutrient deprivation on cells. Also, PBS without $Ca^{2+}$ or $Mg^{2+}$ was used only for washing steps of short duration (<15 min) as it was found to have potentially damaging effects on cell adherence and tissue section integrity.

HEPES, for 2 hours. Then media for all cases was exchanged with $555_{EX}/565_{EM}$ fluorophore-conjugated WGA solution (diluted to a final concentration of 5 μg/ml using high glucose DMEM without phenol red – Thermofisher Scientific Ltd, UK). After 1h of culture with WGA, samples from all cases were recollected, washed three times with ice-cold PBS and were then fixed with 4% PFA for 2h at ambient temperature and were processed into cryosections as described above (see 3.2.2).

After acclimatisation, sections were fixed for 10 minutes with 4% PFA at ambient temperature. Next, sections were washed three times with PBS and they were then stained with Hoechst 33342 (ThermoFisher Scientific Ltd, UK) at a final concentration of 0.1 μg/ml for 20 minutes. Subsequently, sections were washed three times with PBS ($Mg^{2+}$ and $Ca^{2+}$) and were mounted with mounting medium (Fluoromount™ – ThermoFisher Scientific Ltd, UK). Finally, samples were sealed with clear nail polish and stored at 4°C until imaging. Imaging was done with a Leica SP8 Confocal microscope (Leica, Germany). Three images from representative regions within the specimen core (beyond 200 μm from specimen surface) were collected from one section from each sample. Fluorescence intensity was quantified using ImageJ (NIH) (Schindelin , Schneider, Rasband et al. 2012), after thresholding each image to exclude vessel lumens and section inconsistencies.

### 3.2.5 Particle delivery

To examine the benefit for mass transport in specimens perfused in the device described herein, fluorescent polystyrene beads were used to visualise the flow (if any) occurring through the vasculature and the interstitium. Particle delivery within statically cultured, peri-fused and perfused specimens was quantified spectrometrically in sample lysate after culture in media supplemented with fluorescent tracers. For the data presented in Fig. 3.2(A), six specimens from two mice were used per culture condition (three specimens for each mouse). After specimen isolation, all 3-mm mouse liver samples (same as above) were washed three times with ice-cold KH buffer and then incubated for 15 minutes in static conditions with media (high glucose DMEM, no phenol red, supplemented with 20 mM HEPES) added with carboxylate-modified, 0.2 μm thick $580_{EX}/605_{EM}$ polystyrene beads (Invitrogen Ltd, UK), at a final concentration of ~$4.5\times10^{12}$ particles/ml. Next, samples were divided into three cultures: (i) maintained as static controls, (ii) transferred into the peri-fused control devices and (iii) transferred into the perfused devices (Fig. 3.2(B)). After peri-fused and perfused specimens were incorporated in the corresponding devices, specimens were perfused with media containing tracers (same mixture as above) for 45 minutes at 100 nl/min. Similarly, static culture was maintained for 45 minutes. At the end of the culture period, all specimens (static, peri-fused and perfused) were recollected and washed three times with PBS (without $Ca^{2+}$ or $Mg^{2+}$). Subsequently, each specimen was placed in an Eppendorf with 1 ml of lysis buffer, where the sample was lysed manually with a pestle. The lysis buffer used comprised 10 mM Tris pH=7.5, 2 mM NaCl, 20 mM EDTA and 2 mg/ml Triton X-100 (Sigma-Aldrich Company Ltd, UK) in distilled water. Each lysate was then mixed well for 30 seconds using a vortex mixer and then

diluted 1:2 with lysis buffer. Triplicates of 150 µl from each specimen lysate were placed in a clear, flat bottom 96-well plate (Corning, US) and fluorescence intensity was measured with a Varioskan LUX Multimode Microplate Reader (Thermofisher Scientific Ltd, UK).

The delivery routes employed for the induced perfusion through the specimens were visualised by fluorescent tracers in the media used for all culturing conditions. Initially, static specimens were cultured in DMEM high glucose with 20 mM HEPES, whilst peri-fused and perfused specimens were incorporated in the corresponding devices under flow using the same media mixture. After which, culture media was exchanged with media added with fluorescent particles (final concentration ~$4.5\times10^{12}$/ml) for all three conditions. Flowrate for the perfused and peri-fused cases was set at 100 nl/min throughout the experiment. Culture with particles lasted 1.5h, then all samples were recollected, washed three times with ice cold PBS (without $Ca^{2+}$ and $Mg^{2+}$) and fixed for 2.5h with 4% PFA at ambient temperature. After fixation, specimens were cryoprotected with 30% sucrose until sink and then embedded in OCT on dry ice and kept at -80$^{o}$C until sectioning. Sections were cut as described above (see 3.2.2) and three sections were collected per specimen, with 100 µm distance between one another, collected serially between slides.

Before microscopy, slides were let to acclimatise at ambient environment in an opaque sealed container for 45 minutes. Then, without any washing steps, a drop of mounting media (Fluoromount – Thermofisher Scientific Ltd, UK) with 1.2 µg/ml Hoechst 33342 (Thermofisher Scientific Ltd, UK) was placed on each section and a coverslip atop before sealing the samples with clear nail polish and were stored at 4$^{o}$C until imaging. Imaging took place with a Leica SP8 Confocal microscope (Leica, Germany).

For live imaging of fluorescent tracer delivery within mouse liver and zebrafish skeletal muscle (epaxialis) specimens, the same process was followed as above and after 1.5h perfusion with the tracers, the flow was ceased, the three-way valve conformation was changed so that flow to the sample was blocked and the platform was taken to the SP8 Leica confocal microscope (Leica, Germany).

### 3.2.6 microCT

To visualise intra-tissue flow in 3D without the limitations of fluorescence-based approaches and examine perfusion efficacy, micro-computed tomography (microCT) was utilised as x-rays can achieve deep tissue imaging due to their shorter wavelength range. A 3 mm mouse liver specimen was incorporated in a perfused device with culture media (high glucose DMEM supplemented with 20 mM HEPES buffer) and it was perfused for 30 minutes. After this period, media upstream of the specimen (i.e. liquid in the reservoir and in the channel inlet up to the interface with the tissue) were exchanged with media with 20 nm gold nanoparticles (Cytodiagnostics Inc., Canada), which are commonly used as contrast agents for imaging (Ashton, West et al. 2015), at a final concentration of ~$6.5\times10^{11}$

particles/ml. A high concentration of gold nanoparticles was selected to compensate for the resolution of tens of microns of the microCT system used. After 3h perfusion at 100 nl/min using a syringe pump (Harvard Apparatus, USA), the device region where the specimen was immobilised at (i.e. constriction and its surrounding area) was manually cut off using a razor blade. PDMS was trimmed off such that only the necessary amount of material to keep the specimen in the constriction was left. The trimmed device-tissue complex was washed three times with ice cold PBS (without $Ca^{2+}$ or $Mg^{2+}$) and then fixed with 4% PFA at 4°C overnight (at least 16 hours).

After fixation, the sample was dehydrated to eventually infiltrate the specimen with paraffin. First, each tissue-device complex was washed for 5 minutes with PBS (without $Ca^{2+}$ or $Mg^{2+}$) and then submerged in 70% ethanol for 2 hours. Then, the complex was moved to 100% ethanol for 1 hour. This step was repeated with renewed pure ethanol for three more times, each lasting an hour. Next, each tissue-device construct was left to incubate in a xylene-substitute, histological clearing agent (Histoclear – National Diagnostics, US) overnight and then transferred to a beaker with melted paraffin in a 65°C oven for overnight incubation. The construct was removed from the beaker and placed on a Petri dish on ice for paraffin to solidify. Finally, the construct was placed in a small beaker, whose top was sealed with parafilm and kept at 4°C until imaging. The microCT imaging took place at the Francis Crick Institute (London, UK) using a ZEISS Xradia 510 Versa (ZEISS, Germany) system. Tomographic imaging was done at 140 KV/10W, yielding 1920 projections and a pixel size of 28 μm.

### 3.2.7 Statistics and image processing

For the WGA delivery experiment, three specimens were used per culture condition, all isolated from the same liver. Tree representative images were collected from the central region of each specimen's section and the reported data points are the mean of the three per specimen. Statistical analysis was performed on ln-transformed data with Welch's t-test.

Particle fluorescence in specimen lysate was reported in each case as the mean of triplicates and the statistical significance between the difference of the means between the different populations was examined with Welch's t-test with the Banferoni correction. Reported values in graphs are presented as the mean ± the margin of error at a 95% confidence level apart from the WGA quantification, where error was set as equal to standard deviation (SD).

Graphs were produced using GraphPad Prism 9.0 (GraphPad Software, Inc., USA). Image processing was performed using ImageJ (NIH) (Schindelin , Schneider, Rasband et al. 2012).

## 3.3 Results

Cell morphology after a two-hour perfusion provided preliminary evidence regarding the efficacy of the employed system to induce flow through native tissue specimens. F-actin visualisation after tissue culture in perfused, peri-fused and static conditions showed that cells of perfused specimens had acclimatised to flow direction (identified

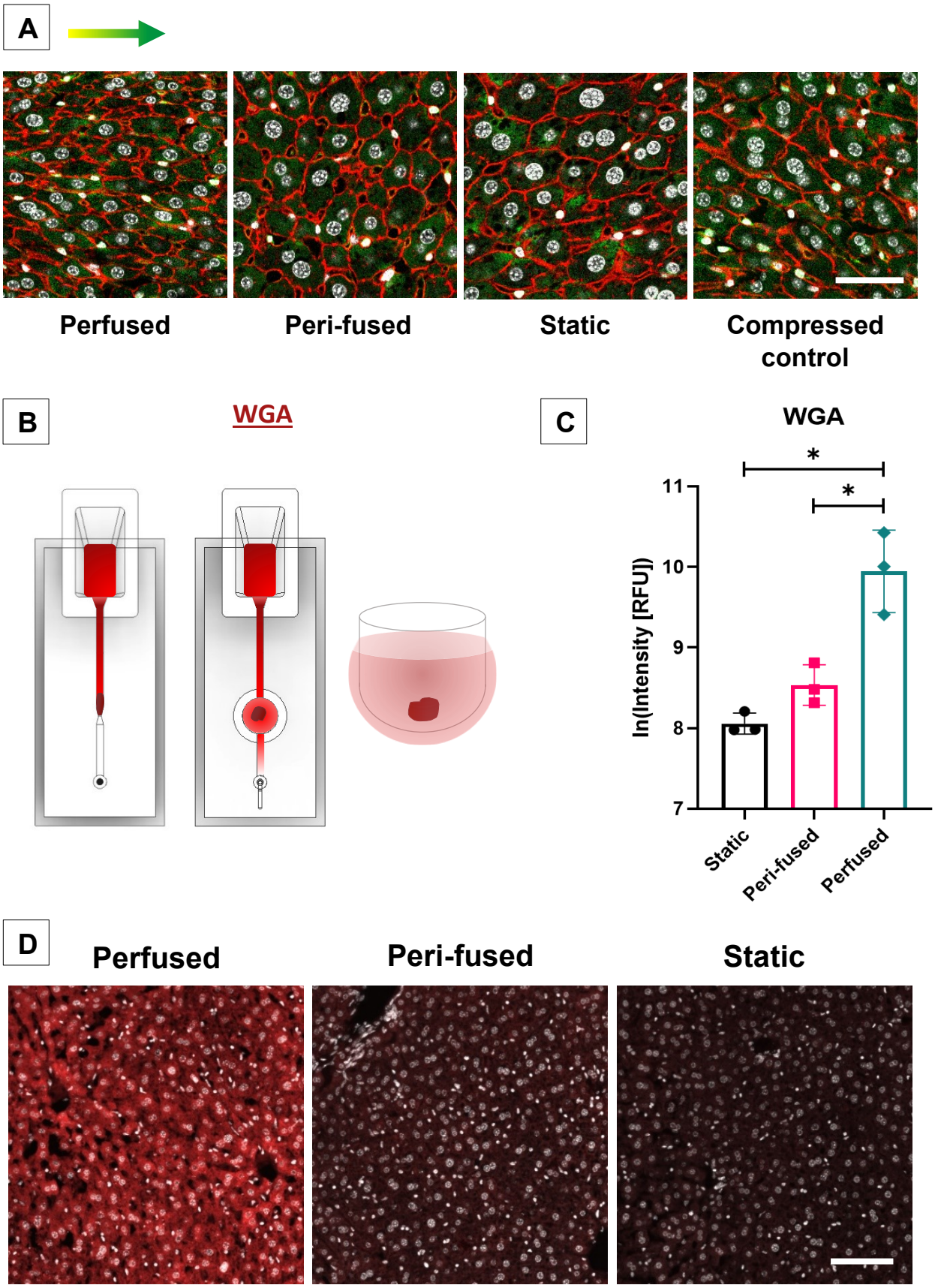


**Figure 3.1** (A) Cell morphology in perfused, peri-fused, static and compression control cases after 2h of perfusion (scale bar: 8 µm), where F-actin is red, cell nuclei are grey and cytoplasm is pseudocoloured green (using cell autofluorescence), The green arrow indicates flow direction for the perfused and peri-fused conditions, (B) Schematic of WGA use for each culture condition, (C) Graph showing fluorescence intensity for WGA in each specimen group, (D) Representative images from the core of perfused, peri-fused and static samples (three specimens per culture condition, all from a single animal) showing WGA in red and cell nuclei in grey (scale bar: 40 µm). *$p < 0.05$.

with respect to specimen adaptation to channel's shape), presenting an elongated shape. On the contrary, cells within tissue specimens in the peri-fused and static controls appeared morphologically similar, having a rounder, more polygonal shape and stochastic orientation. A specimen immobilised within the constriction region of the developed device without flow was used as a compressed control, to understand whether any of the observed cell morphology features in the perfused case could be induced mainly due to specimen compression within the channel. Cells in the compressed case showed limited elongation parallel to channel base, whilst maintaining a morphology that lacked directional alignment (Fig. 3.1(A)).

A red fluorophore conjugated WGA was used to visualise mass transport within specimens cultured in different settings. Analysis of signal intensity from three representative regions (magnification: 20x) within specimen core showed that the geometric mean of WGA intensity in perfused samples was 4.10 times that of the peri-fused specimens (p=0.023, 95% CI: 1.65-10.22) and 6.62 times that of the static samples (p=0.025, 95% CI: 2.84-15.40) (Fig. 3.1(C,D)).

Particle delivery within tissue specimens was quantified using red fluorescent beads in the culture media. Fluorescence intensity measurements in specimen lysate showed a significantly higher number of particles delivered within perfused specimens (perfused *versus* peri-fused: p=0.0004, 95% CI: 1.17±0.45 RFU; perfused *versus* static: p=0.002, 95% CI: 0.70±0.38 RFU; n=6, N=2) whilst there were insignificant differences between the peri-fused and static samples (p=0.066) (Fig. 3.2(A),(B)). Additionally, the same type of beads was used to map the routes employed for intra-tissue flow within the developed device. Confocal imaging demonstrated that tracer particle delivery co-localised with the Tie2-GFP signal in the vasculature of perfused specimens, whilst particles were absent from fluorescently tagged vessel lumens in peri-fused and static specimens (Fig. 3.2(C)). Live tissue imaging during perfusion of mouse liver specimens from Tie2-GFP mice with the fluorescent tracers showed particle delivery throughout the imaged region (Fig. 3.2(D)). However, imaging efficacy was limited beyond 100 μm from channel base (coverslip) mainly due to tissue opacity. To examine perfusion efficacy with less opaque tissues, skeletal muscle specimen from zebrafish were used, which are inherently most accessible to light due to lower pigmentation and scattering. Addition of the same kind of tracers within the perfusate of zebrafish tissue, enabled deeper tissue imaging and visualisation of particle delivery (red fluorescent signal) within the live explant (black) (Fig. 3.2(E)). However, imaging resolution was significantly limited beyond 300 μm.

As x-ray imaging can provide deep tissue imaging due to the deeper penetration of lower wavelengths, microCT was employed for volumetric visualisation of intra-tissue flow across a whole tissue specimen that had been perfused with gold nanoparticles as contrast agents. After specimen perfusion, the tissue was dehydrated and embedded in paraffin, which presents negligible opacity to x-rays and therefore was selected for sample mounting and high-resolution mapping of the contrast agents perfused into the specimen. Tomographic image reconstruction

showed high levels of contrast throughout the perfused specimen with higher levels of signal in specimen periphery and within the stenotic end of the constriction (Fig. 3.3).

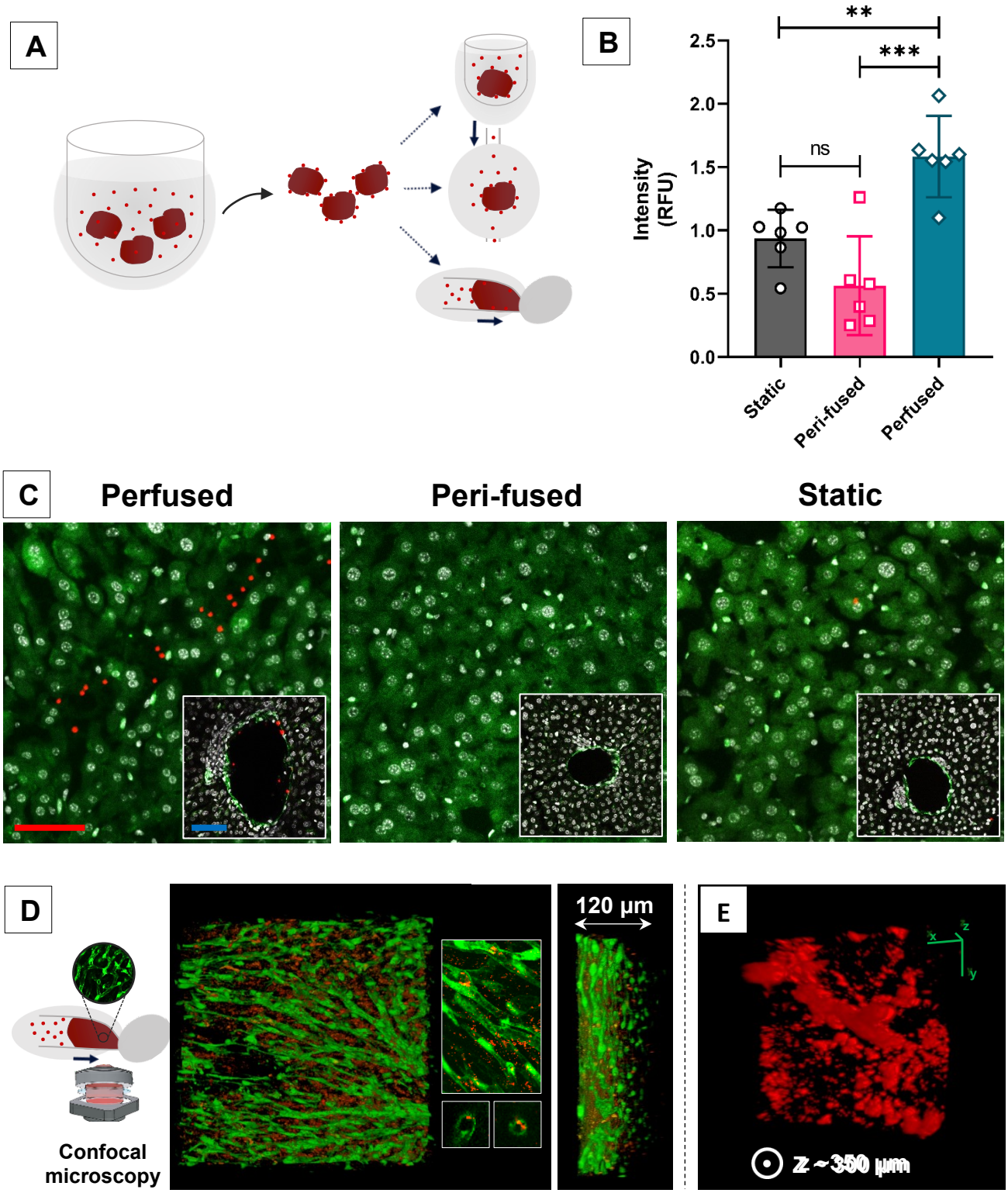


**Figure. 3.2** (A) Experimental protocol for perfusion efficacy assessment using fluorescent particles, including a static culture stage before dividing specimens to different culturing conditions (B) Fuorescence intensity measurement in the lysate of perfused, peri-fused and static samples (C) Fluorescent particle imaging on specimen cryosections·nuclei are white, cytoplasm is psedocoloured green and polystyrene beads are red, red scale bar: 25 µm·Inset: nuclei are white, the vasculature is green (Tie2-GFP) and polystyrene beads are red, blue scale bar: 25 µm (D) Live tracer imaging within a perfused specimen of a Tie2-GFP mouse (representative z-stack from one specimen, 2 specimens used, each coming from a different mouse) (E) Imaging of fluorescent particles within a zebrafish skeletal muscle sample (experimental design: three specimens, each from a different fish). (ns)$p \geq 0.05$, *$p < 0.05$, **$p \leq 0.005$ and ***$p \leq 0.001$.

## 3.4 Discussion

Several currently available systems have attempted to prolong native tissue specimen life *ex vivo* and use them in assays measuring a biologically relevant response to a stimulus. However, diffusion-limited delivery of culture media nutrients and oxygen to cells within sample core has dampened the potential of such technologies. Therefore, demonstrating mass transport within an employed specimen via advection is key in developing a platform that improves tissue preservation. To that end, the developed platform was tested for intra-tissue flow induction efficacy, whilst aiming to visualise which routes can be engaged in specimen perfusion.

Several cell types (Tanaka, Yamato et al. 2006, Piotrowski-Daspit, Nerger et al. 2017, Shi, Graber et al. 2018), but particularly endothelial cells (Wang, Baker et al. 2013, Steward Jr, Tambe et al. 2015)) are known to re-align their orientation to flow direction *in vitro* and *in vivo,* without that being linked to loss of key cell functions or cytotoxicity. On this basis, cell alignment to flow direction was a preliminary indicator that specimen incorporation and perfusion within the developed device was efficacious for intra-tissue flow induction. To confirm that the observed cell morphology was not dominated by compression within the constriction, a compressed control was included in the experimental design. Although cells within the compressed control appeared elongated and had developed some directionality, their appearance was less indicative of cell alignment when compared to the cells in the perfused specimen. This supported the notion that fluid flow had the prime role on cell morphology and orientation in the perfused samples. Moreover, cells in the static and peri-fused cases had similar appearance, with the latter not

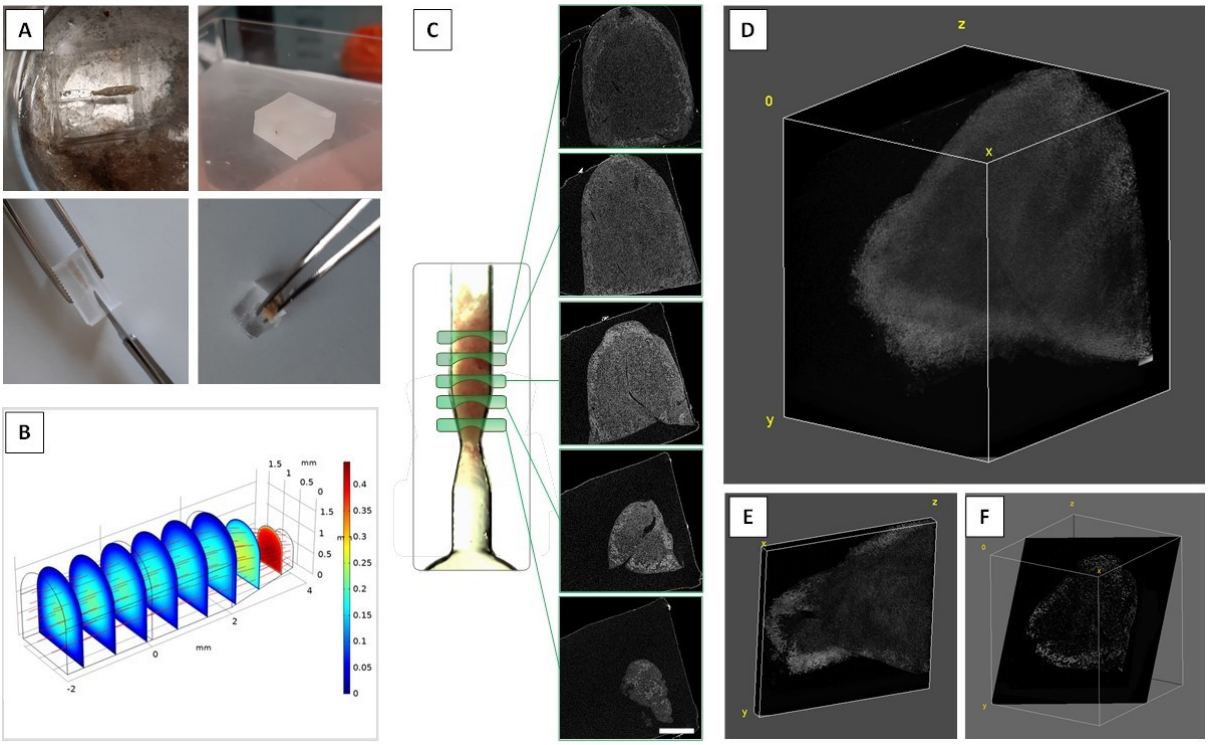


**Figure 3.3** (A) Specimen processing whilst being in the constriction for paraffin infiltration and embedment (B) COMSOL fluid flow simulation within an isotropic porous solid, velocity heatmap range: 0-0.45 m/s (C) Representative microCT sections from different specimen regions (Scale: 0.5 mm) (D) 3D reconstruction of microCT slices for the whole tissue part within the constriction (E) 150-μm thick (median) slice of the 3D view (F) Single-slice, transverse diagonal view through the 3D view.

showing any alignment towards the flow profile. This further supports the absence of peri-fusion and leaks through the tissue-device interface in the perfused condition. Furthermore, the fact that the observed cell patterns were shaped during a 2.5h perfusion suggests that intra-tissue flow was established early within the device and that sufficient specimen sealing of the constriction was achieved during specimen loading. Indeed, if specimen compression due to perfusion were required for the sealing to be formed, cell alignment as a response to flow might not have been noticeable.

Further to the indicators of perfusion, the experimental validation of the platform was focused on studying how mass transport was differentiated across the three culture conditions and whether perfusion in this device could provide significant benefits for substance delivery dynamics. To visualise mass transport to cells, a fluorescent lectin was used, which binds to sialic acid and *N*-acetylglucosaminyl residues on cell membranes. To minimise diffusion's role in WGA transport and primarily focus on advection's effect, a 45-minute perfusion protocol was followed for all three culture settings. For the same purpose, image acquisition was done for all sample categories within specimen core and away from specimen periphery (beyond 200 μm from sample surface), where diffusion could have a drastic effect on dye uptake into the sample.

WGA fluorescence intensity was higher within perfused specimens suggesting delivery within these samples was influenced by fluid flow engagement, as being superior to the amount delivered within samples in the static and peri-fused cases. In other words, the perfused set up was more effective in WGA delivery to the centre of the sample for the same treatment duration when compared with peri-fusion and static tissue culture.

Building on these findings, it was necessary to understand whether the observed mass transport benefit for perfused specimens was also noticeable for larger molecules and particles. To do so, fluorescent particles were added to the culture media that specimens were cultured with in all culture conditions. To quantify total particle number within the employed specimens, tissue samples were lysed after a 1h (in total) culture with particles using sterile pestles and suitable lysis buffer. Despite using carboxylate-modified beads, which were expected to present minimal tissue adherence, the particles still showed a tendency to coat specimen surface. For that reason, all specimens were first incubated for 15min under static conditions with culture media containing particles and were then divided to the three culturing conditions (static, peri-fused and perfused). Particle number was found to be significantly higher within perfused specimens, demonstrating that perfusion in the developed device was a more effective method to deliver 0.2 μm particles within native tissue samples. Notably, this effect was observed despite most of specimen periphery in the perfused case being blocked from access to particles during perfusion. Conversely, sample surface in the static and peri-fused controls remained directly exposed to particles and yet had a much lower overall particle count.

Identifying the routes through which intra-tissue flow was occurring was also necessary to establish the novelty of the developed platform to drive fluid flow through native tissue specimens. Confocal imaging of specimen sections showed fluorescent tracers being present within perfused sample's core, in the extracellular space and importantly, within sinusoids and larger vessels, suggesting the induced intra-tissue flow engaged both sample interstitium and vasculature. Tracer identification within sub-cell-size matrix gaps provided further evidence of sufficient sealing of the tissue-device interface within device constriction, which is necessary for flow to be driven through the various tissue compartments. To improve understanding of perfusion efficacy and unravel any perfusion gradients potentially occurring during specimen culture in the developed device, liver specimens from mice with endothelium with a fluorescent tag were used for live 3D imaging. Live imaging typically enables deeper imaging due to the absence of fixation-induced autofluorescence and artifacts. Imaging of the fluorescent tracers within a perfused specimen revealed widespread particle delivery within the tissue, confirming accumulation of tracers also within vascular routes. However, limited light penetration within murine liver specimens allowed high resolution volumetric imaging only within 120 μm from channel bottom. This was anticipated given the particularly pigment-rich nature of liver tissues, which absorb light significantly in the green channel due to the heme protein. Following the same procedure but with a specimen from zebrafish skeletal muscle (which is significantly less opaque) enabled deeper imaging of fluorescent tracers within a perfused specimen. However, imaging resolution remained poor beyond 300 μm, which prevented full mapping of particle delivery within 3-mm thick specimens.

Attempts to overcome fluorescence imaging limitations were carried out using microCT to perform whole-specimen volumetric imaging of contrast agents that had been added to the perfusate after a period of perfusion acclimatisation. More specifically, mouse liver specimens were perfused for 1h prior to the addition of gold nanoparticles to assure the specimen had fully sealed the constriction and engagement of perfusion routes through the specimen had occurred. After which, gold nanoparticles were added in the upstream region of the channel and perfusion continued for 3h. 3D reconstruction of microCT slices revealed widespread delivery of tracers within the employed sample, with higher contrast agent levels in specimen periphery as well as at the stenotic end of the constriction. It is worth noting that pixel size as a result of electron beam settings and sample characteristics was 28 μm, suggesting that the contrast observed was induced by nanoparticle accumulation within specific regions rather than individual nanoparticles themselves. Widespread delivery of nanoparticles across the specimen suggests that the developed platform and method for *ex vivo* specimen perfusion is likely sufficient to induce intra-tissue flow throughout large 3mm parenchymal specimens. Moreover, the fact that particle delivery across the specimen was observed with tracer incorporation in the perfusate after only an hour of perfusion supports the notion that specimen compression within the constriction as a result of fluid flow does not result in the collapse of perfusable routes for the examined period (4h in total).

Interestingly, contrast in specimen periphery was higher than within most regions in specimen core (Fig. 3.3(C,E,F)). Arguably, this could be attributed to preferential flow through regions close to specimen outer regions and limited perfusion of specimen core. Other possible reasons for higher contrast on specimen periphery and stenotic end could be due to contraction of the tissue regions near the wall resulting in higher percolation through those regions. However, basic computational modelling of culture media flow through a porous body with similar permeability to that of a liver specimen showed that fluid velocity was higher within the specimen core and lower (reaching almost zero) in specimen periphery (Fig. 3.3(B) – for details on the fluid flow modelling see Appendix C). This finding, together with the small dimensions of the used gold nanoparticles (20 nm), support the notion that the less intense contrast observed in specimen core is likely the result of nanoparticle washout due to the higher fluid velocity in that region. Within the stenotic end of the constriction nanoparticle accumulation could be higher due to increased resistance given that there was higher specimen compression, leading to higher nanoparticle entrapment in that part of the specimen and therefore a more intense signal in that region.

Computational exploration of fluid flow through deformable porous media could inform further development of the device. Linking tissue specific Young's modulus to the geometrical characteristics of specimen confinement in the device could be used to account for the varying tissue permeability after specimen entrapment in the constriction-based channel. Additionally, the laminar flow profile of a viscoelastic fluid with properties matching those of the tissue used in the device could inform the development of a more accurate approach to model tissue deformation close to the wall as a result of the friction on specimen surface against the channel wall. Biomechanical effects on cells as a response to advection might influence tissue permeability and perfusion efficacy, however the role of such events in *ex vivo* bulk perfusion remains largely unexplored and modelling of relevant fluid transport systems is lacking.

## 3.5 Conclusion

*Ex vivo* perfusion of native tissue samples (such as those during surgery) has not been demonstrated before, mainly due to the high hydraulic resistance of human tissues and limitations of available modalities for deep tissue imaging in a laboratory setting. Employing fluorescence imaging *in situ* (i.e. when the specimen is perfused within the device) and on specimen cryosections provided evidence which suggest that intra-tissue flow was successfully induced through the vasculature and interstitial space of mouse liver samples in the novel constriction-based device presented in Chapter 2. Volumetric imaging using microCT further supported effective specimen perfusion within the developed device, as demonstrated by contrast agent delivery throughout the sample. The provided data indicate that specimen entrapment and culture within this platform is a suitable method to restore advection through parenchymal tissue specimens, enabling further research on flow's effect on tissue viability and function after isolation. Nevertheless, biological replicates were not included in the above presented experiments, as the variability in liver permeability between animals was considered negligible in comparison to the impact technical

parameters controlling tissue specimen cutting, loading and entrapment have on perfusion. Finally, based on this evidence, the developed device may have potential for *in vitro* drug assays.

# Chapter 4

# Effects of Perfusion on Tissue Viability and Function

## 4.1 Introduction

### 4.1.1 Personalised drug screening

Evidence-based medicine has enabled the development of targeted and reliable medical interventions that have improved patient prognosis for a plethora of conditions. However, especially for multi-parametric, genetically-heterogenous diseases, such as cancer, it is evident that there is no one-drug-fits-all solution, and clinical outcomes can vary significantly even for those with the same type of disease and treatment plan. However, inter-patient heterogeneity, which is limitedly characterised in the clinical setting by a few molecular and histology biomarkers, is rarely considered during first-line treatment. As a result, means for early detection of inherent resistance to taxane- or platinum-based chemotherapy are lacking, and these patients are not currently directed to more effective alternatives. For this reason, there is an emerging need for more patient-specific cancer therapy, accounting for the unique interplay of factors that defines each patient's potential to benefit from a given treatment. In this context, approaches that identify early those patient cohorts that would see no improvement from standard first line interventions (deemed "non-responders") are considered a priority for the research community.

One of the diseases that gain limited benefits from new anti-cancer treatments is ovarian cancer. Ovarian tumours can develop from several different malignant precursors, often outside the ovaries, and rapidly grow beyond their original location (Lengyel 2010). The unknown cell origin of tumourogenesis, the remarkable histopathological complexity of such tumours and their late diagnosis represent major challenges for the clinical handling of ovarian cancer patients. This is illustrated by the fact that ovarian cancer represents the most common gynaecological malignancy, the second most frequent for women and one of the deadlier cancers with less than 20% survival rate 10 years after the original diagnosis. Resistance to chemotherapy is another complication for the treatment of women with ovarian cancer, which limits the options for clinicians to help patients (Cardenas, Alvero et al. 2016).

Ovarian cancer presents significant genetic and phenotypic heterogeneity, which limits the applicability of genetic marker combinations to personalise patient treatment (Jayson, Kohn et al. 2014). High grade serous ovarian cancer (HGSOC), which is the dominant subtype and accounts for up to 80% of all ovarian cancer patient deaths, is almost invariably p53-mutant and positive for CK7, PAX8, WT1 and CDKN2A (Prat 2012, Lisio, Fu et al. 2019). Among these markers, WT1 is considered as the most specific one to differentiate between HGSOC and other types of ovarian cancer (Prat 2012). Several approaches, involving gene sequencing, tumour-specific antigen screening panels and *ex vivo* tissue- or primary cell-based models have been proposed to provide more targeted treatment options for HGSOC patients (Sapiezynski, Taratula et al. 2016). Despite the potential of such technologies, no currently available approach combines high accuracy and sufficient practicality to be applicable for large numbers of patients. Indeed, sequencing data are not available for most patients, whilst patient derived organoids and xenografts usually require laborious processing and long incubation to expand/grow (see 1.2.3). Recently,

organoids have been used to predict patient response to treatment with remarkable success, particularly for advanced colorectal tumours (Vlachogiannis, Hedayat et al. 2018, Ooft, Weeber et al. 2019). Nonetheless, organoids *in vitro* rapidly lose their genetic heterogeneity (Bhaduri, Andrews et al. 2020, Sampaziotis, Muraro et al. 2021), which is critical for the relevance of the drug response they can produce. This progressive genetic "homogenisation" thus limits the predictability of such models and success for use in patient stratification on the basis of potential treatment benefit.

The intrinsic limitations any "bottom-up" model will have for *ex vivo* drug assays, since it requires cell isolation and adaptation to an artificial environment, may be overcome by utilising native tissue specimens. Tissue samples collected during biopsy examination or debulking surgery can be a meaningful alternative for predictive systems of drug response as such specimens comprise most cell types and microenvironment cues influencing drug response (Powley, Patel et al. 2020). Tissue slices have been a standard model in preclinical assessment, but their thickness has been limited to a maximum of approximately 400 μm due to diffusion-limited mass transport in slice-based platforms. However, even within such specimens, oxygen, nutrient and drug gradients are rapidly established a few cell layers deeper than the surface. Therefore, technologies that would enable restoration of advection through an explant would have great potential for improved tissue preservation and more relevant drug response assays. Despite the benefits of advection for explant culture, such technologies remain to be fully tested with patient samples and validated for mimicry of patient response when used for drug screening. Also, the effects of specimen confinement and the induced intra-tissue flow on cell functions and response to treatment remain underexplored.

### 4.1.2 Tissue function and drug response

For a specimen (regardless whether it originates from a tumour or healthy tissue) to be used in a set up where its response to compound is measured, cells' viability and ability to respond to external perturbations need to be preserved *ex vivo*. This ability of cells to rapidly acclimatise to changes in their environment is homeostatically exhibited via a plethora of precisely regulated biochemical reactions that are involved in internalisation, metabolism and elimination of drug molecules. To perform these reactions, cells require continuous flux of various biomolecules, which are provided either passively (i.e. passive diffusion), as in the case of small molecules, such as oxygen, or via active transport, which is required for larger solutes (e.g. glucose or drugs) (Lodish, Berk et al. 2000). Access to substrates for respiration and metabolism depends significantly on the conformation of cell structures, which is regulated by biological, chemical and mechanical elements of the tissue microenvironment. Cell connections with their neighbouring counterparts and the ECM are paramount for cytoskeletal arrangement, which facilitates the formation of receptors and pumps on cell surface that are necessary for physiologic mass transport. Cell surface machinery and unobstructed access to by-product clearance routes, via the interplay of diffusion and advection, preserve physiologic chemical gradients around cells despite waste excretion.

Despite the fundamentality of surface machinery and metabolism for cells, these critical components of cell function are significantly remodelled once cells are removed from their native environment. Indeed, matrix composition and stiffness, cell density, shear stress and oxygen availability *in vitro* often poorly mimic the *in vivo* setting, leading to rapid dedifferentiation of cells and loss of key functions in standard laboratory culturing systems. Liver specimens and hepatocytes, which are substantially susceptible to ischemic injury, are typical examples of quick dedifferentiation and limited preservation *ex vivo* and *in vitro*, which complicate the use of such samples for predictive drug assays. For example, the bile salt export pump (BSEP) and ATP-binding cassette (ABC) drug efflux transporters of hepatocytes are known to be significantly under-expressed *in vitro* and their use in drug assays yields results of poor relevance (Heslop, Rowe et al. 2017). Another significant aspect of cell responsiveness that cannot be fully studied *in vitro* is related to the distinct roles different compartments of tissues have with respect to detoxification. For example, ammonia detoxification is a critical liver function that depends on the compartmentalised distribution of glutaminase and glutamine synthase in different zones within hepatic tissues. Drug-induced injury of periportal hepatocytes can result in net increase of ammonia and reduction of urea, further compromising liver function and rendering cells more susceptible to toxicity. 2D and 3D *in vitro* models poorly mimic such complex functional and concentration gradients, therefore limitedly mimicking liver disease states.

In that context, drug response assays represent a major element in the development of laboratory platforms that involve cells or explants. Response to xenobiotics[1] depends on several key functions of cells and tissue structures, whose preservation or recapitulation is challenging. Therefore, demonstration of cell/tissue response to a known toxicant is widely accepted as convincing evidence of preservation of cell/tissue viability and function. For instance, widespread cytotoxicity induced in an *ex vivo* or *in vitro* model by a chemical with toxic metabolites (such as acetaminophen) demonstrates that the compound has reached cytoplasm successfully via cell surface pumps and that metabolic enzyme levels were sufficient to process the compound into toxic by-products. For this reason, drug response assays have a key role for the validation of tissue-preserving platforms not only due to their potential for testing the benefit or toxicity a compound may have for a tissue, but also for the validation of tissue-based platforms.

### 4.1.3 Cell death mechanisms in ischemia

Decay of cell viability is a key metric for tissue-preserving platforms and/or explant-based drug assays. However, measurement of cell death (i.e. the irreversible disruption of cell membranes and metabolism) remains challenging as mechanism and dynamics of cell degeneration can vary among cells within an explant. After isolation, an ischemic milieu is rapidly established within tissues, which triggers mechanisms that disrupt cell function and tissue structures, ultimately resulting in cell death. Cell death is a multi-step procedure, with the outcome of each stage being determined by the magnitude and duration of the pro-death stimulus. Late stages of cell death are similar,

[1] Xenobiotic is any (mainly chemical) substance that is not physiologically found or produced within an organism.

leading, in most cases, to secondary necrosis and lysis. However, earlier events in death-leading mechanisms can vary significantly with apoptotic, necrotic and autophagic cell death representing the main types occurring during ischemic conditioning of tissues. Recently, further distinction among these three standard types has been enabled as more specialised types of cell death have been identified (Galluzzi, Vitale et al. 2018).

Nutrient deprivation, hypoxia, materials leaking from damaged cells and the formation of reactive species, are the main factors triggering pro-death processes within an explant's cells. However, each of these factors and/or combination can result to a different type of cell death. Apoptosis is arguably the type of cell death with the most triggers, such as growth factor withdrawal, DNA damage, ROS and ER stress. Apoptotic death is intrinsically mediated by BCL2, BAX and BAK1 proteins, resulting in irreparable MOMP, cytosolic release of mitochondrial proteins and cleavage of executioner caspases 3 and 7. Hypoxia, ischemic cues and starvation can also trigger (mainly non-selective) autophagic cell death, where cell constituents are engulfed in autophagosomes and degraded by resident hydrolases. The Atk gene family has a key role in autophagic signalling, however autophagy can proceed independently of Atk regulation in several tissues (such as fat) (Sadoshima 2008, Altman and Rathmell 2012, Doherty and Baehrecke 2018). Autophagy-dependent Autosis is a recently identified cell death form, characterised by the involvement of the $Na^+$,$K^+$-ATPase pump and morphological changes within cell (Liu and Levine 2015) compartments, such as perinuclear space ballooning and fragmentation of ER (Liu, Shoji-Kawata et al. 2013).

Reactive species and disruption of solute gradients within cells can lead to apoptosis- and autophagy-independent cell death. Under favourable iron concentrations and glutathione depletion, ROS generation and lipid peroxidation within the cell microenvironment can result to ferroptosis, which manifests through a necrotic morphotype (Cao and Dixon 2016). Mitochondrial Permeability Transition (MPT)-driven necrosis is an alternative, more catastrophic kind of cell death, which is induced by severe intracellular ROS and cytosolic $Ca^{2+}$ overload. Notably, permeabilisation of the inner mitochondrial membrane differentiates this necrotic cell degeneration mechanism from apoptosis, which occurs in the case of mitochondrial outer membrane permeabilisation MOMP (Loor, Kondapalli et al. 2011). Reactive nitrogen species typically generated during ischemia, can lead to Parthanatos, a distinct type of cell death triggered by the hyperactivation of the DNA damage response machinery (primarily PARP proteins). Also, recently, glucose deprivation has been shown to result in loss of integrins and cell detachment from the ECM, and eventually internalisation and degradation of the detached cell by adjacent cells. This type of cell cannibalism is termed Entosis. Finally, intracellular materials are often released during various death-leading events and mechanisms, activating the involvement of immune cells in cell death. For example, ATP leaking from cells with compromised membranes can attract macrophages and dendritic cell precursors, exhibiting an immunostimulatory effect, with the potential to result in immunogenic cell death.

Within the heterogenous ischemic environment, cells experience varying levels of oxygen and nutrient deprivation, and build-up of metabolic byproducts and reactive species with respect to their position from explant surface. As extreme solute gradients are rapidly established between explant's core and surface, cells may die via different mechanisms based on their location within the specimen. Similarly, the varying environmental cues within a sample can also alter the dynamics of cell death even for cells dying due to the same combination of triggers. Eventually, under ischemia, there is a progressively growing mosaic of degenerating cells within the explant, which will be dying through different death mechanisms and at dissimilar rate. This increases the necessity for a combination of generic cell viability and death markers to study tissue preservation *ex vivo*.

### 4.1.4 Markers of viability, cell death and drug response

Ischemia limits the timeline for native tissue sample use in drug response assays via several degenerating mechanisms. Obstruction of advection (*in vivo* and/or due to explantation) leads to the occlusion of several small size vessels, primarily capillaries (no reflow phenomenon – see 1.2.2), whilst T-cell extravasation and swelling within vascular routes increase further the number of obstructed vessels within the explant. In parallel, these vessel-blocking phenomena result in higher levels of edema within the tissue sample and increase the rate of explant degeneration within culture. Furthermore, the ischemic milieu aggravates the dedifferentiation of explant cells in culture, often at a significantly quicker rate than that viability reduces at. As most drug-response assays depend on markers of tissue viability and function, progressive tissue degeneration in culture can interfere with the cytotoxic effect induced by a compound and reduce assay validity. Moreover, cells within an explant experience concurrent death-promoting stimuli (Gujral, Bucci et al. 2001, Unal-Cevik, Kılınç et al. 2004, Baines 2011, Puyal, Ginet et al. 2013), which complicate the differentiation between different cell death types and the identification of suitable markers and time-windows to study loss of viability.

On a tissue level, explant viability, cytotoxicity and molecular fingerprint can be evaluated via various marker quantification approaches (Kepp, Galluzzi et al. 2011). An explant can be lysed after culture via enzymatic means, suitable lysis buffers and/or mechanically to measure the total quantity of intracellular markers in the lysate and normalise with total protein of the sample. In this case, the marker of interest is most often an intracellular enzyme necessary at relatively constant levels for a vital cell function. Examples of such enzymes that have been successfully used as markers of cell viability (in specimen lysate) are LDH and intracellular proteases. Similarly, such enzymes have been used as relative markers of cell death when quantified in cell supernatant or in the media used in a tissue culture. In a different approach, substances involved in active cell metabolism are widely used as indicators of cell viability. ATP is the main compound that has been utilised as a measure of the number of viable cells within an explant, as ATP depletion and degeneration of redox homeostasis are fundamental elements of all cell death pathways.

Cell-permeable, redox sensitive compounds (such as resazurin and MTT) that can be reduced to a fluorescent or coloured product by elements of active cell metabolism are also used as a measure of aerobic respiration, primarily when endpoint assays are avoided. Also, negatively charged, cell-impermeable substances that depend on a cell-permeable intermediate electron-coupling agent (for instance MTS, XTT and WST-1) are typically used in assays of metabolic activity of cells (Kepp, Galluzzi et al. 2011, Powley, Patel et al. 2020). Compounds that can bind to intracellular components (such as the DNA) and are normally unable to cross the intact cell membranes of viable cells have been used to assess the number of dead cells within an un-fixed tissue sample, with Propidium Iodide and Ethidium bromide being noticeable examples of that group (Kepp, Galluzzi et al. 2011). Despite the several benefits of these compounds for the determination of cell viability or death in a culturing system, such as the low-cost, technical simplicity and low cell toxicity, these markers come with limitations. Indeed, such assays are generic, providing limited insights about the type of death a cell undergoes. Additionally, a meaningful measurement can only happen after sufficient incubation time has passed so that the molecules have diffused deep in the explant and the redox conversion and/or attachment to DNA has progressed. The long duration of this process can often limit measurement accuracy and the reliability of results, particularly for thick (>1mm) tissue specimens.

In the clinic, paraffin sections of tissues and staining with Haematoxylin and Eosin (H&E) are the gold standard for identifying the extent of necrotic and apoptotic processes within a specimen. Alternatively, immunohistochemistry and radio- or chemical labelling of cell epitopes represents a common approach for *in situ* visualisation of specific molecules involved in various metabolic and death-leading processes. Most of these molecules have specificity for one cell death mechanism, enabling differentiation between different types of cell degeneration within a sample (Li, Wu et al. 2014). For apoptosis, commonly used markers are activated (i.e. cleaved) caspases and poly (ADP-ribose) polymerase (PARP) proteins, and BCL proteins. ATK and LC3 proteins, and Beclin-1 are widely used as markers of autophagic cell death, whilst RIP proteins have been used for the identification of necroptotic cell death. Beyond protein markers, labelling of degenerated structures within cells has been a common approach to evaluate cytotoxicity. For example, probing the 3′- hydroxyl termini of the double strand-breaks of DNA that can lead to cell death is a standard assay (termed Terminal deoxynucleotidyl transferase dUTP nick end labeling – TUNEL) linked to apoptosis (Cannan and Pederson 2016). Recently, improved understanding of metabolic and death-resulting pathways has provided several emerging biomarkers for various stages and types of cell death, increasing the means available to study explant degeneration and drug response.

Maintenance of cell viability after tissue isolation is critical for the development of any cell-or tissue-based drug response assay. However, preservation of cell identifying features is also paramount. Primary cell types can be cultured for days to weeks without noticeable loss of viability although several functions are lost soon after cell isolation and acclimatisation *in vitro*. These functions are regulated by cytoskeletal arrangement, cell connections to the matrix and the presence of multiple cell types in the original environment of the tissue. This rapid

dedifferentiation of some cell types in monolayer cultures is a significant limitation for typical 2D drug screening. For this reason, preservation of several functional marker levels (with respect to the tissue of origin/interest) is another significant aspect of explant-based platform validation. For instance, endothelial cells are expected to produce eNOS and contain high levels of nitric oxide, whilst hepatocytes need to maintain high levels of albumin, urea, glutathione and CYP enzymes to behave in an *in vivo* relevant manner when treated with a drug. In the context of cancer, proliferation markers such as Ki67 (Scholzen and Gerdes 2000) are often used to demonstrate that cells have maintained their high division capability. Also, several tumour markers are used to demonstrate that *in vitro* cultured cancer cells or tumour slices share the same genetic features with the tumour they originate from.

In that context, the main objective for this chapter was to assess to what extent restoration of advection within tissue specimens improves viability and drug delivery in tissue culture. Advection's effect on specimen viability and intra-tissue delivery of compounds was assessed with histology and viability markers. Longer preservation of native tissue samples due to perfusion would expand the currently possible timeline for *ex vivo* experimentation with explants, whilst advection would enable wider, more *in vivo*-relevant delivery of compounds to the employed tissue. This could be the basis for more accurate and clinically applicable, personalised drug testing assays.

## 4.2 Methods

### 4.2.1 Platform set up

PDMS-based devices for individual perfusion of native tissue specimens were fabricated as described in 2.3.2.2. Each device had been connected to Teflon tubing leading to a hose bard adapter, sealed with PDMS and were left to cure at 65˚C overnight. Sets of three devices had been placed in modified pipette tip containers that had an opening for each device's tubing. The area between the opening and the tubing was sealed with two strips of autoclave tape. For biological experiments, all devices and fluidic parts used for the perfusion set up had been first sterilised following standard autoclavation (121˚C, 20 min). After autoclavation, all sterilised components were placed in a 65˚C oven to dry overnight.

On the day of the experiment, each device was connected to a three-way valve and two 1 ml syringes filled with sterile PBS as described in 2.3.5. Once a device had been connected to the fluidic equipment (valve, syringes) the syringes were used to fill the device with PBS up to edge of the open-air reservoir. Then, once the culture media to be used for perfusion had equilibrated to 37˚C in a waterbath, the PBS in device reservoir would be removed and replaced with sterile culture media. Using the two syringes connected to the valve, fluid would be withdrawn until each device reservoir would have roughly less than 1/5 of each original amount so that PBS in the device and tubing would have been exchanged for culture media. Then, 1 ml of equilibrated culture media would be used to refill the inlet reservoirs to their original volume using a pipette.

The original explant or organ would be divided to 3-mm specimens and, using sterile tweezers, a tissue sample would be submerged within each device reservoir and would be directed to the beginning of the device channel. Each specimen was directed to each device's constriction and valve conformation was changed to shut off flow towards the specimens so that they remain immobilised. The same arrangements and process were followed for peri-fused devices. Similarly, for statically cultured specimens, wells of a 24-well plate were originally filled with 1.5 ml of culture media. Once a tissue sample was placed in each well, the media was exchanged for fresh media before placing the plate and the tip containers with the perfused and peri-fused devices in a standard tissue culture incubator, with each (perfused or peri-fused) device's tubing coming off outside the incubator. To initiate perfusion, one syringe from each device was connected to the syringe pump adapters on the syringe pump and the valve was opened so that flow from the syringe connected onto the pump towards the specimen was allowed. Then perfusion at 100 nl/min was initiated.

### 4.2.2 Tissue culture and processing of mouse liver specimens

Tissue samples were taken from C57BL/6J (Charles River Ltd, UK) male mice (12 specimens per culture condition from two mice (i.e. six specimens per culture condition per mouse))., aged 8-18 weeks at the time of culling. All mice were housed in clear individually ventilated cages at 21ºC, with a 12h light-dark cycle, where food and water were supplied *ad libitum*. Mice were culled via neck dislocation and decapitation as a secondary culling method to confirm death. As soon as possible after culling, the mouse liver was resected within a biological laminar flow cabinet and was washed 3 times with sterile and filtered, ice-cold KH buffer (Sigma-Aldrich Company Ltd, UK). Using a biopsy punch (Integra LifeSciences Corporation, USA), 3-mm thick mouse liver specimens were punched out of the liver lobes, washed once with KH buffer and placed in a falcon tube with 30ml buffer on ice. All experiments were done under the authority of a UK Home Office project license.

All reagents were purchased from Life Technologies Ltd, UK unless otherwise stated. Culture media for preservation experiments with mouse liver specimens was DMEM:F12[2], supplemented with 10% Fetal Bovine Serum (FBS), 1% Glutamax™[3], 1% Insulin-Transferrin-Selenium (ITS) mixture, 1% Penicillin-Streptomycin, 1‰ Antioxidants (A1345 - Sigma-Aldrich Company Ltd, UK), 10 μM Dexamethasone (Sigma-Aldrich Company Ltd, UK) and 15mM N-2-hydroxyethylpiperazine-N-2-ethane sulfonic acid (HEPES).

### 4.2.3 Tissue culture and processing of mouse omentum specimens

A syngeneic, immunocompetent, transplantable mouse model ovarian was used to study the device's potential in the preservation of ovarian tumour samples. Briefly, one *Trp53* $^{-/-}$ clone and two *Nf1* $^{-/-}$;*Trp53* $^{-/-}$ (NF1 clones: 1.20

[2] 1:1 mixture of DMEM and Ham's F-12 media that utlises a sodium bicarbonate buffer system
[3] is a 200 mM L-alanyl-L-glutamine dipeptide in 0.85% NaCl that minimises the build-up of ammonia in culture (non-spontaneous breakdown to ammonia) often caused by standard media supplementation with L-glutamine

and 1.23) clones of ID8 cells were generated *in vitro* via Crispr-Cas9 gene editing (Walton, Blagih et al. 2016, Walton, Farquharson et al. 2017). $5x10^6$ cells of one clone were inoculated intraperitoneally to each one of three 6-8 week old female C57Bl/6 mice (Charles River Laboratories, UK) cancer. Mice were monitored regularly and killed upon reaching UK Home Office limits. Immediately after culling, the whole mouse omentum was resected and directly placed in ice-cold PBS until the experiment. All experiments complied with the UK welfare guidelines (Workman, Aboagye et al. 2010) and were conducted under specific personal and project license authority.

Culture media for preservation experiments with mouse omentum specimens was DMEM, supplemented with 4% FBS, 2 mM glutamine, 1% ITS and 1% Penicillin-Streptomycin. After a 48h culture in a 5% $CO_2$ tissue culture incubator, all specimens were recollected, washed once with ice-cold PBS and then placed in freshly made 4% PFA for 48h at 4ºC. After this step, specimens were transferred to 70% ethanol and were kept at 4ºC until tissue processing for paraffin embedment.

### 4.2.4 Tissue culture and processing of human omental tumour specimens

At the time of Maximal-Effort Cytoreductive Surgery (MECS) for advanced primary high-grade serous ovarian cancer (HGSOC), ovarian tumour and tumour nodules from within the peritoneum were collected and immediately transferred to the laboratory for culturing. Upon nodule collection, the explant was directly placed in fresh, ice-cold PBS (pH=7.4) and placed on ice until the set up was ready. The project was performed under the Hammersmith and Queen Charlotte's and Chelsea Research Ethics Committee approval 05/QO406/178 and supplied by the Imperial College Healthcare NHS Trust Tissue Bank, following full patient consent.

The culture media used for viability preservation and drug response experiments with human omental tumours was RPMI 1640 supplemented with 20% FBS, 1% Penicillin–Streptomycin, 2 mM sodium pyruvate (Sigma-Aldrich Company Ltd, UK) and 2.5 µg/ml insulin (Sigma-Aldrich Company Ltd, UK). After a 48h culture in a 5% $CO_2$ tissue culture incubator, all specimens were recollected, transferred to cryovials and snap frozen using liquid nitrogen. Specimens were kept at -80ºC until sectioning.

### 4.2.5 Inhibiting cell metabolism

To evaluate the responsiveness of the tissue specimens to external stimuli, a metabolic poison cocktail comprising 2-Deoxy-D-glucose (2-DG), (2E)-3-(3-Pyridinyl)-1-(4-pyridinyl)-2-propen-1-one (3PO) and sodium azide ($NaN_3$) was used, as described elsewhere (Reina-Torres, Wen et al. 2017). 2-DG, which is a glucose analogue, competitively inhibits hexokinases and the progression of glycolysis, while 3PO blocks the activity of the 6-Phosphofructo-2-kinase/fructose-2,6-bisphosphatase (PFKFB) isoenzyme that is involved in the phosphorylation of fructose-6-phosphate. $NAN_3$ inhibits electron transport within mitochondria, therefore disrupting oxidative phosphorylation.

Sets of four specimens per condition (perfused, peri-fused or static), all isolated from the same animal, were treated with the metabolism-inhibiting cocktail (11mM 2-DG, 4mM $NAN_3$, 0.1mM 3PO in PBS), whilst an isosmotic vehicle (11mM D-glucose, 4mM NaCl, 0.2% DMSO in PBS) was used for their metabolically active counterparts. After specimen incorporation to each culture condition, specimens were treated with either mixture for 2h. After this stage, all specimens were collected, washed three times with ice-cold PBS and then either processed for ATP and total protein quantification or fixed for 24h to be cryosectioned for H&E, Oil Red O and PAS staining.

### 4.2.6 ATP, LDH and total protein quantification

At the end of the culture period, all specimens (static, peri-fused and perfused) were collected and washed three times with ice-cold PBS (without $Ca^{2+}$ or $Mg^{2+}$) on ice. Subsequently, each specimen was placed in an Eppendorf tube with 0.5 ml of ice-cold lysis buffer (10 mM Tris pH=7.5, 2 mM NaCl, 20 mM EDTA, 2 mg/ml Triton X-100, with 0.25% proteases inhibitors (P2714) (all purchased from Sigma-Aldrich Company Ltd, UK) in diethyl-pyrocarbonate (DEPC)-treated water (Life Technologies Ltd, UK). Each specimen was homogenised manually using autoclaved pestles and then each Eppendorf tube was centrifuged for $13.3\times10^3$g for 15 min at 4ºC. After centrifugation, the supernatant from each tube was transferred to a new vial, and 1:10 (for LDH and protein quantification) and 1:100 (for ATP quantification) dilutions were produced using lysis buffer for each sample.

ATP levels were quantified using a luminescence-based ATP-determination kit (A22066 - ThermoFisher Scientific, USA) following manufacturer's instructions. In brief, 10 µl of specimen lysate in a 1:100 dilution in lysis buffer was mixed with 90 µl of assay reagent in a well of a 96-well plate. After a 30-min-incubation at ambient temperature, luminescence was measured.

LDH retention in specimen lysate was measured using a colorimetric determination kit (G1780 – Promega, USA) following manufacturer's instructions. In brief, 50 µl of specimen lysate in a 1:10 dilution in lysis buffer was mixed with 50 µl of assay reagent in a well of a 96-well plate and. After a 30-min-incubation at ambient temperature, 50 µl of 1M acetic acid were added to the mixture and the absorbance signal was measured within 20 min.

To normalise for the quantity of the tissue, total protein per sample was measured using a BCA-reaction based kit (No. 23227 – ThermoFisher Scientific Ltd, UK) following manufacturer's instructions. In brief, 25 µl of specimen lysate in a 1:10 dilution in lysis buffer was mixed with by 200 µl of assay mixture (reagent A to B at a ratio of 1:50) in a well of a 96-well plate. The plate was place on an orbital shaker at low speed for 1 minute and then was left to incubate at 37ºC for 1h. After that, the plate was left to acclimatise at ambient temperature for 5min before the measurement of absorbance.

Luminescence and absorbance (at 562 nm for the BCA assay and at 490 nm for the LDH quantification) for all assays were measured using a Varioskan LUX Multimode Microplate Reader (Thermofisher Scientific Ltd, UK).

### 4.2.7 Immunostaining for cleaved-caspase 3, Ki67 and Wilms Tumour protein

Immunostaining for cleaved-caspase 3 (cC3) on specimen cryosections was used to identify cells dying via apoptosis and other death mechanisms that involve caspase activation (autophagy (Tsapras and Nezis 2017) and necrosis (Yuan, Najafov et al. 2016)). For cryosections, sectioning was performed using a cryostat, with the chamber temperature set at -20ºC and sections were stored at -80ºC until further processing. For staining, sections were first left to acclimatise to ambient temperature for 20 minutes and were then fixed for 10 minutes with 4% PFA at ambient temperature. Next, sections were washed three times with PBS (with $Mg^{2+}$ and $Ca^{2+}$) and they were incubated with 10% normal goat serum (NGS), 0.25% TritonX-100 in PBS (with $Mg^{2+}$ and $Ca^{2+}$) to block non-specific binding and permeabalise the tissue. After this step, sections were incubated at 4ºC overnight with rabbit anti-cleaved-caspase 3 primary antibody (9664T – Cell Signaling Technology, Inc., USA), at a 1:200 dilution in 10% NGS, 0.25% TritonX-100 in PBS (with $Mg^{2+}$ and $Ca^{2+}$). Then, sections were washed three times with PBS and were treated with 0.3% $H_2O_2$ to block endogenous peroxidases. Following this step, sections were washed once with PBS and were then incubated with goat anti-rabbit secondary HRP antibody (ab236469 – Abcam, Ltd, UK) for 20 minutes at ambient temperature. After this, sections were washed three times with PBS and were then incubated with DAB chromogen (ab236469 – Abcam, Ltd, UK) for 1 minute. Finally, specimens were washed with PBS and were then stained with Hematoxylin for 1 minute. Then sections were washed for 5 minutes on a rack, under running lukewarm tap water, Finally, sections were dried and mounted with coverslips and a 90% glycerol, 0.2 g/L $NAN_3$ mounting medium. Slides were sealed using clear nail polish to preserve staining until imaging.

cC3 immunostaining was also performed on paraffin sections of mouse omental tumours, Tissue specimens were dehydrated with ethanol, and Histoclear before being infiltrated with paraffin in a 65ºC oven overnight. 10µm sections were cut with a standard microtome and sections were stored at ambient temperature until further processing. Before staining, sections were first left to incubate in a 65ºC for the paraffin to melt and were then deparaffinised and rehydrated. For immunostaining for cC3 a similar protocol to the one above for cryosections was followed, with the addition of an antigen retrieval step instead of the PFA fixation. Antigen-retrieval was heat-induced (95ºC), using a pH=6 citrate buffer (Roche Diagnostics Ltd, UK).

Paraffin sections of mouse omental tumours were also stained for Ki67 and Wilms tumour protein (WT1). Ki67 is a protein located in cell nucleosome during all active cell cycle phases ($G_1$, S, $G_2$ and mitosis) but it is absent from quiescent cells ($G_0$), therefore being widely used as a proliferation marker (Scholzen and Gerdes 2000). For Ki67 staining the same process for staining paraffin sections was followed as above using a Ki67 targeting primary antibody. WT1 is a transcription factor (located in the nucleosome) regulating cell proliferation and survival that has been linked primarily with ovarian cancer among various malignancies. WT1 staining was performed following the same protocol as for cC3 and Ki67 staining of paraffin sections, using a recombinant anti-WT1 antibody (ab89901 – Abcam Ltd, UK) at a 1:250 dilution.

After immunostaining, all sections were counterstained with Haematoxylin as described below and were mounted with coverslip using a few drops of Dibutylphthalate-Polystyrene-Xylene (DPX) mounting medium (Sigma-Aldrich Company Ltd, UK).

### 4.2.8 Staining with Hematoxylin and Eosin, Periodic acid–Schiff's reagent and Oil Red O

Cell morphology was imaged using Haematoxylin and Eosin (H&E) staining, which was performed on paraffin sections of mouse omental tumours and cryosections of mouse liver as previously described. Briefly, cryosections were fixed with 4% PFA for 10 minutes and then washed with PBS before being stained with Haematoxylin for 3 minutes. Then, sections were differentiated in 70% Ethanol in 1M HCl for 5 seconds. After this, sections were washed with lukewarm tap water for 5 minutes and then sections were stained with Eosin for 1.5 minute. Sections were then washed for 1 minute in tap water and were then dehydrated in absolute ethanol followed by Histoclear. Finally, sections were mounted using a glycerol-based mounting medium.

Staining of tissue sections for cell lipid content was performed using the Oil Red O reagent, as previously described. 10-μm cryosections were fixed with PFA and were then incubated with 60% isopropanol (Alfa Aesar, UK) for 5 minutes. After this step, sections were incubated with Oil Red O reagent for 20 minutes, which was produced fresh an hour before the staining, at a 3:2 ratio with distilled water and filtered with a 0.45μm pore size filter, after vortex mixing. Then, sections were washed three times with PBS and were counterstained with Haematoxylin for 1 minute (without differentiation). Sections were then washed in running lukewarm tap water for 5 minutes and were mounted with a coverslip and a glycerol-based mounting medium.

The Periodic acid–Schiff's (PAS) staining was used to visualise the carbohydrate content of cells as performed previously. In brief, sections were fixed with PFA, washed with PBS and were then oxidised with 0.5% periodic acid for 5 minutes. Sections were then washed once for 5 minutes with distilled water and were then incubated with Schiff’s reagent for 20 minutes. After this step, sections were washed once with distilled water and were then stained with Haematoxylin and mounted.

### 4.2.9 Statistics and Image processing

The data from ATP and LDH quantification was analysed with Welch's t-test with the Banferoni correction, apart from the data from the experiment with the metabolic poison for which a Student’s t-test was sued. Reported values are presented as the mean ± the margin of error at a 95% confidence level apart from the ATP quantification for the 2h experiment with and without treatment with metabolic inhibitors, where error was set as equal to standard deviation (SD). Graphs were produced using GraphPad Prism 9.0 (GraphPad Software, Inc., USA). Image processing was done using ZEN 3.3 (Blue edition) (ZEISS, Germany) and ImageJ (NIH) (Schindelin , Schneider, Rasband et al. 2012).

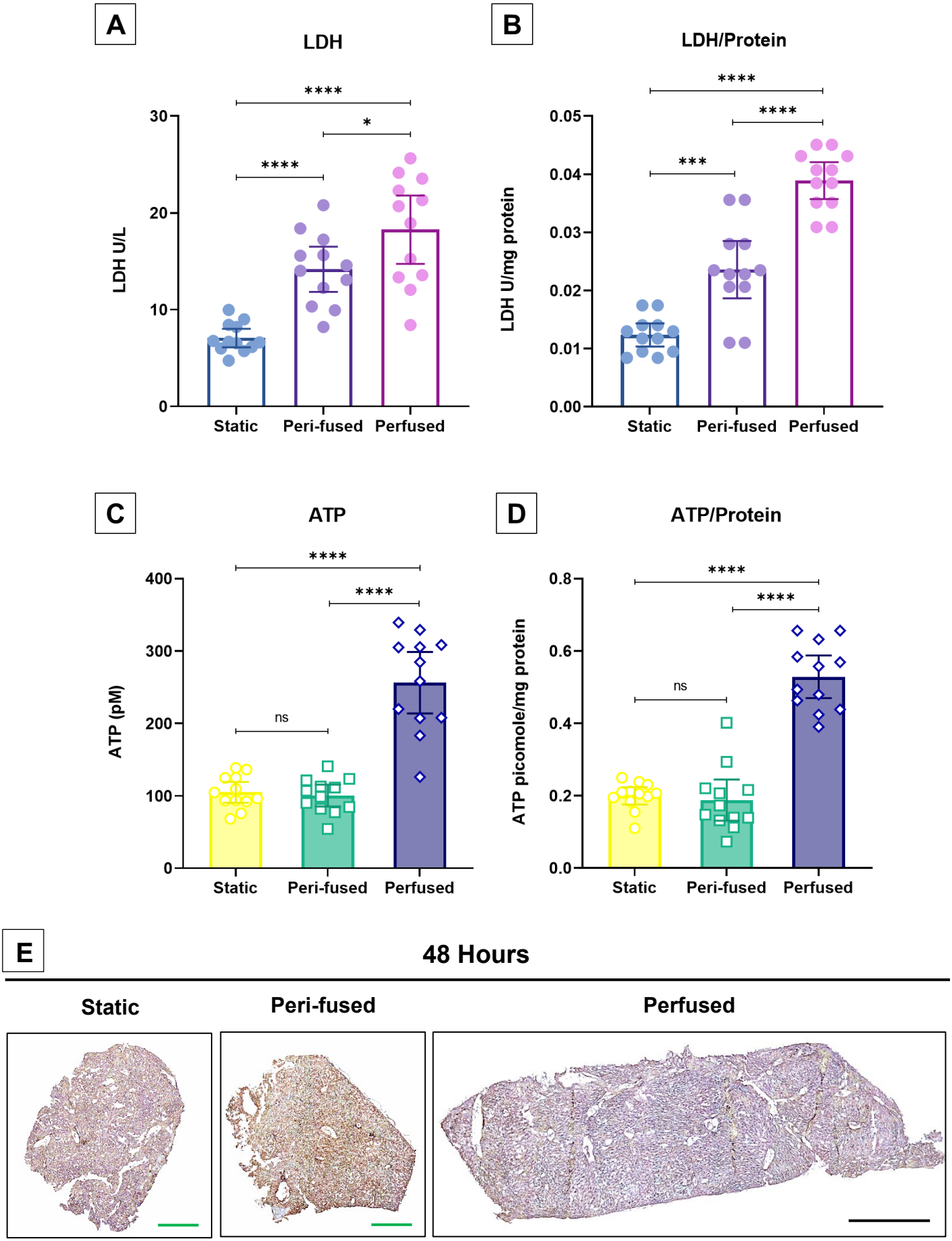


**Figure 4.1** Viability of murine liver explants after 48h of perfusion, peri-fusion or static culture as measured by intracellular retention of (A) total LDH per specimen, (B) normalised LDH to specimen total protein, (C) total ATP per specimen and (D) normalised ATP to specimen total protein. Each datapoint is the average of three technical replicates analysed from each specimen's lysate (N=2, n=6) (E) Cleaved caspase 3 imunolabelling (brown – DAB chromogen) and Hematoxylin staining (blue) on perfused, peri-fused and static specimen cryosections after a 48h culture (Green scale bar: 1 mm, black scale bar: 1 mm). (ns)p ≥0.05, *p < 0.05, **p ≤ 0.005, ***p ≤ 0.001 and ****p < 0.0001.

## 4.3 Results

To examine whether the developed device and method can improve the preservation of native tissue specimen viability *ex vivo*, 3-mm mouse liver specimens were cultured for 48h under static, peri-fused or perfused conditions. LDH quantification in specimen lysate after culture showed significantly higher levels of the metabolic enzyme in the perfused samples compared to peri-fused and static specimens. Moreover, peri-fused samples had higher levels of LDH than static controls. The observed differences in LDH levels were significant both for absolute (perfused versus static: $p<0.0001$, 95% CI: 11.20±3.58 U/L; perfused versus peri-fused: $p=0.047$, 95% CI: 4.10±4.22 U/L; static versus peri-fused: $p<0.0001$, 95% CI: 7.10±2.58 U/L – Fig. 4.1(A)) and normalised with total protein values (perfused versus static: $p<0.0001$, 95% CI: 0.026±0.003 U/mg protein; perfused versus peri-fused: $p<0.0001$, 95% CI: 0.015±0.004 U/mg protein; static versus peri-fused: $p=0.00037$, 95% CI: 0.011±0.006 U/mg protein – Fig. 4.1(B)). Similarly, ATP quantification showed higher ATP levels in perfused samples than in peri-fused and static specimens, whilst no significant difference was observed between static and peri-fused samples (perfused versus static: $p<0.0001$, 95% CI: 151±47 pM; perfused versus peri-fused: $p<0.0001$, 95% CI: 156±48 pM; static versus peri-fused: $p=0.63$ – Fig. 4.1(C)). Normalised ATP levels with total protein were in agreement with the absolute ATP value data (perfused versus static: $p<0.0001$, 95% CI: 0.33±0.07 picomole/mg protein; perfused versus peri-fused: $p<0.0001$, 95% CI: 0.34±0.09 picomole/mg protein; static versus peri-fused: $p=0.68$ – Fig. 4.1(D)). Immunostaining for cleaved caspase 3 on specimen cryosections showed lower levels of caspase 3-dependent degeneration, further suggesting lower cytotoxicity and improved preservation of perfused samples versus peri-fused controls after a 24h culture (Appendix A, SF3) and against peri-fused and static specimens after 48h in culture (Fig. 4.1(E)).

To assess the effects of quicker and wider mass transport within perfused native tissue specimens via advection, perfused, peri-fused and static samples were treated with a cocktail of metabolic inhibitors for 2h and compared with samples perfused with vehicle control for the same duration. Treatment with the metabolic poison led to significant reduction in intracellular levels of ATP in the specimens that were perfused with the inhibitor cocktail versus perfused specimens with vehicle control ($p=0.044$). On the contrary, peri-fused and static samples had no significant difference between their poison-treated and control-treated counterparts (peri-fused: $p=0.49$, static: $p=0.99$) (Fig. 4.2(A). PAS staining showed lower levels of carbohydrate content within perfused samples treated with the metabolic inhibitors, whilst untreated perfused samples had maintained high levels of carbohydrates, similar to those within fresh specimens (Fig. 4.2(B)). No noticeable differences were observed in the treated and untreated cases of peri-fused and static samples (Fig. 4.2(B) - see Appendix C3). Intracellular lipid content, visualised by Oil Red O staining, showed a greater number of larger lipid droplets within specimens perfused with the metabolic poison, which are more indicative of nutrient deprivation and lipid peroxidation under stress (Xu, Donepudi et al. 2013, Jarc and Petan 2019). Nonethelss, perfused samples with vehicle control maintained a

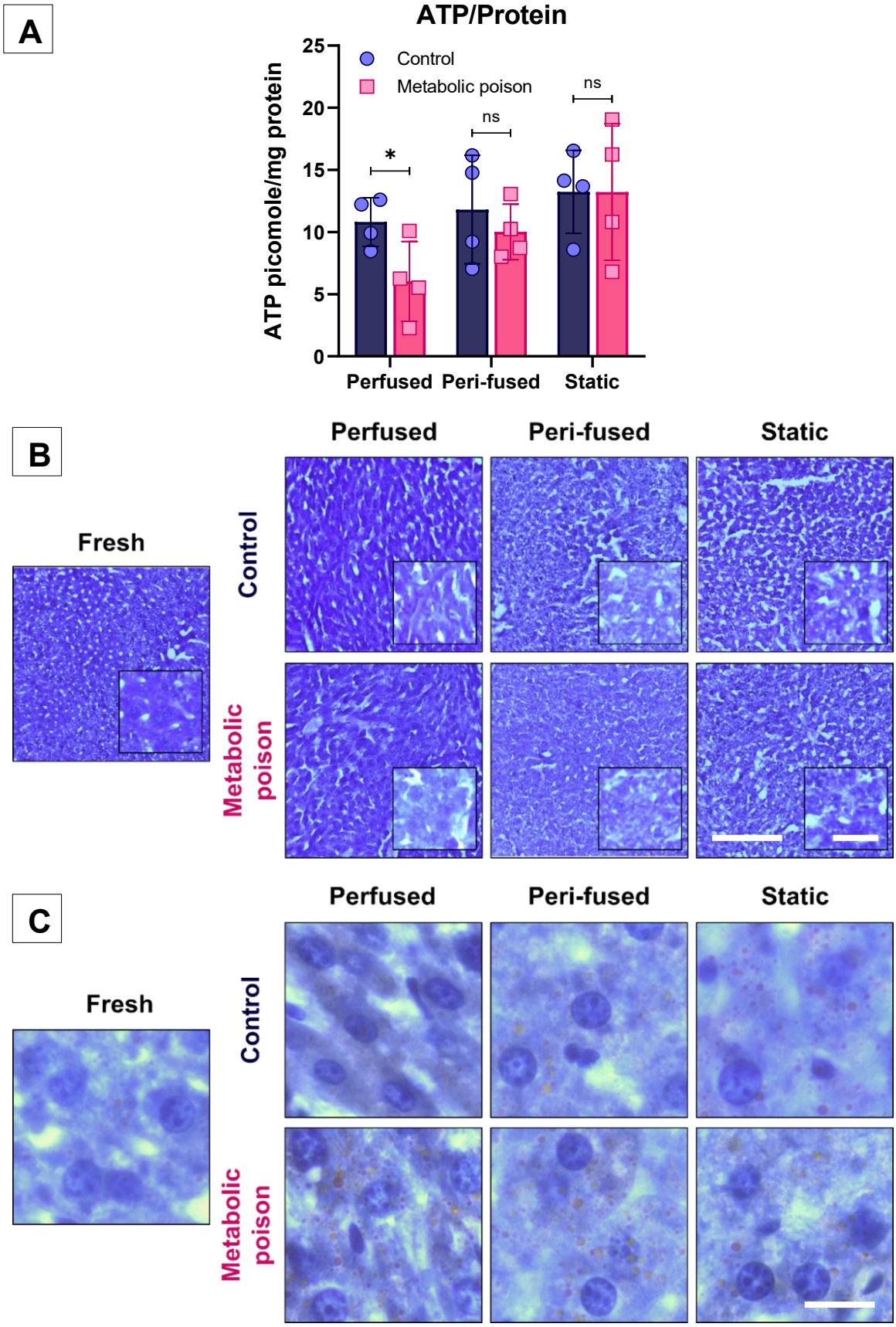


**Figure 4.2** Tissue response to a 2h-treatment with a cocktail of metabolic inhibitors (A) ATP levels in specimen lysate, demonstrating perfusion efficacy to induce inhibition of metabolism in liver specimens. Each datapoint is the average of three technical replicates analysed from each specimen's lysate (N=1, n=4) (B) Periodic-Acid-Schiff's (PAS) (purple) and Haematoxylin (blue) staining showed lower carbohydrate levels in perfused specimens with the metabolic inhibitors *versus* controls (Scale bar:100 µm, Inset scale bar: 25 µm) (C) Oil Red O (red) and Haematoxylin (blue) staining showed larger lipid droplets within cells in specimens perfused with the metabolic poison (Scale bar: 10 µm). (ns)$p \geq 0.05$, *$p < 0.05$.

more physiologic distribution of lipids, similar to that within fresh specimens. Poison-treated static and peri-fused specimens had no noticeable differences in terms of lipid droplet morphology when compared with control cases, with lipid droplets indicative of cell stress within both metabolically inhibited and control samples (Fig. 4.2(C)).

Building on the evidence about the efficacy of this device to prolong the maintenance of tissue samples *ex vivo*, mouse omental tumour samples were used to examine whether perfusion could be used to preserve malignant tissue. The mouse model developed by Walter et al. was selected for the preliminary testing of the system with omental tumour specimens due to its ability to recapitulate a critical mutation (*Trp53-/-*) and key phenotypic traits of human HGSOC (Walton, Blagih et al. 2016, Walton, Farquharson et al. 2017). When mice reached endpoint on the basis of Home Office criteria for animal suffering (median survival of 49 days), animals were culled and specimens of tumour cell-infiltrated mouse omentum were cultured under static, peri-fused or perfused conditions for 48h. H&E staining and WT1 immunostaining on paraffin sections of the cultured samples were used to visualise cancerous regions and the tissue microenvironment within the employed specimens. Microscopy on sections confirmed tumour infiltration within all omental samples (Fig. 4.3). Also, perfused tumour specimens presented limited elongation and shape adaptation to channel architecture compared to healthy liver samples, and tumour islet structures within perfused omental samples were maintained. Staining for Ki67 (used as a marker of cell proliferation) showed intensely stained cells on specimen periphery (particularly for the static tissue fragment), most likely as result of their unobstructed access to the nutrient-rich pool of culture media. Ki67-positive cells were limited in deeper regions of the peri-fused and statically cultured explants, with a higher number of proliferating cells within most of the perfused specimens (Fig. 4.3). However, bibliographical data from the characterisation of the mouse model used for the experiments presented herein suggests that higher levels of Ki67 expression are usually present in such specimens (Walton, Blagih et al. 2016).

Immunostaining for cleaved caspase 3 showed lower apoptosis compared to the peri-fused specimen and static tissue fragment, implying improved viability preservation as a result of perfusion (see Appendix C2 for quantification). Notably, the apoptotic signal was particularly low within the tumour regions for all four perfused samples. Also, necrotic regions were present within most samples (primarily within the peri-fused sample and within 2/4 perfused samples). However, tissue gaps as a result of fully developed primary or secondary necrosis were not anticipated to occur within 48h and therefore were considered to be pre-existing within the omental specimens, as limited regions of necrosis are often found within fat tissue (Fig. 4.4). Tumour specimen preservation in the device was also supported from preliminary evidence of immunostaining for cleaved Caspase 3 on sections of human omental tumour samples after perfusion and in comparison, with samples cultured under static or peri-fused conditions (Appendix A, SF4).

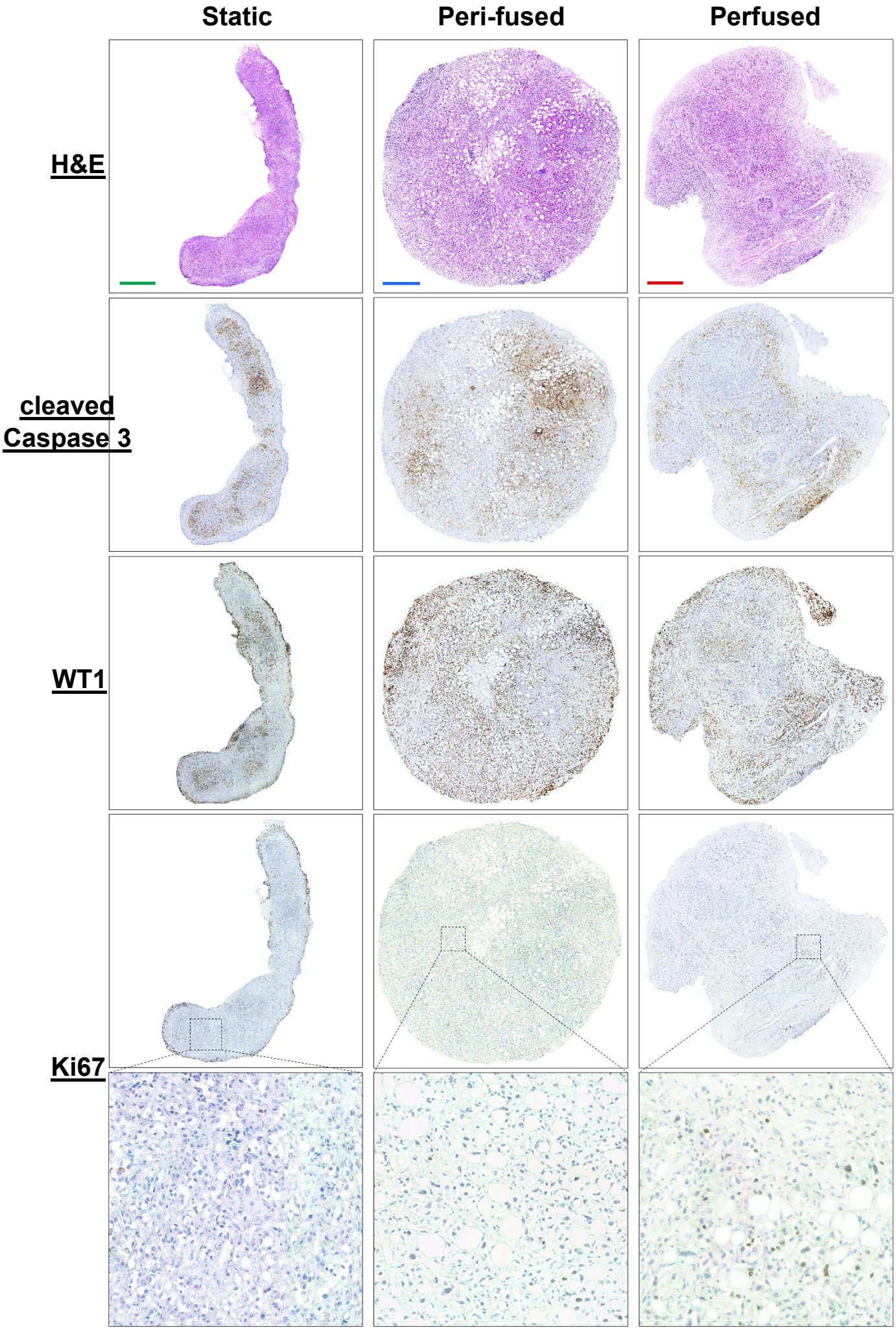


**Figure 4.3** H&E stianing and immunostaining for cleaved Caspase 3, WT1 and Ki67 with Haematoxylin as counterstain for the nuclei on 10 µm formaldehyde fixed, paraffin-embedded tissue sections from a statically cultured tissue fragment and peri-fused and perfused tissue specimens (Green scale bar: 500 µm, red scale bar: 350 µm, blue scale bar: 350 µm)

## 4.4 Discussion

Maintenance of viability and function of native tissue samples is a necessary feature for any system developed to be used for explant-based drug response assays. Most currently available platforms provide limited benefits for explant preservation, primarily due to the absence of advective transport of culture media through the sample. Therefore, the ability of the device to facilitate intra-tissue flow within tissue specimens could provide an improved set up for explant culture and be used for more scalable and reliable diagnostic tests, particularly in cancer. Hence, the developed platform was tested for its efficacy to maintain the viability, structure and function of healthy and malignant tissue specimens, as well as for applications of cell response to external perturbations, such as the inhibition of cell metabolism.

Preservation of viability was tested with mouse liver due to their significant susceptibility to ischemia, to explore the potential of this platform in explant preservation. Levels of LDH and ATP, which are both physiologically present only within the cytoplasm, were used as markers of cell viability, quantified in the lysate of specimens that had been cultured under static, peri-fused and perfused conditions. As normalised values of ATP and LDH are translated to the mean quantity per cell, absolute values were also reported to enable better understanding of the preservation benefit for the entire tissue specimen. Physiologically, variations in intracellular quantity of LDH are limited (Valvona, Fillmore et al. 2016) and therefore, the significantly higher LDH levels within perfused specimens indicated a lower number of cells with compromised membranes. Additionally, absolute and normalised ATP levels were significantly higher for perfused samples against both other conditions (peri-fused and static), indicating a larger part of the specimen remained metabolically active (and hence alive) at the end of the 48h culture period. Taken together, the evidence of higher ATP and LDH levels within perfused samples suggested that advection of culture media through the specimens had a significant benefit for viability preservation. Also, this observation is further supported by the fact that during perfusion more than half of specimen surface is in direct contact with device wall, which limits the area available for nutrient and oxygen diffusion if compared with static and/or peri-fused conditions. Notably, LDH quantity in peri-fused specimens was higher than in static samples, which suggested that the peri-fusion device provided to the cultured samples the beneficial cues occurring in peri-fusion-based technologies over standard static tissue culture.

Cleavage of caspase 3 occurs at different time points as part of several cell death mechanisms (beyond apoptosis alone) (Yuan, Najafov et al. 2016, Tsapras and Nezis 2017), which can be induced by parameters deteriorating specimen condition during culture, such as nutrient deprivation, hypoxia and/or ischemia. Hence, lower levels of cleaved caspase 3-stained cells within perfused samples further supported the notion that resected tissue was better maintained in the device for perfusion. Moreover, Haematoxylin staining showed that the lumens of vessels

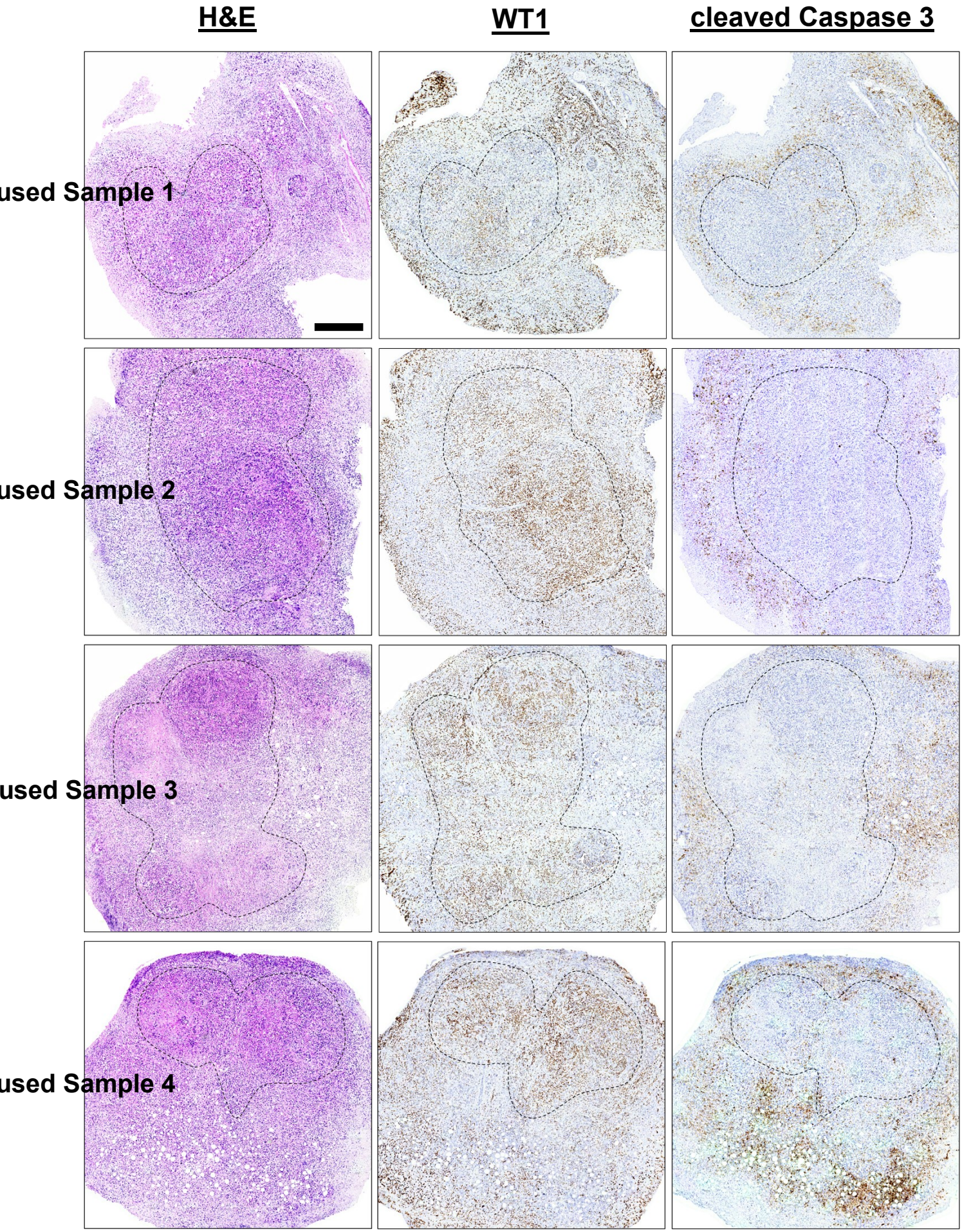


**Figure 4.4** H&E staining and immunostaining for WT1 and cleaved Caspase 3 for all four perfused samples from the same original omental explant. Marked regions show the main tumour infiltrated region within each specimen (Scale bar: 250 µm).

within the perfused explant did not collapse during the culture period, indicating unobstructed engagement of the vasculature throughout the 48h culture. Also, unsurprisingly, no necrotic regions of nonnucleated cells were observed within any of the three cases of cultured explants, indicating that the number of cells dying through necrotic, caspase-independent death mechanisms were negligible.

Treatment of specimens with a cocktail of metabolic inhibitors was used to assess the efficacy of the induced advection to deliver compounds of interest throughout the specimens, at levels sufficient to induce measurable differences in ATP levels in 2h. Indeed, the quantity of ATP within perfused specimens with the metabolic poison were significantly lower than those of the samples perfused with vehicle control, suggesting widespread metabolic inhibition reduced intracellular ATP beyond ischemia and hypoxia could. These observations suggested that perfusion in the device was effective to rapidly deliver the metabolic inhibitors via advection within the treated specimens, sufficiently timely to result in significant ATP reduction within the two-hour examined treatment window. Moreover, this effect was observed soon after isolation, despite the onset of ischemic effects for all conditions examined, and potential re-perfusion injury defects occurring additionally within the perfused samples. On the contrary, static and peri-fused samples treated with the cocktail presented no significant differences from their corresponding control cases.

Further evidence of cell metabolism inhibition after treatment with the metabolic poison were provided using PAS and Oil Red O staining on specimen sections. Static and peri-fused samples presented lower levels of intracellular carbohydrate content and a higher number of larger lipid droplets, both of which are considered to be indicative of cell stress, nutrient deprivation and hypoxia (Lennerz, Hurov et al. 2010, Carmean, Bobe et al. 2013, Xu, Donepudi et al. 2013, Jarc and Petan 2019). These observations suggested that both treated and untreated static, and peri-fused samples suffered the negative effects of ischemia, whilst diffusion-limited delivery of the inhibitor cocktail from specimen surface could not affect substantially cells beyond explant surface. On the contrary, untreated perfused specimens presented more similarities to fresh specimens, which suggested that advection with glucose-containing vehicle control was ameliorating (at least) some of the negative effects from tissue isolation and ischemia. Together the ATP quantification data and PAS and Oil Red O staining evidence support the efficacy of the device to establish intra-tissue flow through native tissue specimens as well as deliver nutrients and/or a compound of interest under terms that can lead to a biologically-relevant response by the employed sample. Nevertheless, static and peri-fused samples did not exhibit comparable ability to respond to metabolic inhibition in the examined conditions.

To explore the potential of this device in cancer-related drug assays, mouse tumour specimens were used to test device effectiveness, focusing on ovarian cancer. Tumours often exhibit significant differences in mechanical properties and tissue structures to healthy tissues (Handorf, Zhou et al. 2015). In ovarian cancer, primary debulking surgery is the main first line treatment prescribed for most patients, resulting in large tissue resections and sufficient

material provided by histopathologists for experimental and/or drug tests (Fig.1.1). To examine device efficacy in the context of cancer, tissue specimens used were from an ovarian cancer mouse model that mimics with high relevance the molecular markup, onset and progression of tumour cancer in human patients. The specimens utilised were from the omentum of animals culled at endpoint, as omental metastasis is present at the majority of patients at the time of diagnosis. Despite its generally small dimensions (Krishnan, Tallapragada et al. 2020), a single tumour-infiltrated mouse omentum provided sufficient material for four perfused samples, one peri-fused sample and a static tissue fragment.

As expected, tumour specimens were empirically found to be stiffer than mouse liver specimens, however that did not compromise the ability of the device to facilitate specimen loading immobilisation and perfusion. Staining showed that after a 48h culture, tumour structures within omental specimens were maintained and sample shape did not adapt noticeably to the flow profile. Immunostaining for cleaved Caspase 3 showed higher levels of cell death within the peri-fused and static specimens, in contrast to the limited number of stained cells within perfused samples. Notably, the statically cultured tissue fragment presented intense signal of caspase 3 cleavage a few cell layers from its surface, in agreement with literature demonstrating that nutrient and oxygen delivery via diffusion is limited beyond 100 μm from explant surface (Milotti, Stella et al. 2017). Similarly, proliferating (Ki67-positive) cells were present at explant surface but where largely absent within the viable, tumour infiltrated regions of static and peri-fused samples. On the contrary, sporadic Ki67-postive cells were present widely within the perfused sample, particularly in each core and heavily infiltrated regions by tumour cells. Ki67-positive cells within perfused samples further support improved preservation in the device for perfusion, however the limited number of proliferating cells even in the perfused condition suggests that further optimisation of this device for tumour specimens may be required.

H&E staining and WT1 immunostaining enabled identification of tumour regions within each perfused specimen. This allowed direct examination of whether cleaved Caspase 3 signal and tumour cells colocalise, demonstrating that tumour regions within perfused specimens were the ones benefitting the most from perfusion, exhibiting negligible levels of cell death. This observation suggests that the induced intra-tissue flow through specimens particularly benefits and preserves tumour cells within thick specimens from resected tissue, which could serve as a novel system for more biologically-relevant and scalable personalised drug response assays. The encouraging evidence from preliminary experiments with human ovarian tumour samples (Appendix A, SF4) further support the potential of this device for preservation and use of native patient specimens towards the treatment personalisation in the clinic.

## 4.5 Conclusions

The potential benefits advection can have for the preservation of isolated native tissue specimens had not been previously explored at large due to the technical complexity of cannulation-dependent technologies and diffusion-limited mass transport in peri-fused systems. The device described in this work was effective to induce intra-tissue flow of culture media through mouse liver and omental tumour explants, enabling their preservation for at least 48h. Perfusion also mediated effective delivery of compounds of interest within explant's cells, resulting in a timely, measurable response. Therefore, beyond tissue culture, the developed platform may have potential in the personalisation of drug response assays in the context of ovarian cancer and other parenchymal tissue malignancies.

# Chapter 5

# General Discussion and Future Work

## 5.1 General discussion

Currently, tissue resection is a standard treatment in the clinic when a region within an organ is identified to comprise genetic and functional defects that are irreversible and may induce further harm. Typically, in cancer, debulking surgery to remove most or all the clinically apparent tumour nodules is part of the first-line treatment recommended for the majority of cancer types and tumour grades. Despite tumour resection being standard in clinical practice, technologies that utilise the resected tissue whilst cells are alive remain underdeveloped, largely due to the difficulty to maintain tissue viability *ex vivo*. Indeed, most currently available platforms provide culture media only to the explant's periphery, where diffusion-limited mass transport only benefits cells located a few layers from the surface of the tissue sample. This limitation is partially addressed in tissue slice models, where an explant is sectioned into slices sufficiently thin (up to 400 μm) for diffusion to be effective (Powley, Patel et al. 2020). However, the labour-intensive protocols to set up slice-based models, the significantly reduced delivery of oxygen beyond 100 μm into the tissue (Milotti, Stella et al. 2017) and the severely limited flux of larger molecules, such as glucose (Bashkatov, Genina et al. 2009) towards cells have restricted the applicability and scalability of such platforms in the clinic.

In the last decades significant progress has been made in the development of cancer therapeutics, however treatment personalisation is required due to tumour heterogeneity, to achieve optimal patient outcomes. Hence, there is an emerging need for scalable platforms that can preserve native tumour specimens *ex vivo* and facilitate circulation-mimicking mass transport that can deliver nutrients and drug molecules timely within specimens. Towards addressing this need, a device was developed, presented in Chapter 2, to facilitate loading, immobilisation and perfusion of 3mm native tissue samples that were collected with a biopsy punch.

Using mouse liver samples as testing material, the device was shown to effectively entrap tissue samples and restore intra-tissue flow through them using a syringe pump in Chapter 3. Despite the absence of surface functionalisation within the lumen of device's channel, no perfusate leak through the tissue-device interface was observed, providing further evidence of perfusion efficacy. Also, advection through the explants was shown to engage both the vasculature and the interstitium, delivering molecules and particles up to 200 nm big within the two tissue compartments. microCT visualised perfusion gradients within specimens, suggesting that flow through the samples follows the parabolic profile of fluid flow through a porous body. Microscopy, microCT and immunostaining data also showed that specimen compression within device constriction did not result in vessel collapse within the samples, indicating vasculature engagement in perfusion throughout the 48h culture period.

The ability of this device to extend the viability of healthy and cancerous *ex vivo* specimens via perfusion was explored in Chapter 4. Perfusion led to higher levels of metabolically active cells and lower cytotoxicity within perfused liver samples, overcoming the limitations of diffusion-limited mass transport and improving specimen

preservation in a 48h culture. Notably, viability maintenance was validated with liver specimens, which exhibit substantial susceptibility to ischemia post-isolation. Moreover, the perfusion-dependent benefit for tissue viability *ex vivo* was significant despite the occurrence of reperfusion injury in liver tissues upon re-establishment of intra-tissue flow. *In vivo*, restoration of perfusion as soon as possible after occlusion of the circulation is the most critical factor for graft survival. Therefore, improved liver specimen preservation in the perfused device suggested that restoration of instar-tissue flow occurred immediately after system set up, protecting (perfused) samples from further ischemic harm throughout the culture period. Notably, the preservation benefit was significant despite the inevitable cell injury upon *ex vivo* reperfusion.

Despite the complexity of liver tissue maintenance *ex vivo*, hepatic tissues are highly porous, which renders them a promising candidate for a technology that induced intra-tissue flow. Indeed, liver tissues are characterised by low stiffness (Colombo, Belloli et al. 2011, MacManus, Maillet et al. 2019) and high permeability (Sarin 2010), with the latter being the result of the dense network of porous capillaries (named sinusoids) isotopically branched throughout the liver. Therefore, although restoration of perfusion was effective through highly vascularised liver specimens that could have not been the case for tumour specimens, which are generally considered as less permeable due to the irregularly branched and poorly functioning vascular routes and avascular regions often comprised within tumours (Jain 2005, Farnsworth, Lackmann et al. 2014). For this reason, the device was tested with tumour-infiltrated omental specimens, showing that the developed system could benefit tumour explant preservation through intra-tissue flow restoration. Notably, the tumour cells within the perfused malignant explants benefited the most by culture media flow through the specimen. This observation further supports the potential of this device and the use of *ex vivo* perfusion to preserve thick (>1mm) tumour samples in the lab for research or diagnostic purposes, hitherto considered as impossible without xenotransplantation.

Building on the evidence for effective advective delivery of nutrients within tissue specimens, mouse liver samples were treated with a cocktail of metabolic inhibitors for 2h, which resulted in significant reduction of cell metabolism and starvation-indicative cell morphology. These observations emphasise the efficacy of the developed device and perfusion method to directly and timely deliver a compound or combination of compounds within a tissue specimen and, most importantly, induce a biologically-relevant response to explant's cells. Notably, metabolic inhibition was measured after a 2h-treatment following sample incorporation in the perfusion set up, during which warm ischemia and/or reperfusion injury could be expected to overshadow the effects a compound may have to the cells within the explant. Therefore, the ability to measure a significant response to the treatment with the metabolic poison strengthens evidence for this device's potential for drug response applications, where different drugs are tested on patient samples to personalise patient treatment.

Beyond the promising results from this device's use in specimen perfusion and preservation, the developed technology comes with limitations, which may be overcome by further development of the platform in the future.

The current system depends on compression for specimen immobilisation and perfusion, therefore potentially limiting the possibility to extent perfusion duration and device use with tissues that are sensitive to mechanical stress (such as the brain). On another aspect, the current system depends on endpoint assays for assessing perfusion's effects on explants as the device currently lacks the means for real-time measurement of markers of viability and function. Additionally, the existing set up is based on an artificial material (PDMS), which cannot provide biological support to tissues, such as cell adherence, amelioration of inflammation or cell sprouting towards vessel formation.

Beyond these limitations, the role of several factors on specimen perfusion and maintenance of viability remains to be understood. As discussed in Chapter 2, intra-tissue flow in specimens perfused in this device is determined by the complex interplay between the flowrate, specimen compression and tissue properties. As different constriction slopes change the compressive force experienced by the specimen and sample's friction with the PDMS, a methodology for the identification of an optimal combination of flowrate and channel geometry remains to be found. Similarly, for a given channel design, a suitable approach to flowrate optimisation, so that explant's oxygen and nutrient needs are met with minimal compression and secured specimen immbolisation is pending. On this basis, it also remains unclear if the current design can be effective with specimens from tissues with varying mechanical properties and permeability or tissue-specific customisation of the design might be necessary on some occasions. Additionally, further study of perfusion's effect on specimen viability and function is needed, as well as identification of more sensitive markers of advection's effects on explants. Such markers would be useful to optimise the design of the device and perfusion parameters, and potentially contribute towards the use of this system for personalised drug screening.

## 5.2 Future work

The device developed in the context of this thesis represents a novel prototype that can be used to perfuse native tissue specimens *ex vivo*. The induced perfusion has been shown to improve and prolong the preservation of explants, with great potential for drug response assays. In the future, we aim to explore further the dynamics and mechanisms involved in the establishment of advection through native tissue samples and optimise the device geometry and perfusion parameters for several tissues and drug response applications.

Future work on the device would aim to improve understanding regarding the establishment of fluid flow through the explant. Research efforts shall quantify the perfusate volumes travelling through the vasculature and the interstitium, to unravel the engagement level of each compartment in the induced perfusion and assess how closely vascular perfusion in this device mimics the circulation. Moreover, mapping the pressure and permeability gradients occurring within the specimen as a result of perfusion and specimen compression within the constriction could shed light on the factors requiring further optimisation to improve and prolong tissue viability maintenance. Optimisation

of constriction geometry and perfusion parameters should target the absence of anoxic and glucose-deprived regions within the specimen, for a specimen size and flowrate that channel sealing sample entrapment are maintained. Channel surface functionalisation and roughness modification could also be used to promote specimen adherence to PDMS and reduce sample deformation and slipping further into the constriction. Also, perfusion parameter ranges should be selected with caution so that extreme, cell-harming pressure gradients are not established across the explant. The complex interplay of the numerous parameters influencing specimen entrapment and perfusion within the device could result in different optimal device geometry, channel processing and/or perfusion protocol for samples of different origin due to the varying mechanical (mainly stiffness and permeability) and biological properties (for instance susceptibility to injury by ischemia and/or compression) among the various tissues.

The optimisation of explant perfusion may result in higher levels of viability for the perfused specimens for an extended culture duration, beyond the currently possible 48h. This is desirable both for biological experiments and drug response tests were non-acute, inducible effects are examined, such as the development of resistance to a chemotherapeutic. Also, higher levels of viability preserved for longer enable more accurate and sensitive measurements of cell response to treatment with a compound, whilst potentially reducing the number of samples required to have a statistically significant effect.

The development of tailored systems for different types of tumour specimens would provide a useful platform to predict the potential benefit of a drug for a patient and identify early those with inherent resistance to a drug. Improved understanding of perfusion parameters will allow the development of drug perfusion protocols (dosage, treatment duration) that will result in a drug-induced response that matches well with the response of the patient that the samples originate from. Follow-up data from patients during and after treatment will be required to validate the perfusion protocols and assess the accuracy of the developed technology.

# References

Aalkjaer, C., & Nilsson, H. (2005). Vasomotion: cellular background for the oscillator and for the synchronization of smooth muscle cells. *British journal of pharmacology, 144*(5), 605-616.

Abdelaal, H. M., Kim, H. O., Wagstaff, R., Sawahata, R., Southern, P. J., & Skinner, P. J. (2015). Comparison of Vibratome and Compresstome sectioning of fresh primate lymphoid and genital tissues for in situ MHC-tetramer and immunofluorescence staining. *Biological procedures online, 17*(1), 2.

Abe, Y., Hines, I. N., Zibari, G., Pavlick, K., Gray, L., Kitagawa, Y., & Grisham, M. B. (2009). Mouse model of liver ischemia and reperfusion injury: method for studying reactive oxygen and nitrogen metabolites in vivo. *Free Radical Biology and Medicine, 46*(1), 1-7.

Achilli, T.-M., Meyer, J., & Morgan, J. R. (2012). Advances in the formation, use and understanding of multi-cellular spheroids. *Expert opinion on biological therapy, 12*(10), 1347-1360.

Altman, B. J., & Rathmell, J. C. (2012). Metabolic stress in autophagy and cell death pathways. *Cold Spring Harbor perspectives in biology, 4*(9), a008763.

Amoedo, N., Obre, E., & Rossignol, R. (2017). Drug discovery strategies in the field of tumor energy metabolism: Limitations by metabolic flexibility and metabolic resistance to chemotherapy. *Biochimica et Biophysica Acta (BBA)-Bioenergetics, 1858*(8), 674-685.

Androjna, C., Gatica, J. E., Belovich, J. M., & Derwin, K. A. (2008). Oxygen diffusion through natural extracellular matrices: implications for estimating “critical thickness” values in tendon tissue engineering. *Tissue Engineering Part A, 14*(4), 559-569.

Ardehali, A., Esmailian, F., Deng, M., Soltesz, E., Hsich, E., Naka, Y., . . . Leprince, P. (2015). Ex-vivo perfusion of donor hearts for human heart transplantation (PROCEED II): a prospective, open-label, multicentre, randomised non-inferiority trial. *The Lancet, 385*(9987), 2577-2584.

Ashton, J. R., West, J. L., & Badea, C. T. (2015). In vivo small animal micro-CT using nanoparticle contrast agents. *Frontiers in pharmacology, 6*, 256.

Astolfi, M., Peant, B., Lateef, M. A., Rousset, N., Kendall-Dupont, J., Carmona, E., . . . Gervais, T. (2016). Micro-dissected tumor tissues on chip: an ex vivo method for drug testing and personalized therapy. *Lab Chip, 16*(2), 312-325. doi:10.1039/c5lc01108f

Ataç, B., Wagner, I., Horland, R., Lauster, R., Marx, U., Tonevitsky, A. G., . . . Lindner, G. (2013). Skin and hair on-a-chip: in vitro skin models versus ex vivo tissue maintenance with dynamic perfusion. *Lab on a chip, 13*(18), 3555-3561.

Azau, A., Markowicz, P., Corbeau, J., Cottineau, C., Moreau, X., Baufreton, C., & Beydon, L. (2014). Increasing mean arterial pressure during cardiac surgery does not reduce the rate of postoperative acute kidney injury. *Perfusion, 29*(6), 496-504.

Baines, C. P. (2009). The mitochondrial permeability transition pore and ischemia-reperfusion injury. *Basic research in cardiology, 104*(2), 181-188.

Baines, C. P. (2011). How and when do myocytes die during ischemia and reperfusion: the late phase. *Journal of cardiovascular pharmacology and therapeutics, 16*(3-4), 239-243.

Bankhead, P., Loughrey, M. B., Fernández, J. A., Dombrowski, Y., McArt, D. G., Dunne, P. D., . . . Coleman, H. G. (2017). QuPath: Open source software for digital pathology image analysis. *Scientific reports, 7*(1), 1-7.

BÁRÁNY, E. H. (1964). Simultaneous measurement of changing intraocular pressure and outflow facility in the vervet monkey by constant pressure infusion. *Investigative ophthalmology & visual science, 3*(2), 135-143.

Bashkatov, A. N., Genina, E. A., & Tuchin, V. V. (2009). Measurement of glucose diffusion coefficients in human tissues. *Chap, 19*, 587-621.

Bastien, O., Piriou, V., Aouifi, A., Flamens, C., Evans, R., & Lehot, J. J. (2000). Relative importance of flow versus pressure in splanchnic perfusion during cardiopulmonary bypass in rabbits. *Anesthesiology: The Journal of the American Society of Anesthesiologists, 92*(2), 457-457.

Becker, H., & Locascio, L. E. (2002). Polymer microfluidic devices. *Talanta, 56*(2), 267-287.
Beckwith, A. L., Borenstein, J. T., & Velásquez-García, L. F. (2018). Monolithic, 3D-printed microfluidic platform for recapitulation of dynamic tumor microenvironments. *Journal of Microelectromechanical Systems, 27*(6), 1009-1022.
Bedard, P. L., Hansen, A. R., Ratain, M. J., & Siu, L. L. (2013). Tumour heterogeneity in the clinic. *Nature, 501*(7467), 355-364.
Bell, G. I., Kayano, T., Buse, J. B., Burant, C. F., Takeda, J., Lin, D., . . . Seino, S. (1990). Molecular biology of mammalian glucose transporters. *Diabetes care, 13*(3), 198-208.
Benam, K. H., Dauth, S., Hassell, B., Herland, A., Jain, A., Jang, K. J., . . . Ingber, D. E. (2015). Engineered in vitro disease models. *Annu Rev Pathol, 10*, 195-262. doi:10.1146/annurev-pathol-012414-040418
Bergh, N., Ekman, M., Ulfhammer, E., Andersson, M., Karlsson, L., & Jern, S. (2005). A new biomechanical perfusion system for ex vivo study of small biological intact vessels. *Annals of biomedical engineering, 33*(12), 1808-1818.
Berkowitz, A. (2020). Playing the genome card. *Journal of Neurogenetics*, 1-9.
Berretta, R., Patrelli, T. S., Migliavacca, C., Rolla, M., Franchi, L., Monica, M., . . . Gizzo, S. (2014). Assessment of tumor size as a useful marker for the surgical staging of endometrial cancer. *Oncology reports, 31*(5), 2407-2412.
Bhaduri, A., Andrews, M. G., Leon, W. M., Jung, D., Shin, D., Allen, D., . . . Salma, J. (2020). Cell stress in cortical organoids impairs molecular subtype specification. *Nature, 578*(7793), 142-148.
Bhatia, S. N., & Ingber, D. E. (2014). Microfluidic organs-on-chips. *Nature biotechnology, 32*(8), 760.
Bilzer, M., & Gerbes, A. L. (2000). Preservation injury of the liver: mechanisms and novel therapeutic strategies. *Journal of hepatology, 32*(3), 508-515.
Bissell, D. M. (1981). *Primary hepatocyte culture: substratum requirements and production of matrix components.* Paper presented at the Federation proceedings.
Bosch, A. M., Kessels, A. G., Beets, G. L., Rupa, J. D., Koster, D., van Engelshoven, J. M., & von Meyenfeldt, M. F. (2003). Preoperative estimation of the pathological breast tumour size by physical examination, mammography and ultrasound: a prospective study on 105 invasive tumours. *European journal of radiology, 48*(3), 285-292.
Boucher, Y., Baxter, L. T., & Jain, R. K. (1990). Interstitial pressure gradients in tissue-isolated and subcutaneous tumors: implications for therapy. *Cancer research, 50*(15), 4478-4484.
Boudreault, F., & Grygorczyk, R. (2004). Cell swelling-induced ATP release is tightly dependent on intracellular calcium elevations. *The Journal of physiology, 561*(2), 499-513.
Bowers, C. A., Burns, G., Salzman, K. L., McGill, L. D., & MacDonald, J. D. (2014). Comparison of tissue effects in rabbit muscle of surgical dissection devices. *International Journal of Surgery, 12*(3), 219-223.
Bral, M., Gala-Lopez, B., Bigam, D., Kneteman, N., Malcolm, A., Livingstone, S., . . . Coussios, C. (2017). Preliminary single-center Canadian experience of human normothermic ex vivo liver perfusion: results of a clinical trial. *American Journal of Transplantation, 17*(4), 1071-1080.
Brand, M., Granato, M., & Nüsslein-Volhard, C. (2002). Keeping and raising zebrafish. *Zebrafish: a practical approach*, 7-37.
Breeuwer, P., & Abee, T. (2000). Assessment of viability of microorganisms employing fluorescence techniques. *International journal of food microbiology, 55*(1-3), 193-200.
Breslin, S., & O'Driscoll, L. (2016). The relevance of using 3D cell cultures, in addition to 2D monolayer cultures, when evaluating breast cancer drug sensitivity and resistance. *Oncotarget, 7*(29), 45745.
Brown, A. M. (1980). Receptors under pressure. An update on baroreceptors. *Circulation research, 46*(1), 1-10.

Byrne, A. T., Alférez, D. G., Amant, F., Annibali, D., Arribas, J., Biankin, A. V., . . . Chang, D. K. (2017). Interrogating open issues in cancer precision medicine with patient-derived xenografts. *Nature Reviews Cancer, 17*(4), 254.

Caliari, S. R., & Burdick, J. A. (2016). A practical guide to hydrogels for cell culture. *Nature methods, 13*(5), 405.

Cannan, W. J., & Pederson, D. S. (2016). Mechanisms and consequences of double-strand DNA break formation in chromatin. *Journal of cellular physiology, 231*(1), 3-14.

Cao, J. Y., & Dixon, S. J. (2016). Mechanisms of ferroptosis. *Cellular and Molecular Life Sciences, 73*(11), 2195-2209.

Cardenas, C., Alvero, A. B., Yun, B. S., & Mor, G. (2016). Redefining the origin and evolution of ovarian cancer: a hormonal connection. *Endocrine-related cancer, 23*(9), R411-R422.

Carmean, C. M., Bobe, A. M., Justin, C. Y., Volden, P. A., & Brady, M. J. (2013). Refeeding-induced brown adipose tissue glycogen hyper-accumulation in mice is mediated by insulin and catecholamines. *PLoS One, 8*(7), e67807.

Carmean, C. M., Bobe, A. M., Justin, C. Y., Volden, P. A., & Brady, M. J. (2013). Refeeding-induced brown adipose tissue glycogen hyper-accumulation in mice is mediated by insulin and catecholamines. *PLoS One, 8*(7), e67807.

Cauwels, A., Rogge, E., Vandendriessche, B., Shiva, S., & Brouckaert, P. (2014). Extracellular ATP drives systemic inflammation, tissue damage and mortality. *Cell death & disease, 5*(3), e1102-e1102.

Cave, A. C., Ingwall, J. S., Friedrich, J., Liao, R., Saupe, K. W., Apstein, C. S., & Eberli, F. R. (2000). ATP synthesis during low-flow ischemia: influence of increased glycolytic substrate. *Circulation, 101*(17), 2090-2096.

Chang, T. C., Mikheev, A. M., Huynh, W., Monnat, R. J., Rostomily, R. C., & Folch, A. (2014). Parallel microfluidic chemosensitivity testing on individual slice cultures. *Lab on a chip, 14*(23), 4540-4551.

Chen, C., Pore, N., Behrooz, A., Ismail-Beigi, F., & Maity, A. (2001). Regulation of glut1 mRNA by hypoxia-inducible factor-1 Interaction between H-ras and hypoxia. *Journal of Biological Chemistry, 276*(12), 9519-9525.

Cırık, D. A., Kalyoncu, R., Üreyen, I., Taşçı, T., Boran, N., Özfuttu, A., . . . Tulunay, G. (2014). Analysis of non-squamous vulvar cancer cases: A 21-year experience in a single center. *Turkish journal of obstetrics and gynecology, 11*(3), 165.

Cohen, P. P., & Hayano, M. (1946). Urea synthesis by liver homogenates. *J. biol. Chem, 166*, 251.

Colombo, S., Belloli, L., Zaccanelli, M., Badia, E., Jamoletti, C., Buonocore, M., & Del Poggio, P. (2011). Normal liver stiffness and its determinants in healthy blood donors. *Digestive and Liver Disease, 43*(3), 231-236.

Compton, C. C., Butler, C. E., Yannas, I. V., Warland, G., & Orgill, D. P. (1998). Organized skin structure is regenerated in vivo from collagen-GAG matrices seeded with autologous keratinocytes. *Journal of investigative dermatology, 110*(6), 908-916.

Cooper, J., & Giancotti, F. G. (2019). Integrin signaling in cancer: mechanotransduction, stemness, epithelial plasticity, and therapeutic resistance. *Cancer Cell, 35*(3), 347-367.

Correia, A. L., & Bissell, M. J. (2012). The tumor microenvironment is a dominant force in multidrug resistance. *Drug resistance updates, 15*(1-2), 39-49.

Cox, T. R., & Erler, J. T. (2011). Remodeling and homeostasis of the extracellular matrix: implications for fibrotic diseases and cancer. *Disease models & mechanisms, 4*(2), 165-178.

Cukierman, E., Pankov, R., & Yamada, K. M. (2002). Cell interactions with three-dimensional matrices. *Current opinion in cell biology, 14*(5), 633-640.

Cunningham, D., Humblet, Y., Siena, S., Khayat, D., Bleiberg, H., Santoro, A., . . . Verslype, C. (2004). Cetuximab monotherapy and cetuximab plus irinotecan in irinotecan-refractory metastatic colorectal cancer. *New England Journal of Medicine, 351*(4), 337-345.

Cypel, M., Neyrinck, A., & Machuca, T. N. (2019). Ex vivo perfusion techniques: state of the art and potential applications. In: Springer.

da Silva-Diz, V., Lorenzo-Sanz, L., Bernat-Peguera, A., Lopez-Cerda, M., & Muñoz, P. (2018). *Cancer cell plasticity: Impact on tumor progression and therapy response.* Paper presented at the Seminars in cancer biology.

Dagogo-Jack, I., & Shaw, A. T. (2018). Tumour heterogeneity and resistance to cancer therapies. *Nature reviews Clinical oncology, 15*(2), 81.

Daly, S. M., & Leahy, M. J. (2013). 'Go with the flow': a review of methods and advancements in blood flow imaging. *Journal of biophotonics, 6*(3), 217-255.

Damiano, J. S., Cress, A. E., Hazlehurst, L. A., Shtil, A. A., & Dalton, W. S. (1999). Cell adhesion mediated drug resistance (CAM-DR): role of integrins and resistance to apoptosis in human myeloma cell lines. *Blood, The Journal of the American Society of Hematology, 93*(5), 1658-1667.

Darcy, H. (1856). *Les fontaines publiques de la ville de Dijon: exposition et application*: Victor Dalmont.

Davis, M. J., Hill, M. A., & Kuo, L. (2008). Local regulation of microvascular perfusion. In *Microcirculation* (pp. 161-284): Elsevier.

De Backer, D. (2003). Lactic acidosis. *Intensive care medicine, 29*(5), 699-702.

de Castro Fonseca, M., Araujo, B. H. S., Dias, C. S. B., Archilha, N. L., Neto, D. P. A., Cavalheiro, E., . . . Franchini, K. G. (2018). High-resolution synchrotron-based X-ray microtomography as a tool to unveil the three-dimensional neuronal architecture of the brain. *Scientific reports, 8*(1), 1-13.

De Palma, M., Biziato, D., & Petrova, T. V. (2017). Microenvironmental regulation of tumour angiogenesis. *Nature Reviews Cancer, 17*(8), 457.

De Villiers, C., & Riley, P. R. (2020). Mouse models of myocardial infarction: comparing permanent ligation and ischaemia-reperfusion. *Disease models & mechanisms, 13*(11).

Debbaut, C., Vierendeels, J., Casteleyn, C., Cornillie, P., Van Loo, D., Simoens, P., . . . Segers, P. (2012). Perfusion characteristics of the human hepatic microcirculation based on three-dimensional reconstructions and computational fluid dynamic analysis. *Journal of biomechanical engineering, 134*(1).

Denk, W., & Horstmann, H. (2004). Serial block-face scanning electron microscopy to reconstruct three-dimensional tissue nanostructure. *PLoS biology, 2*(11).

Dewhirst, M. W., & Secomb, T. W. (2017). Transport of drugs from blood vessels to tumour tissue. *Nature Reviews Cancer, 17*(12), 738.

Di Lisa, F., Canton, M., Menabò, R., Kaludercic, N., & Bernardi, P. (2007). Mitochondria and cardioprotection. *Heart failure reviews, 12*(3-4), 249-260.

Dinenno, F. A., Jones, P. P., Seals, D. R., & Tanaka, H. (1999). Limb blood flow and vascular conductance are reduced with age in healthy humans: relation to elevations in sympathetic nerve activity and declines in oxygen demand. *Circulation, 100*(2), 164-170.

Dirkx, A. E., oude Egbrink, M. G., Castermans, K., Van Der Schaft, D. W., Thijssen, V. L., Dings, R. P., . . . ter Steege, J. C. B.-. (2006). Anti-angiogenesis therapy can overcome endothelial cell anergy and promote leukocyte-endothelium interactions and infiltration in tumors. *The FASEB Journal, 20*(6), 621-630.

Doherty, J., & Baehrecke, E. H. (2018). Life, death and autophagy. *Nature cell biology, 20*(10), 1110-1117.

Don, F. K., & Huch, M. (2021). Organoids, Where We Stand and Where We Go. *Trends in molecular medicine*.

Downey, G. P., Doherty, D. E., Schwab 3rd, B., Elson, E., Henson, P., & Worthen, G. (1990). Retention of leukocytes in capillaries: role of cell size and deformability. *Journal of applied physiology, 69*(5), 1767-1778.

Du Plessis, A., Broeckhoven, C., Guelpa, A., & Le Roux, S. G. (2017). Laboratory x-ray micro-computed tomography: a user guideline for biological samples. *GigaScience, 6*(6), gix027.

Du, Y., Han, R., Wen, F., San San, S. N., Xia, L., Wohland, T., . . . Yu, H. (2008). Synthetic sandwich culture of 3D hepatocyte monolayer. *Biomaterials, 29*(3), 290-301.

Duval, K., Grover, H., Han, L.-H., Mou, Y., Pegoraro, A. F., Fredberg, J., & Chen, Z. (2017). Modeling physiological events in 2D vs. 3D cell culture. *Physiology, 32*(4), 266-277.

Eberhard, A., Kahlert, S., Goede, V., Hemmerlein, B., Plate, K. H., & Augustin, H. G. (2000). Heterogeneity of angiogenesis and blood vessel maturation in human tumors: implications for antiangiogenic tumor therapies. *Cancer research, 60*(5), 1388-1393.

Eichelberger, L. E., Koch, M. O., Eble, J. N., Ulbright, T. M., Juliar, B. E., & Cheng, L. (2005). Maximum tumor diameter is an independent predictor of prostate-specific antigen recurrence in prostate cancer. *Modern pathology, 18*(7), 886-890.

Eltzschig, H. K., & Collard, C. D. (2004). Vascular ischaemia and reperfusion injury. *British medical bulletin, 70*(1), 71-86.

Eltzschig, H. K., & Eckle, T. (2011). Ischemia and reperfusion—from mechanism to translation. *Nature medicine, 17*(11), 1391.

Engler, R., Schmid-Schönbein, G., & Pavelec, R. (1983). Leukocyte capillary plugging in myocardial ischemia and reperfusion in the dog. *The American journal of pathology, 111*(1), 98.

Farnsworth, R. H., Lackmann, M., Achen, M. G., & Stacker, S. A. (2014). Vascular remodeling in cancer. *Oncogene, 33*(27), 3496-3505.

Fischbach, C., Chen, R., Matsumoto, T., Schmelzle, T., Brugge, J. S., Polverini, P. J., & Mooney, D. J. (2007). Engineering tumors with 3D scaffolds. *Nature methods, 4*(10), 855-860.

Fox, R. W., McDonald, A. T., & Mitchell, J. W. (2020). *Fox and McDonald's introduction to fluid mechanics*: John Wiley & Sons.

Frentzas, S., Simoneau, E., Bridgeman, V. L., Vermeulen, P. B., Foo, S., Kostaras, E., . . . Shi, Y. (2016). Vessel co-option mediates resistance to anti-angiogenic therapy in liver metastases. *Nature medicine, 22*(11), 1294.

Galluzzi, L., Vitale, I., Aaronson, S. A., Abrams, J. M., Adam, D., Agostinis, P., . . . Andrews, D. W. (2018). Molecular mechanisms of cell death: recommendations of the Nomenclature Committee on Cell Death 2018. *Cell Death & Differentiation, 25*(3), 486-541.

Gaur, R., Mishra, L., & Gupta, S. K. S. (2014). Diffusion and transport of molecules in living cells. In *Modelling and Simulation of Diffusive Processes* (pp. 27-49): Springer.

Ge, H., & Luo, H. (2018). Overview of advances in vasculogenic mimicry–a potential target for tumor therapy. *Cancer management and research, 10*, 2429.

Ge, L., Zhou, X., Ji, W.-J., Lu, R.-Y., Zhang, Y., Zhang, Y.-D., . . . Li, Y.-M. (2015). Neutrophil extracellular traps in ischemia-reperfusion injury-induced myocardial no-reflow: therapeutic potential of DNase-based reperfusion strategy. *American Journal of Physiology-Heart and Circulatory Physiology, 308*(5), H500-H509.

Geiger, B., Bershadsky, A., Pankov, R., & Yamada, K. M. (2001). Transmembrane crosstalk between the extracellular matrix and the cytoskeleton. *Nature reviews Molecular cell biology, 2*(11), 793-805.

Geraghty, R., Capes-Davis, A., Davis, J., Downward, J., Freshney, R., Knezevic, I., . . . Stacey, G. (2014). Guidelines for the use of cell lines in biomedical research. *British journal of cancer, 111*(6), 1021-1046.

Gerber, D., Dahlberg, S., Sandler, A., Ahn, D., Schiller, J., Brahmer, J., & Johnson, D. (2013). Baseline tumour measurements predict survival in advanced non-small cell lung cancer. *British journal of cancer, 109*(6), 1476-1481.

Gerpe, M. C. R., van Vloten, J. P., Santry, L. A., de Jong, J., Mould, R. C., Pelin, A., . . . Wootton, S. K. (2018). Use of precision-cut lung slices as an ex vivo tool for evaluating viruses and viral vectors for gene and oncolytic therapy. *Molecular Therapy-Methods & Clinical Development, 10*, 245-256.

Godoy, P., Hewitt, N. J., Albrecht, U., Andersen, M. E., Ansari, N., Bhattacharya, S., . . . Boettger, J. (2013). Recent advances in 2D and 3D in vitro systems using primary hepatocytes, alternative hepatocyte sources and non-parenchymal liver cells and their use in investigating mechanisms of hepatotoxicity, cell signaling and ADME. *Archives of toxicology, 87*(8), 1315-1530.

Gomes, A., Guillaume, L., Grimes, D. R., Fehrenbach, J., Lobjois, V., & Ducommun, B. (2016). Oxygen partial pressure is a rate-limiting parameter for cell proliferation in 3D spheroids grown in physioxic culture condition. *PLoS One, 11*(8).

Gotink, K. J., Broxterman, H. J., Labots, M., De Haas, R. R., Dekker, H., Honeywell, R. J., . . . Jansen, G. (2011). Lysosomal sequestration of sunitinib: a novel mechanism of drug resistance. *Clinical Cancer Research, 17*(23), 7337-7346.

Gould, I. G., Tsai, P., Kleinfeld, D., & Linninger, A. (2017). The capillary bed offers the largest hemodynamic resistance to the cortical blood supply. *Journal of Cerebral Blood Flow & Metabolism, 37*(1), 52-68.

Graham, N. A., Tahmasian, M., Kohli, B., Komisopoulou, E., Zhu, M., Vivanco, I., . . . Lo, R. S. (2012). Glucose deprivation activates a metabolic and signaling amplification loop leading to cell death. *Molecular systems biology, 8*(1).

Granger, D. N., & Kvietys, P. R. (2015). Reperfusion injury and reactive oxygen species: the evolution of a concept. *Redox biology, 6*, 524-551.

Griffioen, A. W., Damen, C. A., Blijham, G. H., & Groenewegen, G. (1996). Tumor angiogenesis is accompanied by a decreased inflammatory response of tumor-associated endothelium.

Griffith, C. K., Miller, C., Sainson, R. C., Calvert, J. W., Jeon, N. L., Hughes, C. C., & George, S. C. (2005). Diffusion limits of an in vitro thick prevascularized tissue. *Tissue engineering, 11*(1-2), 257-266.

Griffith, L. G., & Swartz, M. A. (2006). Capturing complex 3D tissue physiology in vitro. *Nature reviews Molecular cell biology, 7*(3), 211-224.

Grimes, D. R., Kelly, C., Bloch, K., & Partridge, M. (2014). A method for estimating the oxygen consumption rate in multicellular tumour spheroids. *Journal of The Royal Society Interface, 11*(92), 20131124.

Gu, F.-f., Zhang, Y., Liu, Y.-y., Hong, X.-h., Liang, J.-y., Tong, F., . . . Liu, L. (2016). Lung adenocarcinoma harboring concomitant SPTBN1-ALK fusion, c-Met overexpression, and HER-2 amplification with inherent resistance to crizotinib, chemotherapy, and radiotherapy. *Journal of hematology & oncology, 9*(1), 66.

Guimarães, C. F., Gasperini, L., Marques, A. P., & Reis, R. L. (2020). The stiffness of living tissues and its implications for tissue engineering. *Nature Reviews Materials*, 1-20.

Gujral, J. S., Bucci, T. J., Farhood, A., & Jaeschke, H. (2001). Mechanism of cell death during warm hepatic ischemia-reperfusion in rats: apoptosis or necrosis? *Hepatology, 33*(2), 397-405.

Hakanson, M., Cukierman, E., & Charnley, M. (2014). Miniaturized pre-clinical cancer models as research and diagnostic tools. *Adv Drug Deliv Rev, 69-70*, 52-66. doi:10.1016/j.addr.2013.11.010

Hall, M., Savvatis, K., Nixon, K., Kyrgiou, M., Hariharan, K., Padwick, M., . . . Farthing, A. (2019). Maximal-effort cytoreductive surgery for ovarian cancer patients with a high tumor burden: variations in practice and impact on outcome. *Annals of surgical oncology, 26*(9), 2943-2951.

Halsøy, K., Kondratiev, T., Tveita, T., & Bjertnaes, L. J. (2016). effects of constant Flow vs. constant Pressure Perfusion on Fluid Filtration in severe hypothermic isolated Blood-Perfused rat lungs. *Frontiers in Medicine, 3*, 70.

Han, S., Khuri, F. R., & Roman, J. (2006). Fibronectin stimulates non–small cell lung carcinoma cell growth through activation of Akt/mammalian target of rapamycin/S6 kinase and inactivation of LKB1/AMP-activated protein kinase signal pathways. *Cancer research, 66*(1), 315-323.

Hanahan, D., & Weinberg, R. A. (2011). Hallmarks of cancer: the next generation. *Cell, 144*(5), 646-674. doi:10.1016/j.cell.2011.02.013

Handorf, A. M., Zhou, Y., Halanski, M. A., & Li, W.-J. (2015). Tissue stiffness dictates development, homeostasis, and disease progression. *Organogenesis, 11*(1), 1-15.

Harunaga, J. S., & Yamada, K. M. (2011). Cell-matrix adhesions in 3D. *Matrix Biology, 30*(7-8), 363-368.

Hasan, J., Byers, R., & Jayson, G. C. (2002). Intra-tumoural microvessel density in human solid tumours. *British journal of cancer, 86*(10), 1566-1577.

Hasanin, A., Mukhtar, A., & Nassar, H. (2017). Perfusion indices revisited. *Journal of intensive care, 5*(1), 1-8.

Heldin, C.-H., Rubin, K., Pietras, K., & Östman, A. (2004). High interstitial fluid pressure—an obstacle in cancer therapy. *Nature Reviews Cancer, 4*(10), 806-813.

Helgason, C. D., & Miller, C. L. (2005). *Basic cell culture protocols* (Vol. 1): Springer.

Helmlinger, G., Yuan, F., Dellian, M., & Jain, R. K. (1997). Interstitial pH and pO 2 gradients in solid tumors in vivo: high-resolution measurements reveal a lack of correlation. *Nature medicine, 3*(2), 177-182.

Heslop, J. A., Rowe, C., Walsh, J., Sison-Young, R., Jenkins, R., Kamalian, L., . . . Malik, H. Z. (2017). Mechanistic evaluation of primary human hepatocyte culture using global proteomic analysis reveals a selective dedifferentiation profile. *Archives of toxicology, 91*(1), 439-452.

Hoarau-Véchot, J., Rafii, A., Touboul, C., & Pasquier, J. (2018). Halfway between 2D and animal models: are 3D cultures the ideal tool to study cancer-microenvironment interactions? *International journal of molecular sciences, 19*(1), 181.

Hoffman, R. M. (2015). Patient-derived orthotopic xenografts: better mimic of metastasis than subcutaneous xenografts. *Nature Reviews Cancer, 15*(8), 451-452.

Holohan, C., Van Schaeybroeck, S., Longley, D. B., & Johnston, P. G. (2013). Cancer drug resistance: an evolving paradigm. *Nature Reviews Cancer, 13*(10), 714-726.

Holton, A. B., Sinatra, F. L., Kreahling, J., Conway, A. J., Landis, D. A., & Altiok, S. (2017). Microfluidic biopsy trapping device for the real-time monitoring of tumor microenvironment. *PLoS One, 12*(1).

Howat, W. J., & Wilson, B. A. (2014). Tissue fixation and the effect of molecular fixatives on downstream staining procedures. *Methods, 70*(1), 12-19.

Huang, Y., Williams, J. C., & Johnson, S. M. (2012). Brain slice on a chip: opportunities and challenges of applying microfluidic technology to intact tissues. *Lab Chip, 12*(12), 2103-2117. doi:10.1039/c2lc21142d

Huch, M., Knoblich, J. A., Lutolf, M. P., & Martinez-Arias, A. (2017). The hope and the hype of organoid research. *Development, 144*(6), 938-941.

Hynes, R. O. (2009). The extracellular matrix: not just pretty fibrils. *Science, 326*(5957), 1216-1219. doi:10.1126/science.1176009

Idrees, A., Chiono, V., Ciardelli, G., Shah, S., Viebahn, R., Zhang, X., & Salber, J. (2018). Validation of in vitro assays in three-dimensional human dermal constructs. *The International journal of artificial organs, 41*(11), 779-788.

Im, W. J., Kim, M. G., Ha, T. K., & Kwon, S. J. (2012). Tumor size as a prognostic factor in gastric cancer patient. *Journal of gastric cancer, 12*(3), 164-172.

Iurlaro, R., Püschel, F., León-Annicchiarico, C. L., O'Connor, H., Martin, S. J., Palou-Gramón, D., . . . Muñoz-Pinedo, C. (2017). Glucose deprivation induces ATF4-mediated apoptosis through TRAIL death receptors. *Molecular and cellular biology, 37*(10), e00479-00416.
Jain, R. K. (2005). Normalization of tumor vasculature: an emerging concept in antiangiogenic therapy. *Science, 307*(5706), 58-62.
Jarc, E., & Petan, T. (2019). Focus: Organelles: Lipid Droplets and the Management of Cellular Stress. *The Yale journal of biology and medicine, 92*(3), 435.
Jayson, G. C., Kohn, E. C., Kitchener, H. C., & Ledermann, J. A. (2014). Ovarian cancer. *The Lancet, 384*(9951), 1376-1388.
Jen, A. C., Wake, M. C., & Mikos, A. G. (1996). Hydrogels for cell immobilization. *Biotechnology and bioengineering, 50*(4), 357-364.
Jose, C., Bellance, N., & Rossignol, R. (2011). Choosing between glycolysis and oxidative phosphorylation: a tumor's dilemma? *Biochim Biophys Acta, 1807*(6), 552-561. doi:10.1016/j.bbabio.2010.10.012
Jun, Y. W., Kim, H. R., Reo, Y. J., Dai, M., & Ahn, K. H. (2017). Addressing the autofluorescence issue in deep tissue imaging by two-photon microscopy: the significance of far-red emitting dyes. *Chemical science, 8*(11), 7696-7704.
Junttila, M. R., & de Sauvage, F. J. (2013). Influence of tumour micro-environment heterogeneity on therapeutic response. *Nature, 501*(7467), 346-354.
Kaelin Jr, W. G., & Ratcliffe, P. J. (2008). Oxygen sensing by metazoans: the central role of the HIF hydroxylase pathway. *Molecular cell, 30*(4), 393-402.
Kalluri, R. (2003). Basement membranes: structure, assembly and role in tumour angiogenesis. *Nature Reviews Cancer, 3*(6), 422-433.
Kalogeris, T., Baines, C. P., Krenz, M., & Korthuis, R. J. (2012). Cell biology of ischemia/reperfusion injury. In *International review of cell and molecular biology* (Vol. 298, pp. 229-317): Elsevier.
Kanter, R., Monshouwer, M., Meijer, D., & Groothuis, G. (2002). Precision-cut organ slices as a tool to study toxicity and metabolism of xenobiotics with special reference to non-hepatic tissues. *Current drug metabolism, 3*(1), 39-59.
Kapałczyńska, M., Kolenda, T., Przybyła, W., Zajączkowska, M., Teresiak, A., Filas, V., . . . Lamperska, K. (2018). 2D and 3D cell cultures–a comparison of different types of cancer cell cultures. *Archives of medical science: AMS, 14*(4), 910.
Karageorgiou, V., & Kaplan, D. (2005). Porosity of 3D biomaterial scaffolds and osteogenesis. *Biomaterials, 26*(27), 5474-5491.
Katt, M. E., Placone, A. L., Wong, A. D., Xu, Z. S., & Searson, P. C. (2016). In vitro tumor models: advantages, disadvantages, variables, and selecting the right platform. *Frontiers in bioengineering and biotechnology, 4*, 12.
Kepp, O., Galluzzi, L., Lipinski, M., Yuan, J., & Kroemer, G. (2011). Cell death assays for drug discovery. *Nature reviews Drug discovery, 10*(3), 221-237.
Kienle, A., & Hibst, R. (2006). Light guiding in biological tissue due to scattering. *Physical review letters, 97*(1), 018104.
Kim, N., Lee, J., Kim, K. H., Park, J. W., Lee, C. G., & Keum, K. C. (2016). Early hypopharyngeal cancer treated with different therapeutic approaches: a single-institution cohort analysis. *Radiation oncology journal, 34*(4), 280.
Kim, S. H., Turnbull, J., & Guimond, S. (2011). Extracellular matrix and cell signalling: the dynamic cooperation of integrin, proteoglycan and growth factor receptor. *J Endocrinol, 209*(2), 139-151. doi:10.1530/joe-10-0377
Kornprat, P., Pollheimer, M. J., Lindtner, R. A., Schlemmer, A., Rehak, P., & Langner, C. (2011). Value of tumor size as a prognostic variable in colorectal cancer: a critical reappraisal. *American journal of clinical oncology, 34*(1), 43-49.

Kornuta, J. A., & Dixon, J. B. (2014). Ex vivo lymphatic perfusion system for independently controlling pressure gradient and transmural pressure in isolated vessels. *Annals of biomedical engineering, 42*(8), 1691-1704.
Krishnan, V., Tallapragada, S., Schaar, B., Kamat, K., Chanana, A. M., Zhang, Y., . . . Folkins, A. K. (2020). Omental macrophages secrete chemokine ligands that promote ovarian cancer colonization of the omentum via CCR1. *Communications biology, 3*(1), 1-13.
Kristián, T., Katsura, K.-i., Gidö, G., & Siesjö, B. K. (1994). The influence of pH on cellular calcium influx during ischemia. *Brain research, 641*(2), 295-302.
Kristián, T., & Siesjö, B. K. (1998). Calcium in ischemic cell death. *Stroke, 29*(3), 705-718.
Kuczynski, E. A., Vermeulen, P. B., Pezzella, F., Kerbel, R. S., & Reynolds, A. R. (2019). Vessel co-option in cancer. *Nature reviews Clinical oncology, 16*(8), 469-493.
Kvietys, P. R., & Granger, D. N. (2012). Role of reactive oxygen and nitrogen species in the vascular responses to inflammation. *Free Radical Biology and Medicine, 52*(3), 556-592.
Lacroix, G., Koch, W., Ritter, D., Gutleb, A. C., Larsen, S. T., Loret, T., . . . Rothen-Rutishauser, B. (2018). Air–liquid Interface in vitro models for respiratory toxicology research: consensus workshop and recommendations. *Applied in vitro toxicology, 4*(2), 91-106.
Lambin, P., Kramar, A., Haie-Meder, C., Castaigne, D., Scalliet, P., Bouzy, J., . . . Gerbaulet, A. (1998). Tumour size in cancer of the cervix. *Acta oncologica, 37*(7-8), 729-734.
Land, W. G. (2005). The role of postischemic reperfusion injury and other nonantigen-dependent inflammatory pathways in transplantation. *Transplantation, 79*(5), 505-514.
Latacz, E., Caspani, E., Barnhill, R., Lugassy, C., Verhoef, C., Grünhagen, D., . . . Dirix, M. (2019). Pathological features of vessel co-option versus sprouting angiogenesis. *Angiogenesis*, 1-12.
Leary, E., Rhee, C., Wilks, B. T., & Morgan, J. R. (2018). Quantitative live-cell confocal imaging of 3D spheroids in a high-throughput format. *SLAS TECHNOLOGY: Translating Life Sciences Innovation, 23*(3), 231-242.
Lengyel, E. (2010). Ovarian cancer development and metastasis. *The American journal of pathology, 177*(3), 1053-1064.
Lennerz, J. K., Hurov, J. B., White, L. S., Lewandowski, K. T., Prior, J. L., Planer, G. J., . . . Piwnica-Worms, H. (2010). Loss of Par-1a/MARK3/C-TAK1 kinase leads to reduced adiposity, resistance to hepatic steatosis, and defective gluconeogenesis. *Molecular and cellular biology, 30*(21), 5043-5056.
Lever, M. J. (1995). Mass transport through the walls of arteries and veins. In *Biological Flows* (pp. 177-197): Springer.
Levick, J. (1987). Flow through interstitium and other fibrous matrices. *Quarterly Journal of Experimental Physiology: Translation and Integration, 72*(4), 409-437.
Li, K., Wu, D., Chen, X., Zhang, T., Zhang, L., Yi, Y., . . . Wang, H. (2014). Current and emerging biomarkers of cell death in human disease. *BioMed research international, 2014*.
Liberti, M. V., & Locasale, J. W. (2016). The Warburg effect: how does it benefit cancer cells? *Trends in biochemical sciences, 41*(3), 211-218.
Lin, A. Y., Maniotis, A. J., Valyi-Nagy, K., Majumdar, D., Setty, S., Kadkol, S. H., . . . Folberg, R. (2005). Distinguishing fibrovascular septa from vasculogenic mimicry patterns. *Archives of pathology & laboratory medicine, 129*(7), 884-892.
Lisio, M.-A., Fu, L., Goyeneche, A., Gao, Z.-h., & Telleria, C. (2019). High-grade serous ovarian cancer: basic sciences, clinical and therapeutic standpoints. *International journal of molecular sciences, 20*(4), 952.
Liu, R., Hu, R., Zeng, Y., Zhang, W., & Zhou, H.-H. (2020). Tumour immune cell infiltration and survival after platinum-based chemotherapy in high-grade serous ovarian cancer subtypes: A gene expression-based computational study. *EBioMedicine, 51*, 102602.
Liu, T., Zhou, L., Li, D., Andl, T., & Zhang, Y. (2019). Cancer-associated fibroblasts build and secure the tumor microenvironment. *Frontiers in Cell and Developmental Biology, 7*.

Liu, Y., & Levine, B. (2015). Autosis and autophagic cell death: the dark side of autophagy. *Cell Death & Differentiation, 22*(3), 367-376.

Liu, Y., Shoji-Kawata, S., Sumpter, R. M., Wei, Y., Ginet, V., Zhang, L., . . . Xavier, R. J. (2013). Autosis is a Na+, K+-ATPase–regulated form of cell death triggered by autophagy-inducing peptides, starvation, and hypoxia–ischemia. *Proceedings of the National Academy of Sciences, 110*(51), 20364-20371.

Lodder, W. L., Teertstra, H. J., Tan, B., Pameijer, F. A., Smeele, L. E., van Velthuysen, M.-L. F., & van den Brekel, M. W. (2011). Tumour thickness in oral cancer using an intra-oral ultrasound probe. *European radiology, 21*(1), 98-106.

Lodish, H., Berk, A., Zipursky, S. L., Matsudaira, P., Baltimore, D., & Darnell, J. (2000). Active Transport by ATP-Powered Pumps. In *Molecular Cell Biology. 4th edition*: WH Freeman.

Loor, G., Kondapalli, J., Iwase, H., Chandel, N. S., Waypa, G. B., Guzy, R. D., . . . Schumacker, P. T. (2011). Mitochondrial oxidant stress triggers cell death in simulated ischemia–reperfusion. *Biochimica et Biophysica Acta (BBA)-Molecular Cell Research, 1813*(7), 1382-1394.

Lu, P., Takai, K., Weaver, V. M., & Werb, Z. (2011). Extracellular matrix degradation and remodeling in development and disease. *Cold Spring Harbor perspectives in biology, 3*(12), a005058.

Lugano, R., Ramachandran, M., & Dimberg, A. (2019). Tumor angiogenesis: causes, consequences, challenges and opportunities. *Cellular and Molecular Life Sciences*, 1-26.

Luo, S., Lei, H., Qin, H., & Xia, Y. (2014). Molecular mechanisms of endothelial NO synthase uncoupling. *Current pharmaceutical design, 20*(22), 3548-3553.

MacManus, D. B., Maillet, M., O'Gorman, S., Pierrat, B., Murphy, J. G., & Gilchrist, M. D. (2019). Sex-and age-specific mechanical properties of liver tissue under dynamic loading conditions. *Journal of the mechanical behavior of biomedical materials, 99*, 240-246.

MacManus, D. B., Menichetti, A., Depreitere, B., Famaey, N., Vander Sloten, J., & Gilchrist, M. (2020). Towards animal surrogates for characterising large strain dynamic mechanical properties of human brain tissue. *Brain Multiphysics, 1*, 100018.

Madekurozwa, M. (2019). *Aqueous Humour Outflow Dynamics in Mice.*

Madekurozwa, M., Reina-Torres, E., Overby, D. R., & Sherwood, J. M. (2017). Direct measurement of pressure-independent aqueous humour flow using iPerfusion. *Experimental eye research, 162*, 129-138.

Majmundar, A. J., Wong, W. J., & Simon, M. C. (2010). Hypoxia-inducible factors and the response to hypoxic stress. *Molecular cell, 40*(2), 294-309.

Manallack, D. T., Prankerd, R. J., Yuriev, E., Oprea, T. I., & Chalmers, D. K. (2013). The significance of acid/base properties in drug discovery. *Chemical society reviews, 42*(2), 485-496.

Marcu, R., Choi, Y. J., Xue, J., Fortin, C. L., Wang, Y., Nagao, R. J., . . . Murry, C. E. (2018). Human organ-specific endothelial cell heterogeneity. *iScience, 4*, 20-35.

Marquart, J., Chen, E. Y., & Prasad, V. (2018). Estimation of the percentage of US patients with cancer who benefit from genome-driven oncology. *JAMA oncology, 4*(8), 1093-1098.

Marusyk, A., Almendro, V., & Polyak, K. (2012). Intra-tumour heterogeneity: a looking glass for cancer? *Nature Reviews Cancer, 12*(5), 323-334.

Matzinger, P. (2002). The danger model: a renewed sense of self. *Science, 296*(5566), 301-305.

McDonald, M. E., Salinas, E. A., Devor, E. J., Newtson, A. M., Thiel, K. W., Goodheart, M. J., . . . Gonzalez-Bosquet, J. (2019). Molecular Characterization of Non-responders to Chemotherapy in Serous Ovarian Cancer. *International journal of molecular sciences, 20*(5), 1175.

McDonald-Hyman, C., Turka, L. A., & Blazar, B. R. (2015). Advances and challenges in immunotherapy for solid organ and hematopoietic stem cell transplantation. *Sci Transl Med, 7*(280), 280rv282. doi:10.1126/scitranslmed.aaa6853

McKeown, C., Edwards, V., Phillips, M. J., Harvey, P., Petrunka, C., & Strasberg, S. (1988). Sinusoidal lining cell damage: the critical injury in cold preservation of liver allografts in the rat. *Transplantation, 46*(2), 178-191.

McLean, I. C., Schwerdtfeger, L. A., Tobet, S. A., & Henry, C. S. (2018). Powering ex vivo tissue models in microfluidic systems. *Lab on a chip, 18*(10), 1399-1410.

McMurtrey, R. J. (2016). Analytic models of oxygen and nutrient diffusion, metabolism dynamics, and architecture optimization in three-dimensional tissue constructs with applications and insights in cerebral organoids. *Tissue Engineering Part C: Methods, 22*(3), 221-249.

Mehta, G., Hsiao, A. Y., Ingram, M., Luker, G. D., & Takayama, S. (2012). Opportunities and challenges for use of tumor spheroids as models to test drug delivery and efficacy. *Journal of controlled release, 164*(2), 192-204.

Meijer, T. G., Naipal, K. A., Jager, A., & van Gent, D. C. (2017). Ex vivo tumor culture systems for functional drug testing and therapy response prediction. *Future science OA, 3*(2), FSO190.

Melissaridou, S., Wiechec, E., Magan, M., Jain, M. V., Chung, M. K., Farnebo, L., & Roberg, K. (2019). The effect of 2D and 3D cell cultures on treatment response, EMT profile and stem cell features in head and neck cancer. *Cancer cell international, 19*(1), 16.

Miller, K. D., Siegel, R. L., Lin, C. C., Mariotto, A. B., Kramer, J. L., Rowland, J. H., . . . Jemal, A. (2016). Cancer treatment and survivorship statistics, 2016. *CA: a cancer journal for clinicians, 66*(4), 271-289.

Milotti, E., Stella, S., & Chignola, R. (2017). Pulsation-limited oxygen diffusion in the tumour microenvironment. *Scientific reports, 7*, 39762.

Minsky, M. (1988). Memoir on inventing the confocal scanning microscope. *Scanning, 10*(4), 128-138.

Mir, M. C., Pavan, N., & Parekh, D. J. (2016). Current paradigm for ischemia in kidney surgery. *The Journal of urology, 195*(6), 1655-1663.

Moen, I., Tronstad, K. J., Kolmannskog, O., Salvesen, G. S., Reed, R. K., & Stuhr, L. E. (2009). Hyperoxia increases the uptake of 5-fluorouracil in mammary tumors independently of changes in interstitial fluid pressure and tumor stroma. *BMC cancer, 9*(1), 446.

Monici, M. (2005). Cell and tissue autofluorescence research and diagnostic applications. *Biotechnology annual review, 11*, 227-256.

Mookerjee, S. A., Gerencser, A. A., Nicholls, D. G., & Brand, M. D. (2017). Quantifying intracellular rates of glycolytic and oxidative ATP production and consumption using extracellular flux measurements. *Journal of Biological Chemistry, 292*(17), 7189-7207.

Moore, R. G., Chung, M., Granai, C. O., Gajewski, W., & Steinhoff, M. M. (2004). Incidence of metastasis to the ovaries from nongenital tract primary tumors. *Gynecologic oncology, 93*(1), 87-91.

Morgan, G., Ward, R., & Barton, M. (2004). The contribution of cytotoxic chemotherapy to 5-year survival in adult malignancies. *Clinical oncology, 16*(8), 549-560.

Morgan, S., Hanna, J., & Yousef, G. M. (2020). Knowledge Translation in Oncology: The Bumpy Ride From Bench to Bedside. *American Journal of Clinical Pathology, 153*(1), 5-13.

Moulder, S. (2010). Intrinsic resistance to chemotherapy in breast cancer. *Women's health, 6*(6), 821-830.

Mourant, J. R., Freyer, J. P., Hielscher, A. H., Eick, A. A., Shen, D., & Johnson, T. M. (1998). Mechanisms of light scattering from biological cells relevant to noninvasive optical-tissue diagnostics. *Applied optics, 37*(16), 3586-3593.

Musumeci, G. (2014). Past, present and future: overview on histology and histopathology. *Journal of Histology and Histopathology, 1*(1), 5.

Nallanthighal, S., Heiserman, J. P., & Cheon, D.-J. (2019). The Role of the Extracellular Matrix in Cancer Stemness. *Frontiers in Cell and Developmental Biology, 7*.

Navin, N., Kendall, J., Troge, J., Andrews, P., Rodgers, L., McIndoo, J., . . . Esposito, D. (2011). Tumour evolution inferred by single-cell sequencing. *Nature, 472*(7341), 90.

Netti, P. A., Berk, D. A., Swartz, M. A., Grodzinsky, A. J., & Jain, R. K. (2000). Role of extracellular matrix assembly in interstitial transport in solid tumors. *Cancer research, 60*(9), 2497-2503.

Network, C. G. A. R. (2011). Integrated genomic analyses of ovarian carcinoma. *Nature, 474*(7353), 609.

Niccoli, G., Burzotta, F., Galiuto, L., & Crea, F. (2009). Myocardial no-reflow in humans. *Journal of the American College of Cardiology, 54*(4), 281-292.

Nicholas, Fajar, F. M., Ramadhanty, S., & Abuzairi, T. (2019). *Study of plasma treatment for PDMS surface modification on the fabrication of microfluidic devices.* Paper presented at the AIP Conference Proceedings.

Nikoletopoulou, V., Markaki, M., Palikaras, K., & Tavernarakis, N. (2013). Crosstalk between apoptosis, necrosis and autophagy. *Biochimica et Biophysica Acta (BBA)-Molecular Cell Research, 1833*(12), 3448-3459.

O'Brien, F. J., Harley, B. A., Yannas, I. V., & Gibson, L. J. (2005). The effect of pore size on cell adhesion in collagen-GAG scaffolds. *Biomaterials, 26*(4), 433-441.

O'Leary, D. S. (1991). Regional vascular resistance vs. conductance: which index for baroreflex responses? *American Journal of Physiology-Heart and Circulatory Physiology, 260*(2), H632-H637.

Oliver, C., Starke-Reed, P., Stadtman, E., Liu, G., Carney, J., & Floyd, R. (1990). Oxidative damage to brain proteins, loss of glutamine synthetase activity, and production of free radicals during ischemia/reperfusion-induced injury to gerbil brain. *Proceedings of the National Academy of Sciences, 87*(13), 5144-5147.

Ooft, S. N., Weeber, F., Dijkstra, K. K., McLean, C. M., Kaing, S., van Werkhoven, E., . . . van de Haar, J. (2019). Patient-derived organoids can predict response to chemotherapy in metastatic colorectal cancer patients. *Science translational medicine, 11*(513), eaay2574.

Opie, L. H. (2004). *Heart physiology: from cell to circulation*: Lippincott Williams & Wilkins.

Papalazarou, V., Zhang, T., Paul, N. R., Juin, A., Cantini, M., Maddocks, O. D., . . . Machesky, L. M. (2020). The creatine–phosphagen system is mechanoresponsive in pancreatic adenocarcinoma and fuels invasion and metastasis. *Nature Metabolism, 2*(1), 62-80.

Park, J. S., Burckhardt, C. J., Lazcano, R., Solis, L. M., Isogai, T., Li, L., . . . Bachoo, R. (2020). Mechanical regulation of glycolysis via cytoskeleton architecture. *Nature, 578*(7796), 621-626.

Parrish, A. R., Gandolfi, A. J., & Brendel, K. (1995). Precision-cut tissue slices: applications in pharmacology and toxicology. *Life Sci, 57*(21), 1887-1901. doi:10.1016/0024-3205(95)02176-j

Pauli, C., Hopkins, B. D., Prandi, D., Shaw, R., Fedrizzi, T., Sboner, A., . . . Rosati, R. (2017). Personalized in vitro and in vivo cancer models to guide precision medicine. *Cancer discovery, 7*(5), 462-477.

Peek, C. B., Levine, D. C., Cedernaes, J., Taguchi, A., Kobayashi, Y., Tsai, S. J., . . . Bass, J. (2017). Circadian clock interaction with HIF1α mediates oxygenic metabolism and anaerobic glycolysis in skeletal muscle. *Cell metabolism, 25*(1), 86-92.

Petermann, D., Demartines, N., & Schäfer, M. (2013). Is tumour size an underestimated feature in the current TNM system for malignancies of the pancreatic head? *HPB, 15*(11), 872-881.

Peyton, S. R., Ghajar, C. M., Khatiwala, C. B., & Putnam, A. J. (2007). The emergence of ECM mechanics and cytoskeletal tension as important regulators of cell function. *Cell Biochem Biophys, 47*(2), 300-320. doi:10.1007/s12013-007-0004-y

Piccinini, F., Tesei, A., Arienti, C., & Bevilacqua, A. (2017). Cell counting and viability assessment of 2d and 3d cell cultures: expected reliability of the trypan blue assay. *Biological procedures online, 19*(1), 8.

Pinato, D. J., Howlett, S., Ottaviani, D., Urus, H., Patel, A., Mineo, T., . . . Falconer, A. (2019). Association of prior antibiotic treatment with survival and response to immune checkpoint inhibitor therapy in patients with cancer. *JAMA oncology, 5*(12), 1774-1778.

Pinezich, M., & Vunjak-Novakovic, G. (2019). Bioengineering approaches to organ preservation ex vivo. *Experimental Biology and Medicine, 244*(8), 630-645.

Piotrowski-Daspit, A. S., Nerger, B. A., Wolf, A. E., Sundaresan, S., & Nelson, C. M. (2017). Dynamics of tissue-induced alignment of fibrous extracellular matrix. *Biophysical journal, 113*(3), 702-713.

Place, T. L., Domann, F. E., & Case, A. J. (2017). Limitations of oxygen delivery to cells in culture: An underappreciated problem in basic and translational research. *Free Radical Biology and Medicine, 113*, 311-322.

Polacheck, W. J., Charest, J. L., & Kamm, R. D. (2011). Interstitial flow influences direction of tumor cell migration through competing mechanisms. *Proceedings of the National Academy of Sciences, 108*(27), 11115-11120.

Pon, J. R., & Marra, M. A. (2015). Driver and passenger mutations in cancer. *Annual Review of Pathology: Mechanisms of Disease, 10*, 25-50.

Popel, A. S., & Johnson, P. C. (2005). Microcirculation and Hemorheology. *Annu Rev Fluid Mech, 37*, 43-69. doi:10.1146/annurev.fluid.37.042604.133933

Powley, I. R., Patel, M., Miles, G., Pringle, H., Howells, L., Thomas, A., . . . MacFarlane, M. (2020). Patient-derived explants (PDEs) as a powerful preclinical platform for anti-cancer drug and biomarker discovery. *British journal of cancer*, 1-10.

Prat, J. (2012). Ovarian carcinomas: five distinct diseases with different origins, genetic alterations, and clinicopathological features. *Virchows Archiv, 460*(3), 237-249.

Prigerson, H. G., Bao, Y., Shah, M. A., Paulk, M. E., LeBlanc, T. W., Schneider, B. J., . . . Adelson, K. B. (2015). Chemotherapy use, performance status, and quality of life at the end of life. *JAMA oncology, 1*(6), 778-784.

Puyal, J., Ginet, V., & Clarke, P. G. (2013). Multiple interacting cell death mechanisms in the mediation of excitotoxicity and ischemic brain damage: a challenge for neuroprotection. *Progress in neurobiology, 105*, 24-48.

Qiang, Z., & Wang, M. (2020). 100th Anniversary of Macromolecular Science Viewpoint: Enabling Advances in Fluorescence Microscopy Techniques. *ACS Macro Letters, 9*(9), 1342-1356.

Ragan, T., Kadiri, L. R., Venkataraju, K. U., Bahlmann, K., Sutin, J., Taranda, J., . . . Osten, P. (2012). Serial two-photon tomography for automated ex vivo mouse brain imaging. *Nature methods, 9*(3), 255.

Rambani, K., Vukasinovic, J., Glezer, A., & Potter, S. M. (2009). Culturing thick brain slices: an interstitial 3D microperfusion system for enhanced viability. *Journal of neuroscience methods, 180*(2), 243-254.

Ramirez, C. N., Antczak, C., & Djaballah, H. (2010). Cell viability assessment: toward content-rich platforms. *Expert opinion on drug discovery, 5*(3), 223-233.

Randall, K. J., Turton, J., & Foster, J. R. (2011). Explant culture of gastrointestinal tissue: a review of methods and applications. *Cell biology and toxicology, 27*(4), 267-284.

Rauen, U., & de Groot, H. (2004). New insights into the cellular and molecular mechanisms of cold storage injury. *Journal of investigative medicine, 52*(5), 299-309.

Raza, A., Franklin, M. J., & Dudek, A. Z. (2010). Pericytes and vessel maturation during tumor angiogenesis and metastasis. *American journal of hematology, 85*(8), 593-598.

Reina-Torres, E., Wen, J. C., Liu, K. C., Li, G., Sherwood, J. M., Chang, J. Y., . . . Allingham, R. R. (2017). VEGF as a paracrine regulator of conventional outflow facility. *Investigative ophthalmology & visual science, 58*(3), 1899-1908.

Ren, K., Zhou, J., & Wu, H. (2013). Materials for microfluidic chip fabrication. *Accounts of chemical research, 46*(11), 2396-2406.
Richardson, D. S., & Lichtman, J. W. (2015). Clarifying tissue clearing. *Cell, 162*(2), 246-257.
RINTOUL, R. C., & SETHI, T. (2002). Extracellular matrix regulation of drug resistance in small-cell lung cancer. *Clinical science, 102*(4), 417-424.
Rodenhizer, D., Dean, T., D'Arcangelo, E., & McGuigan, A. P. (2018). The Current Landscape of 3D In Vitro Tumor Models: What Cancer Hallmarks Are Accessible for Drug Discovery? *Adv Healthc Mater, 7*(8), e1701174. doi:10.1002/adhm.201701174
Rohr, U.-P., Binder, C., Dieterle, T., Giusti, F., Messina, C. G. M., Toerien, E., . . . Schäfer, H. H. (2016). The value of in vitro diagnostic testing in medical practice: a status report. *PLoS One, 11*(3).
Rotte, A. (2019). Combination of CTLA-4 and PD-1 blockers for treatment of cancer. *Journal of Experimental & Clinical Cancer Research, 38*(1), 255.
Rousset, N., Monet, F., & Gervais, T. (2017). Simulation-assisted design of microfluidic sample traps for optimal trapping and culture of non-adherent single cells, tissues, and spheroids. *Scientific reports, 7*(1), 1-12.
Sadoshima, J. (2008). The role of autophagy during ischemia/reperfusion. *Autophagy, 4*(4), 402-403.
Sahai, E., Astsaturov, I., Cukierman, E., DeNardo, D. G., Egeblad, M., Evans, R. M., . . . Hunter, T. (2020). A framework for advancing our understanding of cancer-associated fibroblasts. *Nature Reviews Cancer*, 1-13.
Sakariassen, P. Ø., Prestegarden, L., Wang, J., Skaftnesmo, K.-O., Mahesparan, R., Molthoff, C., . . . Tysnes, B. B. (2006). Angiogenesis-independent tumor growth mediated by stem-like cancer cells. *Proceedings of the National Academy of Sciences, 103*(44), 16466-16471.
Sampaziotis, F., Muraro, D., Tysoe, O. C., Sawiak, S., Beach, T. E., Godfrey, E. M., . . . Garcia-Bernardo, J. (2021). Cholangiocyte organoids can repair bile ducts after transplantation in the human liver. *Science, 371*(6531), 839-846.
Sanderson, T. H., Reynolds, C. A., Kumar, R., Przyklenk, K., & Hüttemann, M. (2013). Molecular mechanisms of ischemia–reperfusion injury in brain: pivotal role of the mitochondrial membrane potential in reactive oxygen species generation. *Molecular neurobiology, 47*(1), 9-23.
Sänger, C., Schenk, A., Schwen, L. O., Wang, L., Gremse, F., Zafarnia, S., . . . Richter, B. (2015). Intrahepatic vascular anatomy in rats and mice—variations and surgical implications. *PLoS One, 10*(11), e0141798.
Sapiezynski, J., Taratula, O., Rodriguez-Rodriguez, L., & Minko, T. (2016). Precision targeted therapy of ovarian cancer. *Journal of controlled release, 243*, 250-268.
Sarin, H. (2010). Physiologic upper limits of pore size of different blood capillary types and another perspective on the dual pore theory of microvascular permeability. *J Angiogenes Res, 2*, 14. doi:10.1186/2040-2384-2-14
Schaaf, M. B., Garg, A. D., & Agostinis, P. (2018). Defining the role of the tumor vasculature in antitumor immunity and immunotherapy. *Cell death & disease, 9*(2), 1-14.
Schindelin, J. Fiji: An open-source platform for biological-image analysis. Nature Methods9, 676–682. In.
Schmidt, R. F., & Thews, G. (2013). *Physiologie des Menschen*: Springer-Verlag.
Schmidt-Nielsen, K., & Pennycuik, P. (1961). Capillary density in mammals in relation to body size and oxygen consumption. *American Journal of Physiology-Legacy Content, 200*(4), 746-750.
Schnabel, M., Marlovits, S., Eckhoff, G., Fichtel, I., Gotzen, L., Vecsei, V., & Schlegel, J. (2002). Dedifferentiation-associated changes in morphology and gene expression in primary human articular chondrocytes in cell culture. *Osteoarthritis and Cartilage, 10*(1), 62-70.

Schneider, C. A., Rasband, W. S., & Eliceiri, K. W. (2012). NIH Image to ImageJ: 25 years of image analysis. *Nature methods, 9*(7), 671-675.

Scholzen, T., & Gerdes, J. (2000). The Ki-67 protein: from the known and the unknown. *Journal of cellular physiology, 182*(3), 311-322.

Schumacher, K., Khong, Y.-M., Chang, S., Ni, J., Sun, W., & Yu, H. (2007). Perfusion culture improves the maintenance of cultured liver tissue slices. *Tissue engineering, 13*(1), 197-205.

Schwartz, B. G., & Kloner, R. A. (2012). Coronary no reflow. *Journal of molecular and cellular cardiology, 52*(4), 873-882.

Seethala, R. R., Thompson, L. D., Gnepp, D. R., Barnes, E. L., Skalova, A., Montone, K., . . . Simpson, R. H. (2012). Lymphadenoma of the salivary gland: clinicopathological and immunohistochemical analysis of 33 tumors. *Modern pathology, 25*(1), 26-35.

Seidel, J. A., Otsuka, A., & Kabashima, K. (2018). Anti-PD-1 and anti-CTLA-4 therapies in cancer: mechanisms of action, efficacy, and limitations. *Frontiers in oncology, 8*, 86.

Sekine, W., Haraguchi, Y., Shimizu, T., Umezawa, A., & Okano, T. (2011). Thickness limitation and cell viability of multi-layered cell sheets and overcoming the diffusion limit by a porous-membrane culture insert. *J Biochip Tissue Chip S, 1*, 2153-0777.

Sethi, T., Rintoul, R. C., Moore, S. M., MacKinnon, A. C., Salter, D., Choo, C., . . . Strieter, R. (1999). Extracellular matrix proteins protect small cell lung cancer cells against apoptosis: a mechanism for small cell lung cancer growth and drug resistance in vivo. *Nature medicine, 5*(6), 662-668.

Sherman-Baust, C. A., Weeraratna, A. T., Rangel, L. B., Pizer, E. S., Cho, K. R., Schwartz, D. R., . . . Morin, P. J. (2003). Remodeling of the extracellular matrix through overexpression of collagen VI contributes to cisplatin resistance in ovarian cancer cells. *Cancer Cell, 3*(4), 377-386. doi:10.1016/s1535-6108(03)00058-8

Sherwood, J. M., Reina-Torres, E., Bertrand, J. A., Rowe, B., & Overby, D. R. (2016). Measurement of Outflow Facility Using iPerfusion. *PLoS One, 11*(3), e0150694. doi:10.1371/journal.pone.0150694

Shi, Z., Graber, Z. T., Baumgart, T., Stone, H. A., & Cohen, A. E. (2018). Cell membranes resist flow. *Cell, 175*(7), 1769-1779. e1713.

Shweiki, D., Neeman, M., Itin, A., & Keshet, E. (1995). Induction of vascular endothelial growth factor expression by hypoxia and by glucose deficiency in multicell spheroids: implications for tumor angiogenesis. *Proceedings of the National Academy of Sciences, 92*(3), 768-772.

Siena, S., Sartore-Bianchi, A., Di Nicolantonio, F., Balfour, J., & Bardelli, A. (2009). Biomarkers predicting clinical outcome of epidermal growth factor receptor–targeted therapy in metastatic colorectal cancer. *Journal of the National Cancer Institute, 101*(19), 1308-1324.

Slaoui, M., & Fiette, L. (2011). Histopathology procedures: from tissue sampling to histopathological evaluation. In *Drug safety evaluation* (pp. 69-82): Springer.

Solaini, G., Baracca, A., Lenaz, G., & Sgarbi, G. (2010). Hypoxia and mitochondrial oxidative metabolism. *Biochimica et Biophysica Acta (BBA)-Bioenergetics, 1797*(6-7), 1171-1177.

Soller, E. C., Tzeranis, D. S., Miu, K., So, P. T., & Yannas, I. V. (2012). Common features of optimal collagen scaffolds that disrupt wound contraction and enhance regeneration both in peripheral nerves and in skin. *Biomaterials, 33*(19), 4783-4791.

Spear, B. B., Heath-Chiozzi, M., & Huff, J. (2001). Clinical application of pharmacogenetics. *Trends in molecular medicine, 7*(5), 201-204.

St Peter, S. D., Imber, C. J., & Friend, P. J. (2002). Liver and kidney preservation by perfusion. *The Lancet, 359*(9306), 604-613.

Steward Jr, R., Tambe, D., Hardin, C. C., Krishnan, R., & Fredberg, J. J. (2015). Fluid shear, intercellular stress, and endothelial cell alignment. *American Journal of Physiology-Cell Physiology, 308*(8), C657-C664.

Stylianopoulos, T., & Jain, R. K. (2015). Design considerations for nanotherapeutics in oncology. *Nanomedicine: Nanotechnology, Biology and Medicine, 11*(8), 1893-1907.
Stylianopoulos, T., Poh, M.-Z., Insin, N., Bawendi, M. G., Fukumura, D., Munn, L. L., & Jain, R. K. (2010). Diffusion of particles in the extracellular matrix: the effect of repulsive electrostatic interactions. *Biophysical journal, 99*(5), 1342-1349.
Susaki, E. A., & Ueda, H. R. (2016). Whole-body and whole-organ clearing and imaging techniques with single-cell resolution: toward organism-level systems biology in mammals. *Cell chemical biology, 23*(1), 137-157.
Swartz, M. A., & Fleury, M. E. (2007). Interstitial flow and its effects in soft tissues. *Annu. Rev. Biomed. Eng., 9*, 229-256.
Szydlowska, K., & Tymianski, M. (2010). Calcium, ischemia and excitotoxicity. *Cell calcium, 47*(2), 122-129.
Tainaka, K., Kubota, S. I., Suyama, T. Q., Susaki, E. A., Perrin, D., Ukai-Tadenuma, M., . . . Ueda, H. R. (2014). Whole-body imaging with single-cell resolution by tissue decolorization. *Cell, 159*(4), 911-924.
Tanaka, Y., Yamato, M., Okano, T., Kitamori, T., & Sato, K. (2006). Evaluation of effects of shear stress on hepatocytes by a microchip-based system. *Measurement science and technology, 17*(12), 3167.
Thompson, R. H., Kurta, J. M., Kaag, M., Tickoo, S. K., Kundu, S., Katz, D., . . . Russo, P. (2009). Tumor size is associated with malignant potential in renal cell carcinoma cases. *The Journal of urology, 181*(5), 2033-2036.
Thorsson, V., Gibbs, D. L., Brown, S. D., Wolf, D., Bortone, D. S., Yang, T.-H. O., . . . Eddy, J. A. (2018). The immune landscape of cancer. *Immunity, 48*(4), 812-830. e814.
Tsapras, P., & Nezis, I. P. (2017). Caspase involvement in autophagy. *Cell Death & Differentiation, 24*(8), 1369-1379.
Unal-Cevik, I., Kılınç, M., Can, A., Gürsoy-Özdemir, Y., & Dalkara, T. (2004). Apoptotic and necrotic death mechanisms are concomitantly activated in the same cell after cerebral ischemia. *Stroke, 35*(9), 2189-2194.
Valvona, C. J., Fillmore, H. L., Nunn, P. B., & Pilkington, G. J. (2016). The regulation and function of lactate dehydrogenase A: therapeutic potential in brain tumor. *Brain pathology, 26*(1), 3-17.
Verpoorte, E., & De Rooij, N. F. (2003). Microfluidics meets MEMS. *Proceedings of the IEEE, 91*(6), 930-953.
Vinten-Johansen, J. (2004). Involvement of neutrophils in the pathogenesis of lethal myocardial reperfusion injury. *Cardiovascular research, 61*(3), 481-497.
Vlachogiannis, G., Hedayat, S., Vatsiou, A., Jamin, Y., Fernández-Mateos, J., Khan, K., . . . Burke, R. (2018). Patient-derived organoids model treatment response of metastatic gastrointestinal cancers. *Science, 359*(6378), 920-926.
Wakai, K., Utsumi, T., Oka, R., Endo, T., Yano, M., Kamijima, S., . . . Suzuki, H. (2016). Clinical predictors for high-grade bladder cancer before first-time transurethral resection of the bladder tumor: a retrospective cohort study. *Japanese journal of clinical oncology, 46*(10), 964-967.
Walton, J., Blagih, J., Ennis, D., Leung, E., Dowson, S., Farquharson, M., . . . Mason, S. (2016). CRISPR/Cas9-mediated Trp53 and Brca2 knockout to generate improved murine models of ovarian high-grade serous carcinoma. *Cancer research, 76*(20), 6118-6129.
Walton, J. B., Farquharson, M., Mason, S., Port, J., Kruspig, B., Dowson, S., . . . Kim, J. (2017). CRISPR/Cas9-derived models of ovarian high grade serous carcinoma targeting Brca1, Pten and Nf1, and correlation with platinum sensitivity. *Scientific reports, 7*(1), 1-11.
Wang, C., Baker, B. M., Chen, C. S., & Schwartz, M. A. (2013). Endothelial cell sensing of flow direction. *Arteriosclerosis, thrombosis, and vascular biology, 33*(9), 2130-2136.

Wang, J. P., & Hielscher, A. (2017). Fibronectin: How Its Aberrant Expression in Tumors May Improve Therapeutic Targeting. *J Cancer, 8*(4), 674-682. doi:10.7150/jca.16901

Wang, M., Zhao, J., Zhang, L., Wei, F., Lian, Y., Wu, Y., . . . Cao, K. (2017). Role of tumor microenvironment in tumorigenesis. *Journal of Cancer, 8*(5), 761.

Wang, X.-M., Xu, Y.-Y., Yu, G., Rong, Z., Geng, R.-C., Wang, R., . . . Liu, G. (2020). Pure transanal total mesorectal excision for rectal cancer: experience with 55 cases. *Gastroenterology Report, 8*(1), 42-49.

Wanner, A., Kirschmann, M., & Genoud, C. (2015). Challenges of microtome-based serial block-face scanning electron microscopy in neuroscience. *Journal of microscopy, 259*(2), 137-142.

Weeber, F., Ooft, S. N., Dijkstra, K. K., & Voest, E. E. (2017). Tumor organoids as a pre-clinical cancer model for drug discovery. *Cell chemical biology, 24*(9), 1092-1100.

Weidner, N. (1995). Intratumor microvessel density as a prognostic factor in cancer. *The American journal of pathology, 147*(1), 9.

Weisgrab, G., Ovsianikov, A., & Costa, P. F. (2019). Functional 3D Printing for Microfluidic Chips. *Advanced Materials Technologies, 4*(10), 1900275.

Welbourn, C., Goldman, G., Paterson, I., Valeri, C., Shepro, D., & Hechtman, H. (1991). Pathophysiology of ischaemia reperfusion injury: central role of the neutrophil. *British Journal of Surgery, 78*(6), 651-655.

White, D., Coombe, D., Rezania, V., & Tuszynski, J. (2016). Building a 3D virtual liver: Methods for simulating blood flow and hepatic clearance on 3D structures. *PLoS One, 11*(9), e0162215.

Willis, C., Fiander, M., Tran, D., Korytowsky, B., Thomas, J.-M., Calderon, F., . . . Stenehjem, D. D. (2019). Tumor mutational burden in lung cancer: a systematic literature review. *Oncotarget, 10*(61), 6604.

Workman, P., Aboagye, E., Balkwill, F., Balmain, A., Bruder, G., Chaplin, D., . . . Glennie, M. (2010). Guidelines for the welfare and use of animals in cancer research. *British journal of cancer, 102*(11), 1555-1577.

Wu, D.-Q., Zhang, G.-L., Shen, C., Zhao, Q., Li, H., & Meng, Q. (2005). Evaluation of diffusion in gel entrapment cell culture within hollow fibers. *World Journal of Gastroenterology: WJG, 11*(11), 1599.

Wu, M.-y., Yiang, G.-t., Liao, W.-T., Tsai, A. P.-Y., Cheng, Y.-L., Cheng, P.-W., . . . Li, C.-J. (2018). Current mechanistic concepts in ischemia and reperfusion injury. *Cellular Physiology and Biochemistry, 46*(4), 1650-1667.

Wu, T., & Dai, Y. (2017). Tumor microenvironment and therapeutic response. *Cancer letters, 387*, 61-68.

Xing, F., Saidou, J., & Watabe, K. (2010). Cancer associated fibroblasts (CAFs) in tumor microenvironment. *Frontiers in bioscience: a journal and virtual library, 15*, 166.

Xu, J., Donepudi, A. C., Moscovitz, J. E., & Slitt, A. L. (2013). Keap1-knockdown decreases fasting-induced fatty liver via altered lipid metabolism and decreased fatty acid mobilization from adipose tissue. *PLoS One, 8*(11), e79841.

Xu, X., Farach-Carson, M. C., & Jia, X. (2014). Three-dimensional in vitro tumor models for cancer research and drug evaluation. *Biotechnology advances, 32*(7), 1256-1268.

Yamaguchi, N., & Garceau, D. (1980). Correlations between hemodynamic parameters of the liver and norepinephrine release upon hepatic nerve stimulation in the dog. *Canadian journal of physiology and pharmacology, 58*(11), 1347-1355.

Yao, T., & Asayama, Y. (2017). Animal-cell culture media: History, characteristics, and current issues. *Reproductive medicine and biology, 16*(2), 99-117.

Yellon, D. M., & Hausenloy, D. J. (2007). Myocardial reperfusion injury. *New England Journal of Medicine, 357*(11), 1121-1135.

Yuan, J., Najafov, A., & Py, B. F. (2016). Roles of caspases in necrotic cell death. *Cell, 167*(7), 1693-1704.

Zanoni, M., Piccinini, F., Arienti, C., Zamagni, A., Santi, S., Polico, R., . . . Tesei, A. (2016). 3D tumor spheroid models for in vitro therapeutic screening: a systematic approach to enhance the biological relevance of data obtained. *Scientific reports, 6*(1), 1-11.

Zeybek, A., Erdoğan, A., Gülkesen, K. H., Ergin, M., Sarper, A., Dertsiz, L., & Demircan, A. (2013). Significance of tumor length as prognostic factor for esophageal cancer. *International surgery, 98*(3), 234-240.

Zhai, Y., Petrowsky, H., Hong, J. C., Busuttil, R. W., & Kupiec-Weglinski, J. W. (2013). Ischaemia–reperfusion injury in liver transplantation—from bench to bedside. *Nature reviews Gastroenterology & hepatology, 10*(2), 79.

Zhang, J., Gold, K. A., Lin, H. Y., Swisher, S. G., Xing, Y., Lee, J. J., . . . William Jr, W. N. (2015). Relationship between tumor size and survival in non–small-cell lung cancer (NSCLC): an analysis of the surveillance, epidemiology, and end results (SEER) registry. *Journal of Thoracic Oncology, 10*(4), 682-690.

Zhang, J.-Z., Behrooz, A., & Ismail-Beigi, F. (1999). Regulation of glucose transport by hypoxia. *American Journal of Kidney Diseases, 34*(1), 189-202.

Zhao, H.-C., Wu, R.-L., Liu, F.-B., Zhao, Y.-J., Wang, G.-B., Zhang, Z.-G., . . . Geng, X.-P. (2016). A retrospective analysis of long term outcomes in patients undergoing hepatic resection for large (> 5 cm) hepatocellular carcinoma. *HPB, 18*(11), 943-949.

Zhao, J., Chen, J., Ma, S., Liu, Q., Huang, L., Chen, X., . . . Wang, W. (2018). Recent developments in multimodality fluorescence imaging probes. *Acta Pharmaceutica Sinica B, 8*(3), 320-338.

Zhao, P., Gu, H., Mi, H., Rao, C., Fu, J., & Turng, L.-s. (2018). Fabrication of scaffolds in tissue engineering: a review. *Frontiers of Mechanical Engineering, 13*(1), 107-119.

Zhou, Z.-B., Meng, L., Gelb, A. W., Lee, R., & Huang, W.-Q. (2016). Cerebral ischemia during surgery: an overview. *Journal of biomedical research, 30*(2), 83.

# Appendix A: Supplementary Figures

**Supplementary figure (SF) 1:** Multi-channel device design for testing the efficacy of various combinations of constriction shapes and lengths in tissue specimen entrapment.

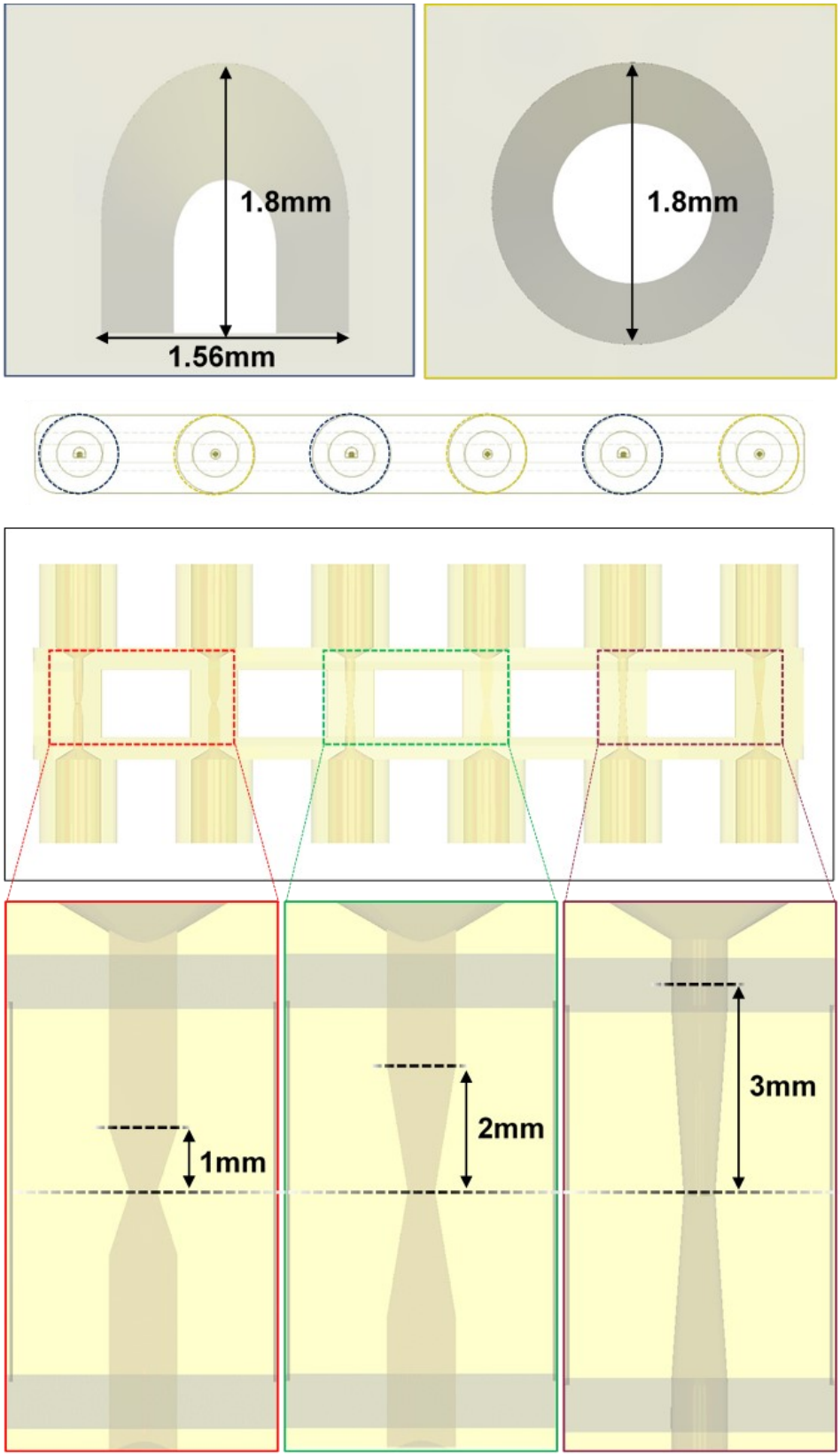

**Supplementary figure (SF) 2:** Three-part syringe pump adapter designed by Foivos Chatzidimitriou, allowing simultaneous control of six 1 ml syringes by each PHD Ultra syringe pump (Harvard Apparatus, USA).

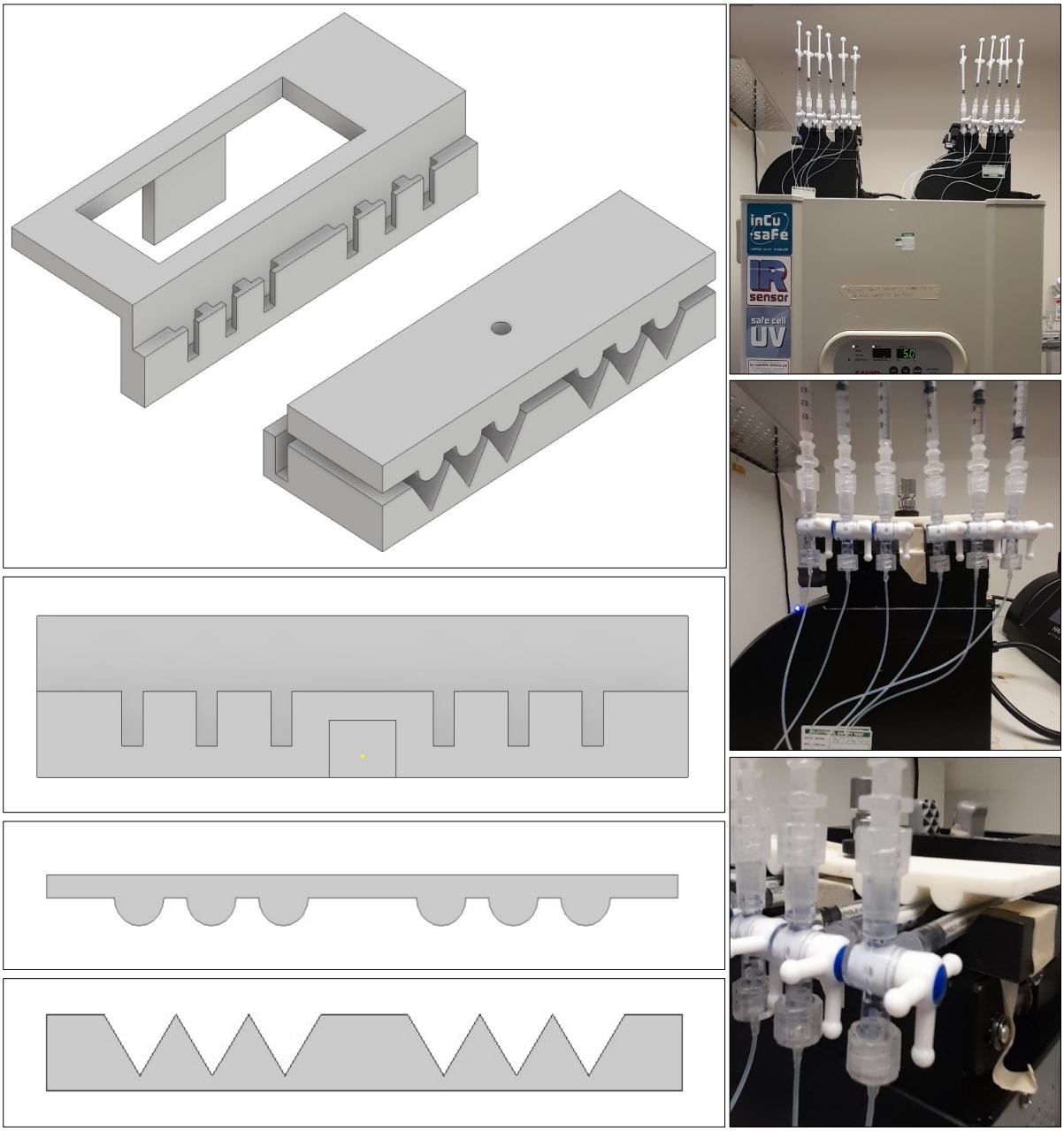

**Supplementary figure (SF) 3:** Cleaved-Caspase 3 immunostaining (brown) and Haematoxylin (blue) on 10µm cryosections of 3mm peri-fused and perfused mouse liver specimens for 24h, at 100 nl/min, at standard cell culture incubator conditions (37ºC, 5% $CO_2$ atmosphere).

## Peri-fused sample

## Peri-fused samples

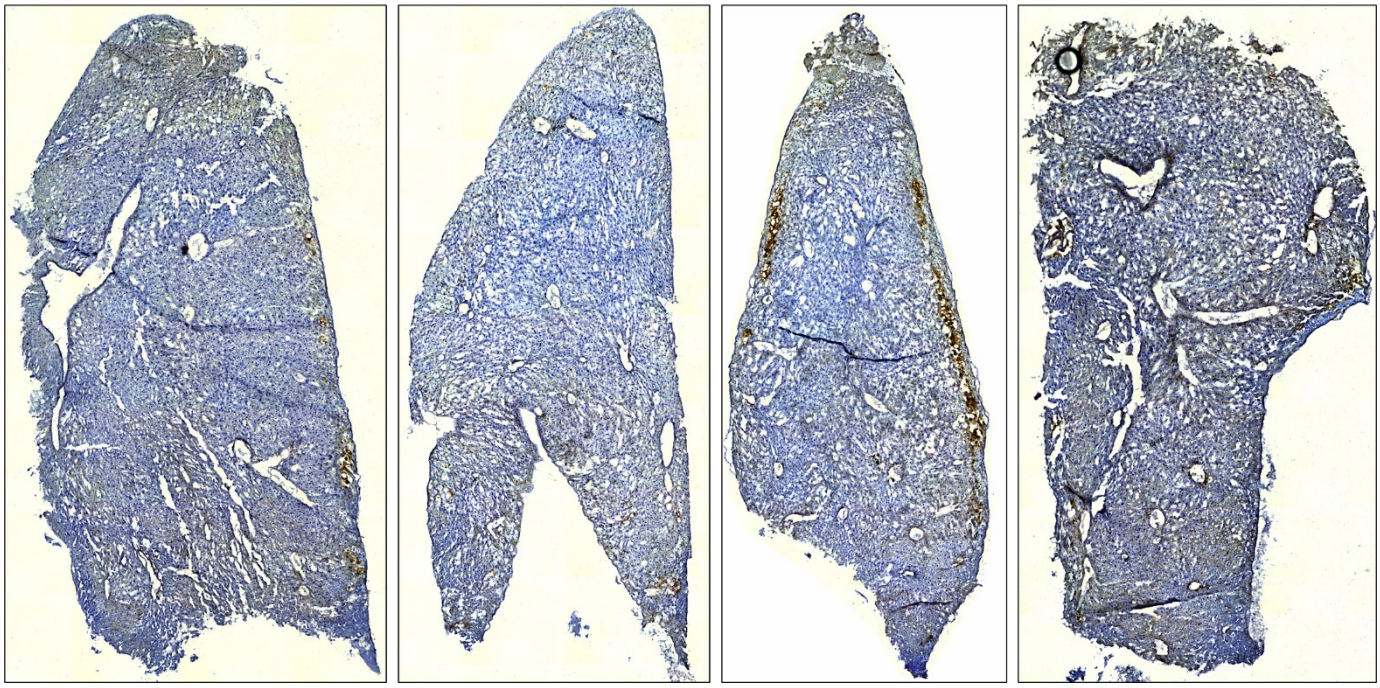

**Supplementary figure (SF) 4:** Cleaved-Caspase 3 immunostaining (brown) and Haematoxylin (blue) on 10µm cryosections of 3mm static, peri-fused and perfused human omental tumour specimens cultured for 48h, at standard cell culture incubator conditions (37ºC, 5% $CO_2$ atmosphere). Flowrate was set at 100 nl/min.

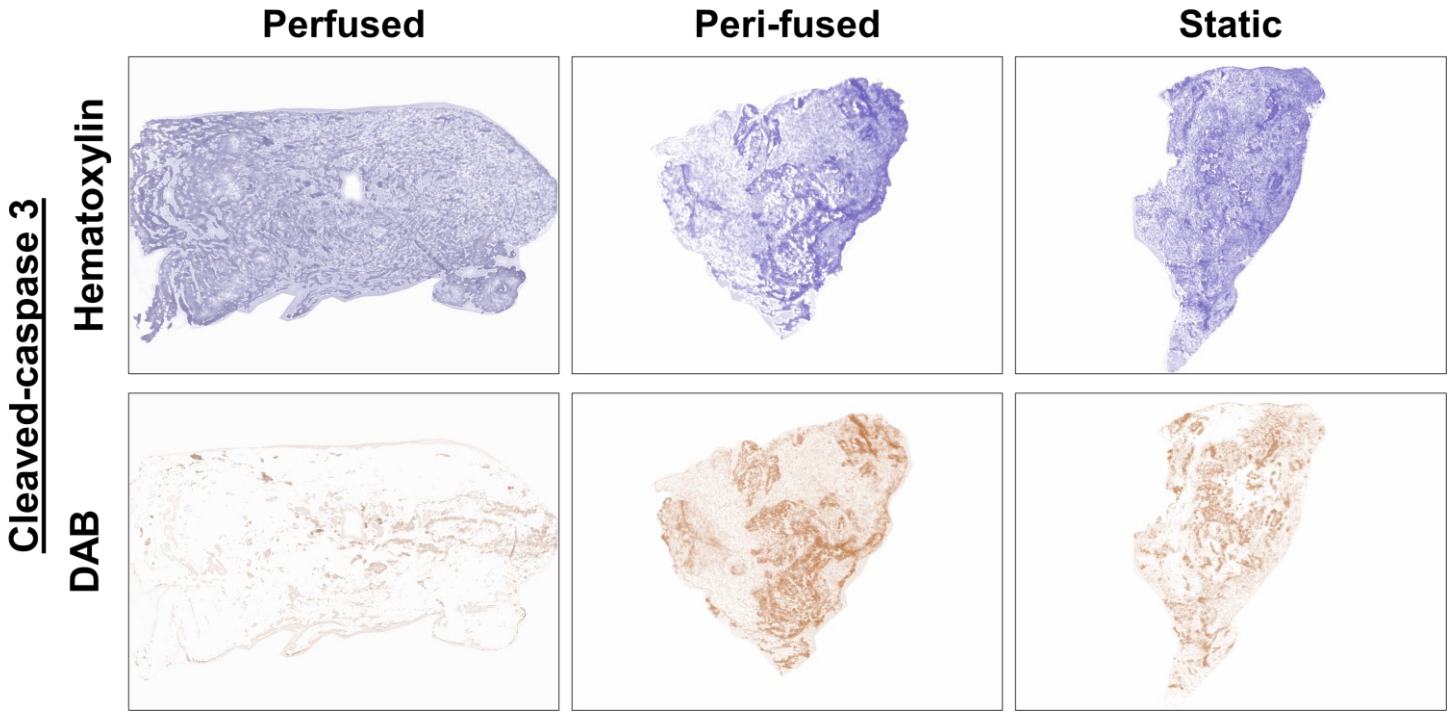

# Appendix B: Protocols

## FABRICATION PROTOCOL

A. The device comprises three layers:

1) Reservoir: Reservoirs are fabricated using a mould, where a mixture of Sylgard 182 (formulated product for PDMS fabrication comprising elastomer, catalyst and clearing agents) and curing agent (10:1) is cast in it. After filling the mould with the mixture, the construct is placed within a desiccator and the mixture is degassed using a common air pump for 45'. Next, PDMS is cured at 65°C for at least 6h.

2) Channel layer: Device main layer with channel architecture is fabricated using a (different) mould, following the same steps as for reservoir fabrication.

3) Bottom layer: A flat layer of the same material and processing is used as the bottom of the device. Usually it is fabricated using a Petri dish.

B. To form the final device the three layers are bonded one on top of the other using plasma treatment.

   a. First, the bottom layer (preferably the surface that was in direct contact with the Petri dish during fabrication) and the surface of the channel layer that was in direct contact with the mould are treated for 45" with a plasma wand.
   b. After that, the two layers are interfaced, manually compressed against each other and then (whilst remaining attached) are cured on a hot plate, indicatively, at 80°C for 2h.
   c. Similarly, the reservoir is bonded on top of the channel layer opening using plasma treatment (same process as 4.). The three-layer construct is let to cure on a hot plate, at 80 °C for 2h.

C. Tubing connection: It is recommended that autoclavable tubing is used so that device sterilisation can be performed in full via autoclave treatment. Indicative tubing length is 80 cm and tubing outer diameter is 1.06 mm.

   a. Using a common biopsy punch, a cylindrical domain is cut out of a flat PDMS layer (similar to the one on 3.).
   b. Similarly, a circular domain that matches tubing's outer diameter (±0.1 mm) is extruded out using a biopsy punch. Each donut-like part is connected to each end of the tubing.
   c. One end of the tubing is interfaced with the device and sealed with 30 μl of uncured PDMS mixture (10:1). The other end is connected to a connector so that is later interfaced with a syringe.
   d. The assembled parts are let to cure on a hot plate, at 65°C for 5h (until PDMS sealing tubing connections has fully polymerised).

## PERFUSION PROTCOL

- Any device, device container, piece of tubing, syringe or reagent that will be used has to be sterile. Any Device fabricated through the fabrication protocol found above can be sterilised with standard autoclave treatment (15 min, 121°C). For heat resistant tubing autoclave sterilisation is preferred. All liquid reagents to be used will be sterile filtered with a sterile 0.2 μm pore filter.
- All steps described below must be followed within a laminar flow biological cabinet to protect equipment and reagent sterility.

- All parts should be removed from the autoclave/plastic bags and devices should be placed within device containers, with the adapters, the tubing and the three-way valves being connected to the devices.
- Recommended equipment for perfusion: syringe A: 1ml; syringe B: 5ml; tubing length: 90 cm.

**A. Setting up the devices:**

1. Fill syringe A (parallel to device tubing; volume depends on syringe pump allowance) and syringe B (perpendicular to device tubing plane; volume depends on total dead volume within device and tubing) with Phosphate Buffered Saline (PBS).

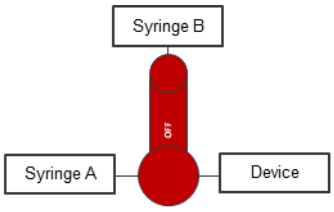


**Configuration 1**

2. Connect each device tubing to a four-way adapter and then connect each adapter to one syringe A and one syringe B. Using configuration 4 dispense enough volume from both so that:
    - The device is filled with media up to reservoir edge.
    - All dead volume is filled with saline – no air bubbles are observed within the device or tubing.

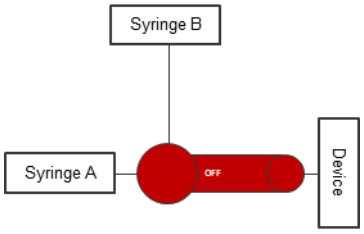


**Configuration 2**

3. Using a pipette empty the reservoir.
4. Using adapter configuration 1 empty syringe A from saline. Using configuration 3 empty syringe B from saline.

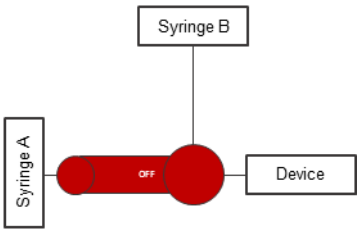


**Configuration 3**

5. Using configuration 2 disconnect syringes A and B. Fill syringes A and B with suitable tissue culture media (depending tissue type and condition) and reconnect them to the adapter as on step 2.
6. Using configuration 4 dispense the whole volume of both syringes.
7. Using a pipette empty the reservoir.
8. Repeat step 5.
9. Using configuration 1 dispense half of the volume within syringe A. Repeat for syringe B using configuration 3. At this point the adapter, the tubing connecting the adapter with the device and the device (up to reservoir edge) should be filled with tissue culture media. No air bubbles should be observed.

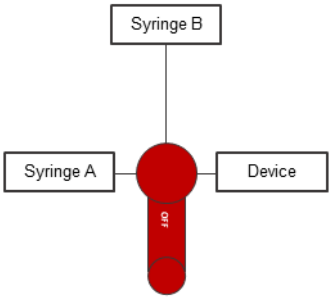


**Configuration 4**

The setup is ready for biological sample incorporation.

**B. Biological sample incorporation:**

1. Using sterile tweezers collect one biological sample unit (e.g. 3-mm murine liver specimen) and place it within the tissue culture media volume in the reservoir so that is submerged. Wait until it sinks to reservoir bottom.
2. Change adapter configuration to configuration 3 and using syringe B induce momentum perturbations (withdraw and dispense) so that the specimen moves within the liquid volume in the reservoir.
3. Once the biological sample is no longer in contact with device bottom, using syringe B withdraw culture media steadily aiming to direct the biological sample to the inlet of the straight channel of the device. This step may need to be repeated several times to successfully direct the specimen in the channel. When syringe B is full and the specimen is still in the reservoir dispense ¾ of syringe B volume and repeat step 3.
4. Once the biological sample reaches channel inlet continue withdrawing media using syringe B, however at a slower rate, forcing the sample to move with no more than 4 mm/s. Withdraw enough volume so that the specimen is directed within the constriction region of the device.
5. Once the specimen macroscopically appears as it seals the constriction region and is immobile stop any flow perturbation and change adapter configuration to configuration 2.

The setup is ready for perfusion initiation.

**C. PERFUSION INITITATION**

1) Place all device containers with devices within a CO2 incubator.
2) Connect syringe A main body to the pump's syringe holder and syringe A end to the moving part of the syringe pump. Configuration 2 allows volume exchange between syringe A and B without the specimen being affected.
3) Once all syringes are connected to the syringe pump, using configuration 1, initiate syringe pump function. (Recommended setting: perfusion at 100 nl/min, withdraw only, no target volume set).

**D. PERFUSION END**

1) Stop syringe pump function.
2) Change valve configuration to configuration 2. Disconnect each four-way valve from the syringe A it is attached to.
3) Remove device containers that carry the devices out of the CO2 incubator and place them immediately within the laminar flow biological cabinet.
4) Disconnect syringe B.

Next steps and biological sample treatment depend on the assays used with the sample.

**RECOMMENDATIONS FOR BIOLOGICAL SAMPLE ISOLATION/PREPARATION**

1. Spray original biological sample container with 70% ethanol and place it in a biological laminar flow cabinet.
2. Remove container lid and using sterile tweezers transfer the biological sample to a sterile petri dish.
3. Wash the biological sample twice with ice cold buffered saline with glucose (recommended glucose concentration 2 g/l).
4. If the biological sample is a tissue specimen divide it in tissue specimens using a sterile biopsy punch. Specimen dimensions are defined by device dimensions. For a given device design tissue samples should be about 3-mm.
5. Wash the specimens twice with ice-cold saline and then transfer them in a sterile container with 5 ml of tissue culture medium.

Biological samples are ready to be incorporated in the device.

# Appendix C: Perfusion model, cell markers

## Appendix C1 – Simulation of perfusion in 3D

The below described model of fluid flow through a porous medium with similar mechanical and hydraulic properties to those of liver grafts was developed by Neophytos Vroulides, whose has allowed reproduction of Fig. 3.3(B) in Chapter 3. This model was developed as part of his UROP under the supervision of Professor Darryl Overby and Foivos Chatzidimitriou.

The fluid flow simulation was developed utilising momentum equations of the Brinkman model and was run in Comsol Multiphysics®. The model comprises two spatial compartments: the channel inlet (xϵ[-2,0]) and the confined specimen ((xϵ(0,4]). Also, it was assumed that fluid flow and pressure were originally zero, the mechanical and hydraulic properties of the body are homogenous and isotropic, no slip on the walls and perfect sealing of the constriction by the specimen. Therefore, the main limitation of the model is that it does not account for the tissue and permeability density gradients established during specimen entrapment in the constriction and their progressive increase due to compression.

The table summarises the parameters used for the calculations.

| Name | Value | Units | Description |
|---|---|---|---|
| $p_i$ | 9930[1] | Pa | Inlet pressure |
| Q | 1.67E-12 | $m^3/s$ | Volumetric flowrate |
| A | 1.0E-06 | $m^2$ | Inlet cross-sectional area |
| ρ | 993.3 | $kg/m^3$ | Fluid density (37ºC) |
| μ | 6.913E-4 | Pa·s | Fluid dynamic viscosity (37ºC) |
| $\varepsilon_p$ | 0.148[2] | - | Tissue porosity |
| $K_l$ | 2E-9[3] | $m^2$ | Liver tissue permeability |

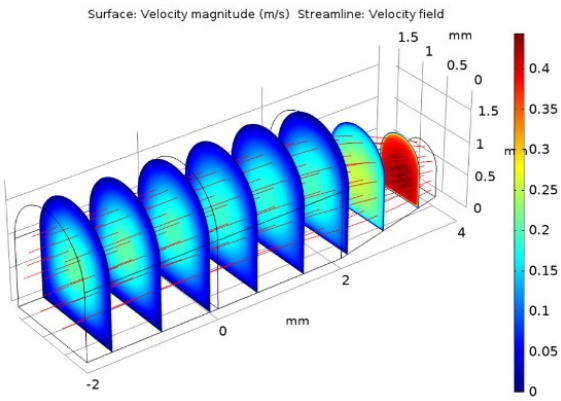


Steady state velocity field in 3D for fluid flow travelling through a specimen entrapped within the constriction of the channel-based device resented herein.

[1] Indicative pressure gradient established across the specimen based on experimental data of a hydraulic resistance of 760 mmHg/μl/min and a flowrate of 100 nl/min.

[2] Debbaut, C., et al. (2012). "Perfusion characteristics of the human hepatic microcirculation based on three-dimensional reconstructions and computational fluid dynamic analysis." Journal of biomechanical engineering **134**(1).

[3] White, D., et al. (2016). "Building a 3D virtual liver: Methods for simulating blood flow and hepatic clearance on 3D structures." PLoS One 11(9): e0162215.

**Appendix C2: cleaved-Caspase 3 quantification**

Quantification of total cleaved Caspase 3 signal of the images presented in Fig. 4.3 was done with QuPath 0.2.3 (Bankhead, Loughrey et al. 2017). Parameters used for positive cell detection after automatic stain vector estimation were Detection image: optical density sum, requested pixel size:0.5 µm, Background radius: 10 µm, Median filter radius: 0 µm, Sigma: 1 µm, Minimum area: 8 µm^2, Maximum area: 500 µm^2, Intensity threshold: 0.05, Maximum background intensity: 5, cell: expansion: 2.0856. Also, the options 'split by shape', 'Include nucleus', Smooth boundaries and 'Make measurements' were selected. Score compartment' was set to 'Nucleus: DAB OD max'.

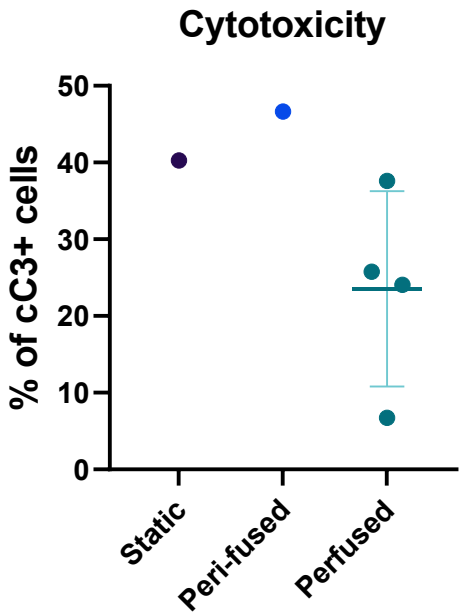


Bankhead, P., et al. (2017). "QuPath: Open source software for digital pathology image analysis." Scientific reports **7**(1): 1-7.

Schneider, C. A., et al. (2012). "NIH Image to ImageJ: 25 years of image analysis." Nature methods **9**(7): 671-675.

**Appendix C3: Filtered PAS images with ImageJ filters (Schneider, Rasband et al. 2012)**